Impact Behavior of Hybrid Thermoplastic Composite Laminates and Sandwich Panels

Sepanta Mandegarian

A Thesis

in

The Department

of

Mechanical, Industrial and Aerospace Engineering

Presented in Partial Fulfillment of the Requirements

for the Degree of

Doctor of Philosophy Mechanical Engineering at

Concordia University

Montreal, Quebec, Canada

March 2025

CONCORDIA UNIVERSITY

School of Graduate Studies

This is to certify that the thesis prepared

By: Sepanta Mandegarian

Entitled: Impact Behavior of Hybrid Thermoplastic Composite Laminates and
                          Sandwich Panels

and submitted in partial fulfillment of the requirements for the degree of

Doctor Of Philosophy (Mechanical Engineering)

complies with the regulations of the University and meets the accepted standards with respect to
originality and quality.

Signed by the final Examining Committee:

_____ Chair
                Farah Hafeez

_____ External Examiner
                Dr. Reza Vaziri

_____ External to Program
                Dr. Ahmed Soliman

_____ Examiner
                Dr. Martin D. Pugh

_____ Examiner
                Dr. Suong Van Hoa

_____ Supervisor
                Dr. Mehdi Hojjati

Approved by

_____
                Chair of Department or Graduate Program Director

11/26/2024   _____
Date of Defence   Dean, Faculty of Engineering and Computer Science

Abstract

Impact Behavior of Hybrid Thermoplastic Composite Laminates and Sandwich Panels

Sepanta Mandegarian, PhD.

Concordia University, 2025.

This thesis explores the development, optimization, and impact behavior of hybrid thermoplastic composite laminates and sandwich panels, focusing on environmentally sustainable materials and advanced reinforcement techniques. Double-belt and compression molding lamination methods were optimized to fabricate full thermoplastic composite sandwich panels with 100% recycled PET foam cores. Analyzing the fabrication parameters and final products' skin-to-core adhesion revealed the critical role of PET foam density and lamination approach in achieving proper bonding. Even though panels made with compression molding outperformed under flexural loads, the continuous nature of the double-belt method offers a reliable and cost-effective alternative production approach.

In the current study, a two-step compression molding method was used to impregnate the metallic mesh layers with PP resin and form a proper connection between the composite layers. Furthermore, the effect of hybridization using stainless-steel mesh layers to reinforce composite laminates and sandwich panels was investigated. Variations of mesh wire size, orientation, and stacking sequence were analyzed to evaluate the energy absorption and damage propagation mechanism of hybrid laminates under different ranges of impact energies. While composite plates show improved performance when the reinforcing metallic layer was positioned at the midplane, it is preferred to reinforce the collision-facing side of sandwich panels for enhanced impact resistance. This strategic placement of the hybrid layer effectively increased the perforation threshold under Low-Velocity Impact (LVI) loading conditions.

In addition, Shape Memory Alloy (SMA) wires were introduced as reinforcing agents of the thermoplastic composite laminates not only to improve the impact performance, but also to take advantage of their specific healing properties to recover the post-impact deformations. Repeated LVI tests demonstrated that the SMA-assisted heating recovery process can restore over 50% of the after-impact deformations, further enhancing the durability and resilience of the composite materials.

Acknowledgments

Dedication

I would like to dedicate this thesis to my beloved family.

To Armita, my love, who has been my unwavering support through every high and low, without whom I would not be where I am today.

To my parents, Farin and Jamshid, for their endless love, guidance, and support, far beyond what I could have ever imagined.

List of journal papers and conference presentations

Journal Papers

[1] Mandegarian S, Hojjati M. "Manufacturing and performance of sandwich composite panels with recycled PET foam core made by continuous roll forming". Manufacturing Letters. 2024; 21: 89-92.

[2] Mandegarian S, Hojjati M, Moghaddar H. "Thermoplastic Composite Sandwich Panels with Recycled PET Foam Core: A Manufacturing Process Assessment". Journal of Thermoplastic Composite Materials, 2024, Accepted.

[3] Mandegarian S., Hojjati M. "Experimental Investigation on the Effects of Stainless-Steel Mesh Reinforcing Layers on Low-Velocity Impact Response of Hybrid Thermoplastic Glass Fiber Composites". Journal of Composite Materials, 2024; 58(16):1887-1904.

[4] Mandegarian S, Hojjati M, Moghaddar H. "Recycled PET Foam Core Sandwich Panels with Reinforced Hybrid Composite Facesheets: A Sustainable Approach for Enhanced Impact Resistance". Journal of Sandwich Structures and Materials, 2025;27(2):396-428.

[5] Mandegarian S, Hojjati M. "Shape Memory Alloy Assisted Healing of Thermoplastic Composite Laminates Under Repeated Impact Loading". Journal of Composite Structures, 2025;358:118977.

Conference Papers / Presentations

[1] Mandegarian S, Hojjati M. "Low velocity impact behavior of thermoplastic glass fiber composites strengthen with stainless steel mesh layers". 23rd International Conference on Composite Materials (ICCM23), Belfast, Northern Ireland, 31 July-4 August 2023.

[2] Mandegarian S, Hojjati M. "Manufacturing and performance of sandwich composite panels with recycled PET foam core made by continuous roll forming". The Sixth International Symposium on Automated Composites Manufacturing (ACM6). South Carolina, SC, USA. 4-8 March 2024.

[3] Mandegarian S, Hojjati M, Moghaddar H. "Fabrication of thermoplastic composite sandwich panels with recycled PET foam core using hot press". 13th Canadian International Conference on Composites (CANCOM 2024), Waterloo, Canada, 6-9 Aug 2024.

Table of Contents

List of Figures

List of Tables

Chapter 1:

Introduction and Motivations

1. Introduction and Motivations

1.1 Introduction

Compared to metals, composite materials offer high strength/stiffness to weight ratio, which is substantial for lightweight load-bearing structures in industries such as aerospace, automotive, and wind power turbines. Nevertheless, composites are inherently susceptible to impact damages caused by hard projectiles such as drop of a tool during maintenance, runaway debris, bird strike or hail. Even impacts that leave barely visible indents can cause internal damages like matrix cracking, delamination, and fiber pull-out which drastically degrade the overall performance of composite panels. To address this issue, numerous research was performed revolving around the topic of low-velocity impact (LVI) behavior of composite materials. It is revealed that modifying the fiber or resin system, fiber architecture, laminate thickness, and stacking sequence can substantially influence impact performance under comparable conditions [1–6].

Composite sandwich panels, often used in these industries because of their specific flexural load-bearing response, thermal and acoustic insulating nature, were a favorite topic for scholars to investigate [7]. These panels show a relatively different response to LVI tests, due to their stepwise failure mechanism, which includes localized core crushing, debonding, fiber breakage and perforation governed by the strikers' energy, skin and core properties [8]. These properties make sandwich panels structurally efficient for impact absorption, yet they remain vulnerable to progressive damage mechanisms that require reinforcement strategies.

Because of the elasto-plastic behavior of metals, they are capable of absorbing higher impact energies; therefore, hybridizing composite materials with metallic reinforcements has proven to be a valuable approach to improving impact resistance. Incorporating metallic reinforcements has been shown to increase energy absorption, delay perforation, and enhance overall LVI performance [9–11]. Moreover, strengthening the composite structures with Shape Memory Alloys (SMA) wires presents a novel method to further enhance impact resistance and after-impact damage recovery. SMA-reinforced composite laminates exhibited the capability to heal specific cracks and delamination during the heat-treatment procedures, activating their recovery behavior [12–18].

2

Despite the promising mechanical improvements expected from hybrid composites, the influence of parameters such as mesh size, wire orientation, stacking sequence, and bonding behavior with thermoplastic resin has not been thoroughly examined. The effectiveness of hybridization on energy absorption, and impact damage propagation, especially in thermoplastic composites, remained unknown. This gap is evident in sandwich panels, where optimizing the placement of metal mesh within the structure could enhance the impact resistance and overall performance of the material.

Thus, this research focuses on addressing previously mentioned gaps by evaluating the applicability and strengthening potential of thermoplastic-based composites hybridized with stainless-steel mesh. The automated fabrication methods and LVI behavior of both composite laminates and sandwich panels are summarized, emphasizing the role of hybridization in improving impact response. Additionally, the potential of SMA reinforced composites to recover from impact damage and enhance energy absorption is discussed.

1.2 Composite plates and sandwich panel lamination

Various manufacturing technologies are available for manufacturing thermoplastic-based composite laminates and composite sandwich panels, including vacuum molding, compression molding, double-belt laminating, automated fiber placement, and in situ foaming. The double-belt laminating process offers the primary advantage of continuous production, making it a cost-effective solution for producing large-scale composite structures, particularly sandwich panels. Figure 1.1 presents a schematic illustration of this automated roll-forming lamination process [7]. Critical parameters across all these methods include heating temperature, cooling rate, manufacturing time, and pressure. Studies have shown that high molding pressure, low melt viscosity, and preheating the foam core significantly enhance the bonding between the facesheet and the core materials [19,20]. The composite skin surface quality and its mechanical properties are another key consideration in the manufacturing of thermoplastic sandwich panels [21–23].
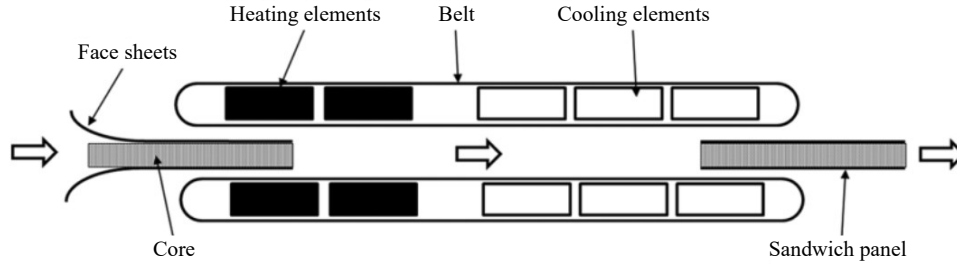
Figure 1.1. Schematic illustration of double-belt laminating procedure of thermoplastic composite sandwich panels [7].

Due to rising environmental concerns, recyclability became popular, with scholars shifting their attention toward developing eco-friendly materials and processes. This trend has also gained momentum in composite manufacturing industries, where sustainable alternatives are actively being used [24–29]; therefore, the present study utilized 100% recycled closed-cell polyethylene terephthalate (PET) foam, sourced from post-consumer plastic water bottles, as the core material for full-thermoplastic sandwich panels. Challenges associated with the high viscosity of polypropylene resin, particularly in achieving effective skin impregnation and interfacial adhesion, were addressed by optimizing key lamination parameters in the double-belt and compression molding processes. Furthermore, the panels' performance under flexural loads was thoroughly assessed, highlighting their potential in practical structural applications.

1.3 Low-velocity impact test

As mentioned earlier, evaluating the LVI response of composite materials is crucial since related damages can significantly compromise structural integrity. Understanding the behavior of composites, the penetration threshold, and subsequent damages are important for real-world applications where impact resistance is a key performance factor. Concordia Center for Composites (CONCOM) has access to an Instron 9340 drop-weight tower, which enables precise assessment of various impact scenarios and gathering essential data. An impact testing machine, like the one used in this study, primarily measures force and time data during LVI tests, which is sufficient to extract complementary information. Using the recorded data, key parameters such as the velocity of the impactor, sample deflection, and energy absorption can be calculated in Equations 1.1, 1.2 and 1.3, respectively [6].

Eq. 1.1.
$$V(t) = V_i + g.t - \int_0^t \left(\frac{F(t)}{m}\right).dt$$

Eq. 1.2.
$$\delta(t) = \delta_i + V_i.t + \frac{g.t^2}{2} + \int_0^t \left(\int_0^t \left(\frac{F(t)}{m}\right).dt\right).dt$$

Eq. 1.3
$$E(t) = \frac{m}{2}\left(V_i^2 - V^2(t)\right) + mg\delta$$

where, V(t), Vi, g, m, F(t), δ(t), and E(t) are the velocity of impactor at time "t", initial velocity, gravitational acceleration, mass of the striker, force, deflection and energy at the time, respectively. Assessing each variable provides crucial insights into different aspects of the composite's response to impact, such as damage initiation, peak force, contact duration, energy absorption, and general impact response. Figure 1.2 depicts the possible force-deflection scenarios of LVI testing. In rebound scenarios, partial deflection recovery occurs, which is indicated by the bounce back of the impactor, while during the perforation all the impact energy is absorbed [6].
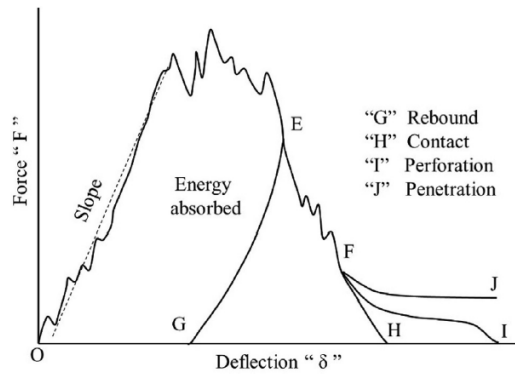
Figure 1.2. Schematic diagram of various force-deflection scenarios under LVI loading [6].

In addition to the force-displacement diagram, energy response of every impact test requires careful evaluation. Each diagram holds specific information about the behavior of the sample in absorbing or restoring specific portions of the applied energy within the impact loading. Thus, in this investigation, not only the energy absorption of hybrid plates and panels were compared to the non-hybrid counterparts, but special attention should be also given to analyzing damage mechanisms at various impact energy levels. Furthermore, the viability and performance of thermoplastic composites reinforced with stainless-steel mesh layers were evaluated to assess their perforation threshold improvement under impact loading conditions.

1.4 Research Motivations

Hybridization using metallic layers has demonstrated its effectiveness in enhancing the energy absorption threshold of composite materials under impact loading. However, there are certain research gaps in the literature regarding the reinforcement potential of stainless-steel mesh in improving impact energy absorption and mechanical performance, particularly for thermoplastic-based composites. Furthermore, full-thermoplastic composites made from polypropylene resin present specific challenges in lamination processes. These challenges were introduced by the industrial partner, Innovative Composite Products Inc. seeking a viable method to enhance the performance of sandwich panels. Addressing these issues required further investigation to optimize reinforcement techniques and overcome the obstacles associated with the fabrication of high-performance composite structures.

1.5 Research Objective

Firstly, this study aims to investigate and optimize available fabrication methods for fully thermoplastic composite plates and sandwich panels with fully recycled PET foam core. This will involve a detailed analysis of compression molding using a hot press and an automated double-belt lamination process, figuring out the proper lamination parameters and evaluating the performance of the final products.

Secondly, due to manufacturing challenges, thermoplastic composite laminates hybridized with stainless-steel mesh layers have not been thoroughly investigated. A multistage approach using a hot press machine, incorporating the pre-impregnation of stainless-steel mesh layers was used to fabricate the composite plate and sandwich panels. To better understand the LVI reinforced of panels reinforced with metal mesh layers, key factors such as mesh wire size, opening area, mesh architecture, and stacking sequence require further assessments. The primary objective is to determine how hybridization influences energy absorption, evaluate the impact behaviors and include response characteristics and damage extent of the reinforced composite laminates. Furthermore, this research intends to investigate the LVI response of PET foam core sandwich panels strengthened with metallic mesh layers. Thus, a comprehensive series of LVI tests were conducted to evaluate the effects of reinforcing layers stacking sequence. In addition to the perforation threshold, visual evaluations of the sectioned views of the panels, accompanied by

microscopic assessments of metal wire fracture and measurements of permanent dents were done, which serve as indicators of damage and plastic deformation.

Finally, the use of hybridization to improve LVI energy absorption by embedding shape memory alloy (SMA) wires in composite structures has been examined. The potential for recovery under repeated LVI loading at lower impact energies, as well as the effectiveness of heat treatment procedures in promoting material recovery or healing after impact has been evaluated. This dual approach of reinforcement and recovery was expected to contribute to the development of more resilient, self-healing composite materials.

1.6 Thesis Layout

The present thesis followed the Concordia manuscript-based thesis guidelines, structuring the details of this study into eight chapters as follows:

Chapter 2: Background and a comprehensive review of previous research on manufacturing, low-velocity impact behavior of composite structures, and reinforcing techniques for composite plates and panels.

Chapter 3: The automated double-belt lamination technique was initially assessed and optimized for its capability to laminate composite sandwich panels. These panels were manufactured with a Glass/PP composite skin, and fully recycled PET foam core on a large scale, and their performance was tested under 3-point bending. The results for this chapter have been published in a special edition of the Journal of Manufacturing Letters.

Chapter 4: The details of two distinct lamination techniques, double-belt and compression molding have been presented and compared to fabricate high-quality composite laminates and PET foam core sandwich panels. A comprehensive evaluation of both methods, qualitative study of skin-to-core bonding and flexural performance of such panel were examined in this chapter. This work has been published in the Journal of Thermoplastic Composite Materials.

Chapter 5: In this chapter, the influence of hybridization, using stainless-steel metal mesh layers to reinforce composite plates has been studied under low-velocity impact loading conditions. The LVI perforation threshold of hybrid and non-hybrid glass/PP composites was carefully determined,

with a detailed investigation of the reinforcing metal mesh wire size, orientation and stacking sequence. The achievements of this part of our study have been published in the Journal of Composite Materials.

Chapter 6: In this chapter, in addition to taking advantage of metal mesh to reinforce the PET foam core composite sandwich panels, respective damages under various impact energies were investigated. The reinforcement stainless-steel mesh layer position with respect to the impactor has been examined for panels with two different core thicknesses.

Chapter 7: Shape memory alloy wires were used to enhance the energy-absorbing capacity of composite plates and present the opportunity to heal the damages under repeated impacts. Thus, in this section, the capability of SMA Nitinol wires to recover the after-impact deformation of composite laminates has been assessed by examining the plates subjected to repeated impacts followed by thermal healing cycles.

Chapter 8: Finally, the conclusions of this research, along with a discussion of potential future work have been presented.

Chapter 2:

Literature Review

2. Literature Review

2.1 Fabrication of composite structures

There is a growing demand to make structures from recycled or recyclable materials, driven by increasing environmental concerns. The recyclability of PET makes it a material of significant interest within the academic and industrial communities. Recent studies on cores made from recycled bottle caps and eco-friendly PET foam sandwich panels further underscore this industry shift [24–29]. Glass fiber composite panels with PET foam cores are being widely used in different fields, including wind turbine structures and prefabricated insulated building components [24,30]. In this context, Kang et al. conducted an extensive investigation into the complete lamination cycle and recycling processes of PET core composite sandwich panels [31].

Numerous studies have been conducted on various fabrication methods aimed at establishing a robust bond between the core and composite facesheets [7]. The fusion bonding method, used in fabrication approaches like double-belt or compression molding, has proven to be particularly effective in achieving satisfactory adhesion between the layers in thermoplastic sandwich panels [1,16–18]. Akermo and Astrom carried out a detailed analysis of the critical factors, which directly affect the interfacial contact in all-thermoplastic sandwich panels, in a compression molding process [32,33].

As mentioned in the previous chapter, the uninterrupted feature of double-belt manufacturing method presents a cost-effective continuous operation technique capable of large-scale lamination of composite plates or panels. As shown in Figure 1.1, this automated fabrication method could potentially include several heating, cooling or laminating sequences which require a comprehensive evaluation. Alongside these manufacturing variable parameters, production speed significantly influences the adequate impregnation of thermoplastic laminates [7,34–37]. An investigation on carbon fiber phenylene sulfide composites made with this automated approach demonstrated that the production rate significantly affects the microstructural characteristics of the laminates [38]. Therefore, the current study necessitates a systematic trial-and-error approach to optimize both the available double-belt and compression molding manufacturing methods prior to

initiating the primary research focused on the composite plates and sandwich panels' LVI performance and the enhancement of hybridization techniques.

2.2 Low-velocity impact behavior of composites

Several attempts have revealed that the LVI behavior of composite structures is dependent on their fabrication, material systems, geometry, impactor parameters and environmental conditions. In addition to the striker's response, compression after impact testing, CT scans, X-rays, and microscopic imaging of the impacted samples have been employed to determine the extent of damage [5]. Previous research has shown that the penetration energy and indentation depth are primarily controlled by laminate thickness, fiber volume fraction, and impactor tup diameter, while resin type, stacking sequence, and fiber architecture play a relatively minor role [1–4].

Robinson and Davies depicted that the magnitude of impact energy governs the LVI test behavior, while the striker's mass and velocity effects are negligible [39]. Similarly, Artero et al. confirmed that peak force, maximum displacement, and damage patterns are independent of impactor mass [40]. Nonetheless, at low energy levels, impactor velocity affects the extent of delamination and residual displacement [41,42]. Besides, studies on fiber architectures, including unidirectional, multidirectional, woven, and 3D woven, revealed that 3D woven composites outperform the other architectures under impact loading [43–45]. Despite significant research efforts to evaluate and improve the LVI performance of composite materials, certain gaps remain in understanding the effects of hybridization with metallic reinforcements, which will be addressed in the following sections.

2.2.1 LVI response of composite laminates

Even barely visible damages occurring under LVI loading can severely compromise the integrity of composite materials. Richardson and Wisheart categorized the damage progression in fiber-reinforced plastics subjected to impact loading into four stages [46]. Initially, matrix cracking occurs parallel to fibers at the edge of the impact zone due to high shear and bending stress, as presented in Figure 2.1. Following that, delamination and fiber breakage occur because of the bending stiffness mismatch, tensile bending stress and compression buckling of fibers,

respectively. Finally, penetration is considered as the catastrophic macroscopic failure of these laminates. Furthermore, since penetrating the laminate requires higher impact energies, the after-impact damages are relatively localized compared to the non-penetrated cases [43,46]. Bibo and Hogg revealed that the matrix and shear cracks influence load drop or compression after impact strength are negligible compared to delamination occurring under LVI loadings [4,47].

a) Transverse view   B) Longitudinal view
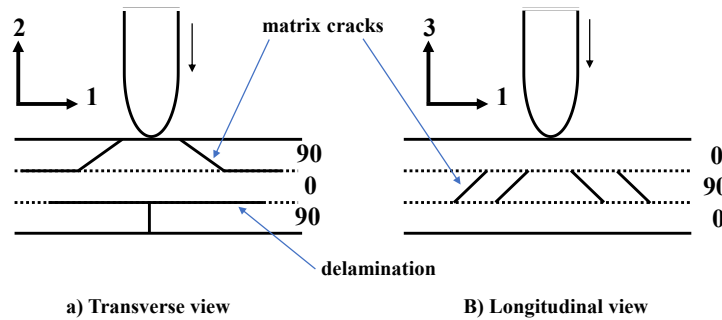
Figure 2.1. Progression of damages in a cross-ply laminated composite plate under impact loading [46].

In addition to fibers' energy absorption capacity, laminate architecture, stacking sequence, and matrix properties play an important role in the impact behavior of composites. Notably, due to their superior fracture toughness, fiber composites reinforced with thermoplastic matrices are more resistant to impact damage in contrast to thermoset ones [5,6,46,48,49]. Ghsemi-Nejhad and Parvizi-Majidi conducted a comprehensive study of woven carbon fiber reinforced PEEK (Polyether Ether Ketone), PPS (Polyphenylene Sulfide), and Epoxy across a range of impact energies [50]. Following a similar pattern in damage sequence, thermoset composite samples reach the defined barely visible impact damage limitation earlier than the thermoplastic ones. Therefore, as expected, the maximum load threshold of Carbon/Epoxy laminates was almost 20 % less than either Carbon/PPS or Carbon/PEEK [51]. Figure 2.2 represents previously described variations in post-impact indentation of composite samples with thermoplastic and thermoset resin systems.
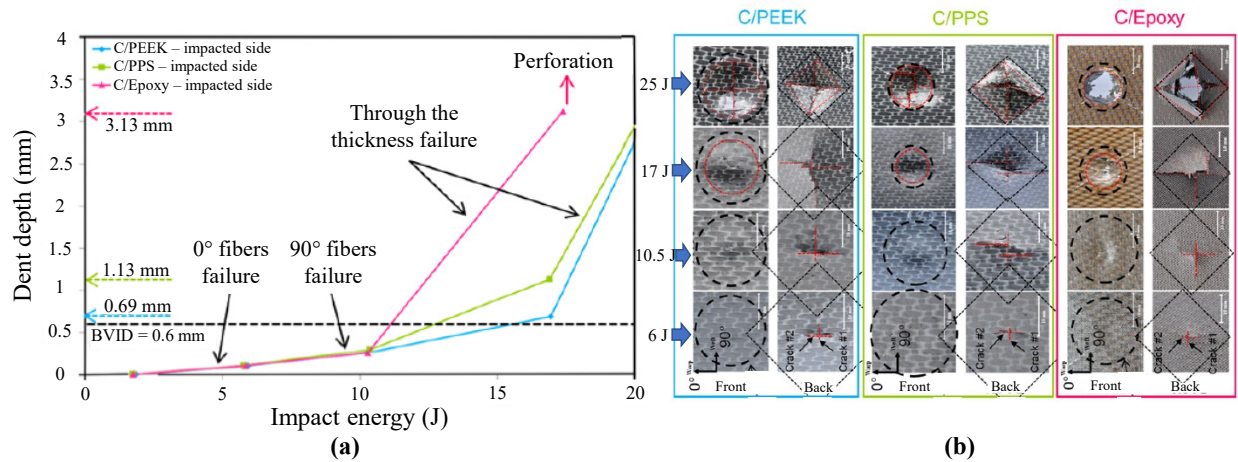
Figure 2.2. (a) Variation of after impact dent depth, and (b) Impact damage patterns of thermoplastic and thermoset carbon fiber composite laminates under different LVI energies [51].

Shah et al. performed an extensive study on LVI response of glass fiber composite with Elium and Epoxy matrices [52]. Confirming the prior scholars' findings, they observed that thermoplastic samples withstand higher impact energies before complete penetration occurs. As Figure 2.3 shows, their observations confirmed that thermoset composites primarily fail through matrix cracking, straining of the fibers, and yarn/matrix debonding, which are the consequence of matrix brittleness. In contrast to that, thermoplastic composites are more prone to matrix plasticization and whole yarn straining as the primary energy-absorbing phenomenon [52].
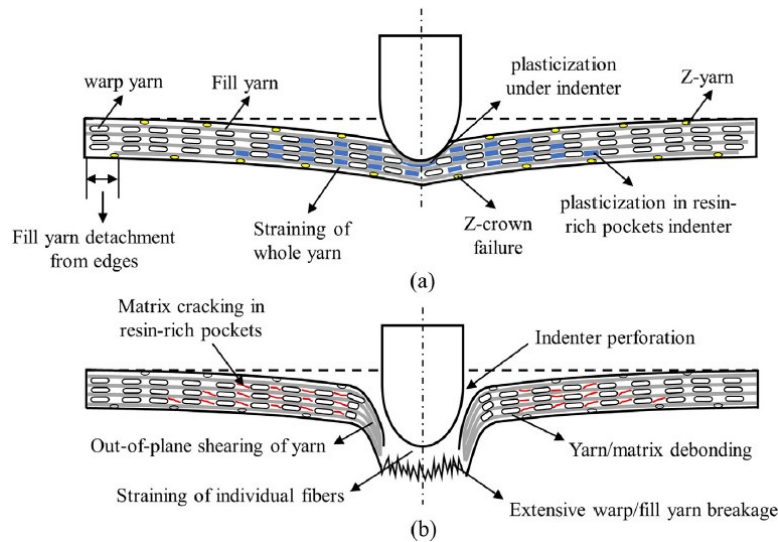
Figure 2.3. Schematic sketch of failure mechanisms of (a) thermoplastic, and (b) thermoset 3D fiber composite laminates under LVI loading conditions [52].

2.2.2   LVI response of composite sandwich panels

There are specific differences between the LVI response of sandwich panels and composite plates that require careful attention. Mines et al. conducted a detailed comparison of the Quasi-static and LVI perforation response composite sandwich panels with different core materials. Figure 2.4.(a) represented sequence of damage progression under static loading in the honeycomb core (Arolam core) sandwich panels with woven glass/Vinyl Ester composite skins, which changes if replaced with an alternative core structure. For honeycomb core sandwich panels, damage initiates in the upper skin and proceeds with tearing of the lower skin, while in Coremat sandwich panels, the failure order is completely reversed. Unlike composite laminates, which exhibit a single loading peak, the LVI force-displacement diagrams of sandwich panels feature two separate peaks, as depicted in Figure 2.4. (a) The scheme of the damage sequence, and (b) Force-displacement diagram of honeycomb core panels under LVI loading [8].[8].
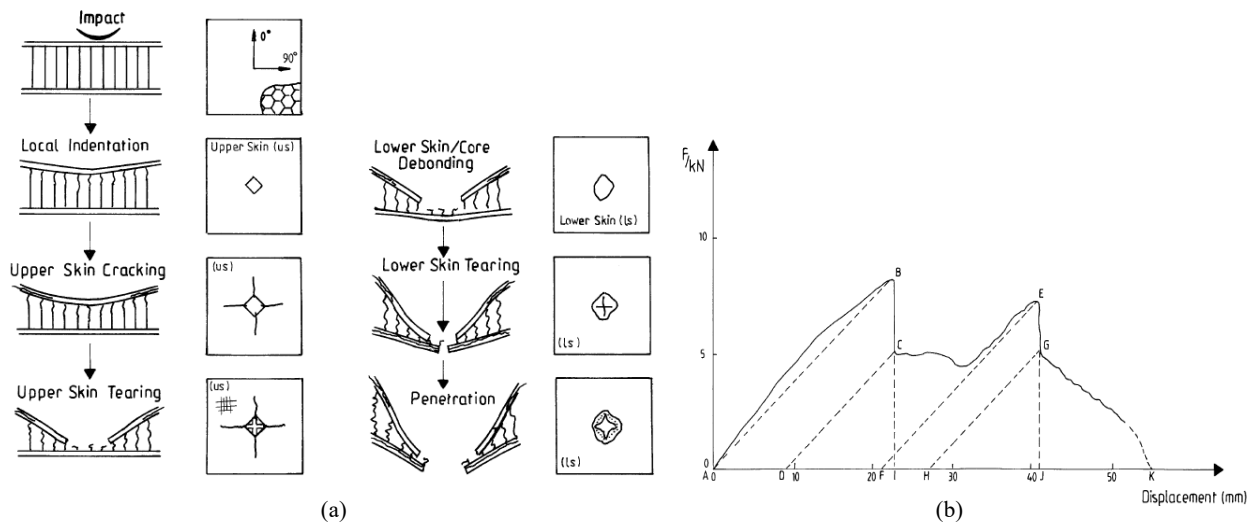
(a)   (b)

Figure 2.4. (a) The scheme of the damage sequence, and (b) Force-displacement diagram of honeycomb core panels under LVI loading [8].

Analogous to composite plates, the behavior of composite sandwich panels under LVI loading is strongly dependent on the boundary condition [53]. A common boundary condition for LVI testing of sandwich panels involves clamping the panels using rigid circular ring fixtures [54–

14

56]. It was revealed that the perforation threshold of sandwich panels directly enhances proportionally with foam core density. Furthermore, investigations on foam core sandwich panels with rigid-backed support, showed that most of the damages occur on the top skin and core, with the core properties playing a critical role in determining the impact response [57]. Dogan and Arikan performed an assessment of LVI response of PVC foam core sandwich panels with four different permutations of E-glass thermoplastic (PP) and thermoset (Epoxy) composite facesheets [56]. It was noted that PP-based composite plates displayed a superior energy absorption behavior under LVI loading. Moreover, sandwich panels with at least one thermoplastic composite skin outperformed those with entirely thermoset counterparts.

2.3 Hybridization effect on LVI behavior of composites

Investigations revealed that reinforcing composite laminates with metal sheets improves both fatigue resistance and impact damage tolerance [58–62]. Metal meshes are increasingly being used not only as reinforcing agents, but also as heating elements in resistance welding of thermoplastic composite panels, offering an alternative to traditional mechanical joints [63,64]. Although steel fiber composites are heavier than carbon or glass fiber, they possess superior toughness and a strain-to-failure capacity of up to four times greater. Because of that, these novel laminates are expected to behave more efficiently under impact loading [65,66]. LVI behavior of stainless-steel fiber/PP composites has shown that regardless of fiber architecture, these composites outperform conventional glass or carbon fiber laminates [67].

Woven ±45° glass/Epoxy composites hybridized with cross-ply steel fiber layers showed superior energy dissipation compared to the non-hybrid ones [68,69]. Besides, the introduction of stainless-steel layers altered the tensile failure mode from a sudden, catastrophic failure to a more localized form, maintaining the post-failure plates' integrity [70]. LVI examinations revealed metal fiber wire diameter directly affects the perforation energy threshold of composite laminates. Moreover, it was depicted that positioning the reinforcing stainless-steel fiber layers at the rear side, considerably enhanced the energy absorption of hybrid composite plates [11,71,72].

Determining factors influencing the mechanical performance of hybrid composites include mesh wire size, opening area, architecture, and stacking sequence [73]. Various techniques, such as sandblasting and chemical treatments, have been employed to enhance the bond between the

metallic mesh and resin [71,74]. Aggressive surface treatment has been proven to benefit the adhesion between the metal wire mesh surface and thermoplastic PEI and PPS polymer resins. Hasselbruch et al. found that hybrid laminates with 45° carbon fibers and 0° metal mesh exhibit superior stiffness, strength, and elongation to failure compared to non-hybrid 45° laminates [75]. Microscopic assessments showed that lowering the pressure during the fabrication process positively affects the connection between resin and metal mesh, which led to less cavity formation. Furthermore, hybrid composites demonstrated a more ductile failure mode, contrasting with the brittle fracture manner of carbon fiber laminates [76]. Recent research on hybrid carbon fiber composites showed that samples strengthened with coarse metal wires offer higher peak loads, increased residual strength, and enhanced strain capacity [9,10].

2.4 Shape Memory Alloy reinforced composites under impact loading

Nowadays, in addition to single-strike LVI tests, studies have increasingly focused on the response of composite laminates to repeated LVI testing. Analogous to single-strike LVI, thermoplastic materials have demonstrated superior performance under recurring LVI strikes [52,77,78]. Under repeated impacts, thermoplastic composites exhibit a more global deformation throughout the entire structure, unlike the localized damage seen in thermoset composites [78]. At energy levels lower than the perforation limits, there is a tendency to take advantage of self-healing approaches to recover and heal some of the damages occurring during their service life [79–87]. The combination of superior impact tolerance in hybrid composites, the specific energy absorption properties of SMA metals, and their recovery capabilities represents a promising synergy in advanced composite design.

Significant advancements have been made in improving the impact resilience of hybrid composites by incorporating SMA wires. SMA wires have been extensively researched for their ability to enhance the energy absorption capabilities of composites, while also providing self-healing properties [88–91]. SMA-assisted heat-treatment is recognized as an extrinsic method that effectively restores specific damages in polymer-based composites. C-scan imaging of SMA-reinforced composites has demonstrated the ability of these metallic wires to facilitate crack closure and healing after-impact damage [92]. Moreover, Konlan et al. [18] examined the potential of z-pinning technique using Flexinol SMA wires to reinforce glass composite laminates, which considerably enhanced impact resistance. Further assessment revealed this technique's capability

16

to facilitate delamination closure during thermal healing cycles, thereby improving the overall performance of the composite [12–18]. However, this area of research is still emerging, with gaps remaining in understanding the full extent of healing, the optimal percentage of reinforcement under LVI loading, and the degree of after-impact deformation recovery.

2.5 Concluding Remarks

In this chapter, in addition to the manufacturing strategies employed for thermoplastic composite plates and sandwich panels, the impact behavior of such structures was briefly reviewed. The expected responses of composite laminates, and progression of damage mechanisms under LVI loading were studied. It was shown that, despite the research progress in introducing hybridization as a viable method to enhance the impact resistance of composites, there is still research gaps to be filled, particularly further assessments on reinforcing thermoplastic-based composites reinforced with stainless-steel mesh layers.

Moreover, the integration of SMA reinforcements, taking advantage of these materials' recovery capabilities, remains in the early stages of research. More in-depth studies were needed to assess their full potential; therefore, a key research gap addressed in this investigation is the extent of deformation recovery achievable through repeated thermal healing cycles following multiple low-energy impacts, particularly in cases where the impact does not result in complete perforation of the composite structure.

Chapter 3:

Manufacturing and Performance of Sandwich Composite Panels with Recycled PET Foam Core Made by Continuous Roll Forming

3. Manufacturing and Performance of Sandwich Composite Panels with Recycled PET Foam Core Made by Continuous Roll Forming

3.1 Abstract

A parametrical study has been conducted for double-belt laminating method to optimize the manufacturing process of composite sandwich panels. Examinations have been done to assess the adhesion bonding characteristics between the skin and core. The outcomes of peel-off and flatwise tests revealed that an adequate connection was formed between the composite facesheets and PET core. Finally, the performance of panels was evaluated under three-point bending conditions. In this test series, while the sandwich panels' main failure mechanism is top facesheet buckling, traces of the proper adhesion formed between the foam core and facesheet were detected within the damaged surfaces.

3.2 Introduction

Thermoplastic-based composite materials are gaining high attention due to their high toughness and economical production specifics. Sandwich panels made of thermoplastic-based materials not only improve the flexural properties, but also are advantageous in terms of thermal or acoustic isolation. Fabrication of thermoplastic sandwich panels introduces specific challenges to the problem, particularly the imperative requirement for achieving adequate adhesion between the facesheet and core material; therefore, several researchers investigated diverse manufacturing approaches for thermoplastic composite sandwich panels [7].

Continuous roll forming, commonly referred as double-belt laminating method, employs a fusion bonding technique to produce composite sandwich panels. The capacity of uninterrupted operation along the production line makes this process financially viable. Resident time, heating and cooling temperatures, and applied roller pressure on the panels are the key variables which should be carefully determined in this technique [7]. Hence, the double-belt lamination parameters have been assessed to accomplish a proper impregnation of composite plates [34–36,38]. It was depicted that the fabrication rate plays a significant role in the microstructural characteristics of the composite laminates. Furthermore, comparable tensile and shear properties were achieved when

restricting the lamination speed. Ishida et al. examined the influence of roller modules on the production of carbon fiber polyamide composite laminates, analyzing the two different types of double-belt presses [37]. It was proven that, circular modules maintain constant pressure throughout the fabrication process, improving the laminate impregnation.

In conjunction with their recyclability, flexural properties of composite sandwich panels with PET core material have been previously studied [31,93]. Because of their relatively high viscosity, impregnation of thermoplastic-based composite laminates and proper bonding of facesheet to core is challenging. Due to the escalating environmental concerns, fully recycled PET closed-cell foam is selected as the core material in the current research. This chapter aims to identify the optimal continuous roll forming lamination process parameters, manufacturing PET foam core composite sandwich panels. Finally, beyond the evaluation of the adhesion between facesheet and core, their flexural behavior is examined under three-point bending conditions.

3.3 Material and manufacturing process

Thermoplastic sandwich composite panels used in this study were made of comingled glass/Polypropylene (PP) facesheets bonded to the Polyethylene Terephthalate (PET) foam core. Two different thicknesses of 10, and 50 mm environmentally friendly 100 % recycled closed-cell PET foam with respective densities of 80, and 100 kg∕m^3 (ArmaPET Struct GR80, GR100) were used. A single layer of 2/2 twill weave glass/PP with a nominal thickness of 1 mm and fiber weight fraction of 60 percent was chosen as facesheets. Figure 3.1 provides comprehensive details about the sequential steps within the manufacturing process, presenting both real and schematic depictions. Because of the relatively higher viscosity of thermoplastic-based resins, specific attention is required during the fabrication process. Consequently, a sequence of iterative experimentation and collaborative efforts were undertaken in partnership with Innovative Composite Product (ICP) Inc. to achieve the optimal production parameters. The glass/PP input sheets experience a temperature of around 160-165° C passing through the primary heating chambers followed by a set of rollers forming the facesheet laminates. Then, the facesheet plates are subjected to the temperature of 160-165° C, while the core is exposed to the set heater temperature of 200-205° C. Finally, facesheets are pressed on the PET core under the secondary set of rollers. The production speed of 0.64 m/min is considered to accomplish the best product quality, keeping the manufacturing rate economically efficient.
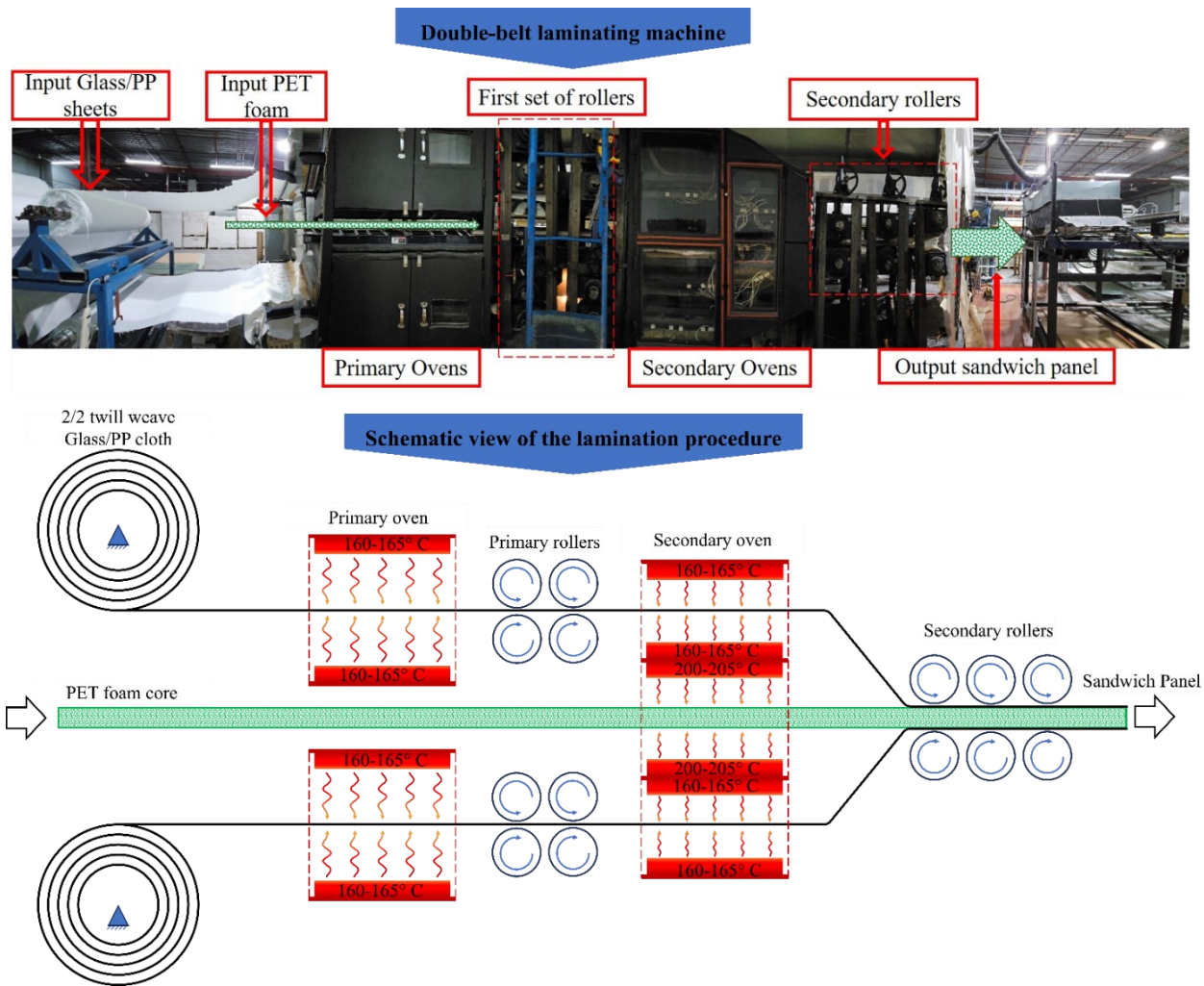
Figure 3.1. The air-cooled double-belt machine and its schematic view used to manufacture thermoplastic-based sandwich panels.

3.4 Sandwich panel assessment test procedures

A seamless connection without detectable gaps between the facesheet and PET foam core is achieved by the current double-belt procedure, as depicted in Figure 3.2. Flatwise tests were done at displacement rate of 0.5 mm/min for the sandwich panels in accordance with the ASTM C297 [94] standard. Sandwich panels with 10, and 50 mm core thickness were cut in cubic specimens with dimensions of 25.4 mm × 25.4 mm, and 50.8 mm × 50.8 mm, respectively. The surfaces of the specimens were sanded and glued to the metallic fixture blocks with the DP 460 epoxy adhesive. Roller drum peel-off fixture was also employed following the ASTM D3167 [95]

guidelines at the head displacement rate of 25.4 mm/min. Panels were cut into the dimensions of 260 mm × 25.4 mm × 10 mm, while facesheet is attached to one side of the trimmed samples with a pre-existing crack of 35 mm. The peel strength is determined by normalizing the data to the specimen width.
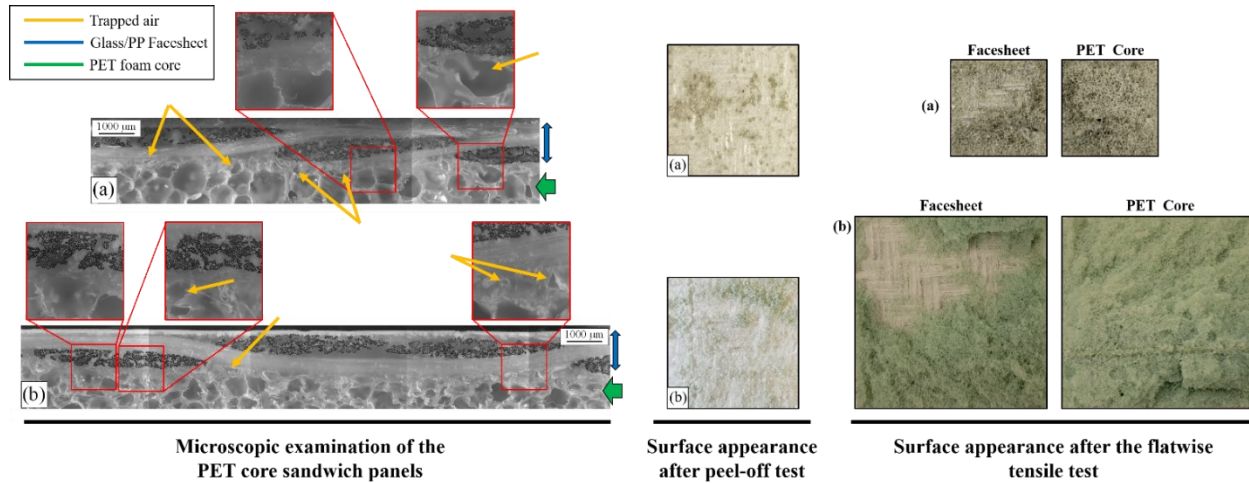
Figure 3.2. Microscopic picture, peel-off and flatwise test surface appearance of PET core sandwich panels with (a) 10 mm, and (b) 50 mm core thicknesses.

To assess the bending properties with the span lengths of 508 mm and 254 mm, 50 mm thick panels were cut into dimensions of 533.4 mm × 76.2 mm, and 279.4 mm × 76.2 mm, respectively. Moreover, 10 mm thick panels were prepared for three-point flexural tests with span lengths of 254 mm and 127 mm. Thus, specimens with the measurements of 300 mm × 30 mm, and 150 mm × 30 mm were cut out of them. According to the ASTM C939 [96], flexural experiments were done at the head displacement rate of 2 mm/min. All the tests were conducted using the universal test machine with the maximum load cell capacities of 5, or 100 kN.

3.5 Results and discussion

The peel and flatwise test results, show appropriate adhesion between the skin and PET core materials. Due to its lower density, the 10 mm PET foam core offers a reduced connecting surface area for the melted skin PP resin to adhere which results in relatively decreased bonding properties. Figure 3.2 illustrates the surface appearance of the separated skin and PET core. The occurrence of adhesive and substrate failures in both tests indicates the robust bonding that has been

established between the facesheet and the PET core. Such a dual failure mode emphasizes the effectiveness and integrity of the bonding achieved through the employed lamination process.

Table 3.1. Peel-off and flatwise tensile strength of glass/PP composite PET foam core sandwich panels.

Sandwich panel PET core thickness [mm]	Peel strength [N/m]	Flatwise tensile strength [MPa]
10	2958.56	0.70
50	3364.60	1.08

Samples with a 10 mm PET core thickness showed two distinct failure modes during a three-point bending test conducted over a 127 mm span length. Given the relatively small span length, one of the samples experienced a shear failure within the core material. When the core of the sandwich panel undergoes failure as a consequence of shear loading, there is an abrupt reduction in the applied load. This phenomenon signifies the structural response, reflecting the importance of the core mechanical properties in bearing and distributing the applied shear stresses. However, buckling occurred on the compression side of the sandwich panel. As depicted in Figure 3.3, the buckled facesheet gradually extends, causing compression of the foam core. Under the larger span length, a combination of facesheet compression failure and buckling is initiated, followed by compression of the core material. This complex failure mode occurs due to the inherited mechanical behavior of sandwich structures, where the skin composite components primarily withstand the applied stress. Generally, the load drop caused by composite facesheet damages can be attributed to structural instability, leading to a rapid loss of load-carrying capacity.
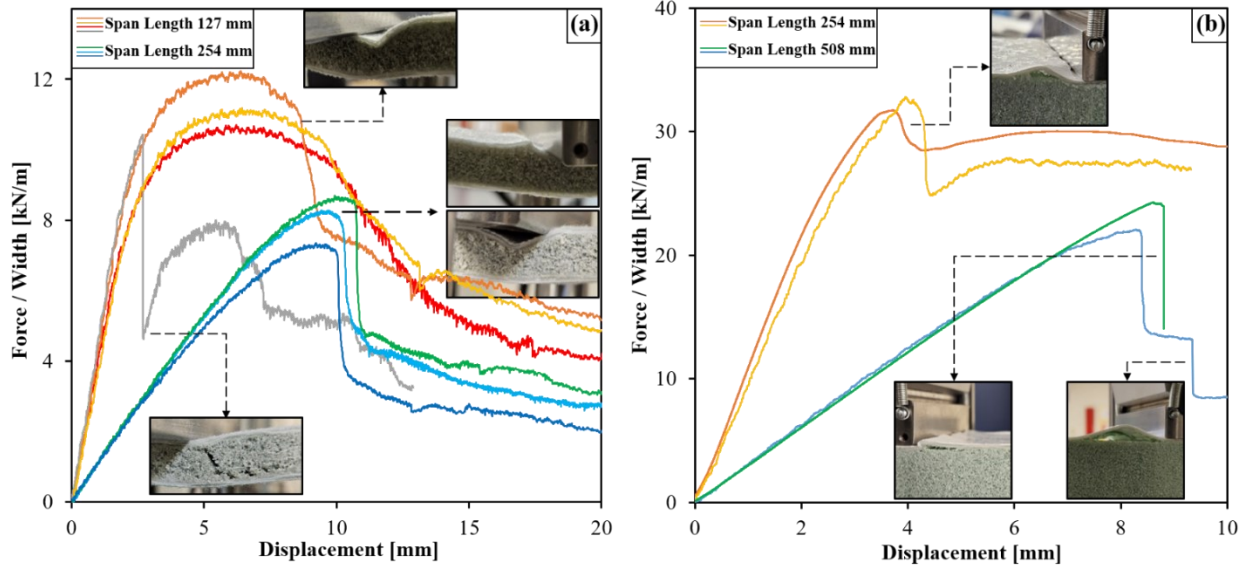
Figure 3.3. Flexural behavior of the sandwich panels with (a) 10 mm , and (b) 50 mm thick PET core under three-point bending load conditions.

Damage initiation is primarily localized at the compression side of sandwich panels with a 50 mm core thickness under three-point bending conditions. Under the shorter span length, the sandwich panels experience compression damage of the skin and PET core material at the loading point. This damage mode is followed by the skin delamination occurring because of the buckling, which results in a sudden load drop. Nevertheless, the extent of damage is higher for the 508 mm span tests, where the cracks are formed by the compression failure of the upper skin. After damage initiation, the composite sandwich panel's top facesheet buckles, which causes delamination of the skin and core material. Even though the skin of the 50 mm thick panels showed debonding after the compression damage initiation, parts of the PET foam material were still connected to the delaminated facesheet. Therefore, the specific failure patterns exhibited under the flexural tests show adequate adhesion between the skin and core in the sandwich panels manufactured by the optimized double-belt method.

3.6 Conclusion

An extensive evaluation of the double-belt lamination method was conducted to achieve reliable production parameters for manufacturing thermoplastic-based sandwich panels. Fully recycled PET foam material with different thicknesses and densities were examined as the

sandwich core component. The selected process parameters for sandwich panel production demonstrated its ability to yield high-quality panels characterized by proper bonding between the skin and the core. The combination of adhesive and PET core substrate failure observed during these tests confirmed the formation of a robust bonding through the lamination process.

In conclusion, the optimization efforts applied to the double-belt lamination procedure have demonstrated their effectiveness in the production of high-quality sandwich panels. Adequate bonding was accomplished between the thermoplastic-based glass/PP composite facesheet and PET foam core material employing the presented technique. Finally, the flexural performance of the manufactured sandwich panels revealed the viability and effectiveness of the employed continuous roll forming procedure.

Chapter 4:

Manufacturing Process Assessment and Comparative Study of Full-Thermoplastic Composite Plates and PET Foam Sandwich Panels

4. Manufacturing Process Assessment and Comparative Study of Full-Thermoplastic Composite Plates and PET Foam Sandwich Panels

This chapter delves deeper into two main processes which were specifically used to fabrication composite panels required for this study. Furthermore, empirical evaluations of the manufactured samples were performed to define the effectivity of each approach, while their bending behavior have been carefully examined. These parts have been published entitled as "Thermoplastic Composite Sandwich Panels with Recycled PET Foam Core: A Manufacturing Process Assessment".

4.1 Abstract

This study attempts to modify two distinct lamination processes of double-belt and compression molding to produce environmentally sustainable full thermoplastic sandwich panels. A precise assessment of fabrication parameters was conducted to ensure the quality of sandwich panels made of glass/Polypropylene composite skin and 100 percent recycled PET foam core sourced from consumer waste bottles. Evaluations of the skin-to-core adhesion properties revealed that the PET foam density in conjunction with the fabrication approach can affect the layers' bonding. The formation of satisfactory interlayer connection under controlled process parameters was confirmed by Peel-off and flatwise tensile test results. Moreover, complementary three-point bending analyses highlighted deviations in panel performance. Panels manufactured by the compression molding method exhibited superior load-bearing capacity compared to those made via a double-belt machine. These observations are attributed to the inherent nature of the lamination procedures, taking single or multiple thermal treatment phases to fabricate the sandwich panels. Finally, the findings suggest that despite potential quality degradation, the production continuity capability of the double-belt method makes it a viable option for meeting industry requirements.

4.2 Introduction

Sandwich panels have been developed to address the industry's demand for load-bearing lightweight structures capable of maintaining proper thermal and acoustic insulation properties. Thermoplastic-based composites are particularly noted for their superior mechanical properties,

manufacturing requirements, and environmental sustainability [97–99]. Numerous research has been performed to assess the performance of sandwich panels incorporating various combinations of skin and core materials [100–102]. Besides, alterations to the composite facesheets, core configuration, or adhesive layer reinforcements can significantly impact the sandwich panels' load-bearing capacity and failure mechanisms [103–107]. Improving the bond between the layers is crucial for an even distribution of load transfer to the composite skin. Thus, several investigations have been conducted focusing on improving the skin-to-core adhesion in thermoplastic composite sandwich panels [108–110].

Glass fiber composite panels with Polyethylene Terephthalate (PET) foam cores are being widely used in different domains, including wind turbine structures and prefabricated insulated building components [24,30]. Certain evaluations are required to simulate the behavior of PET core composite sandwich panels under different loading conditions, particularly fatigue or flexural ones [111–113]. A thorough examination performed by Xie et al. explored the effect of glass fiber composite facesheet and PET core thickness on failure mechanisms and sequence in sandwich panels [93].

Nowadays, there is a discernible shift towards the utilization of panels made of either recycled or recyclable thermoplastic materials, driven by significant environmental concerns. The potential for reuse makes PET material very appealing to scholars. Recent examinations on cores made of recycled bottle caps or eco-friendly PET foam sandwich panels are clear indications of the emerging industry trend around this topic [24–29]. Following this purpose, Kang et al. performed a comprehensive study on a complete lamination cycle and recycling of the glass fiber PET core composite sandwich panel [31].

In addition to the composite facesheet and core material response, the performance of the sandwich panels can be significantly governed by the quality of the skin-to-core bonding. Consequently, several investigations have been performed on different fabrication methods to establish a robust bonding between the core and composite facesheets. The fusion bonding method has demonstrated a notable ability to achieve satisfactory adhesion between the layers in thermoplastic sandwich panels [7,114–116]. Fabrication techniques such as the double-belt lamination method and compression molding capitalize on fusion bonding to process thermoplastic composite panels. Akermo and Astrom performed a comprehensive investigation on the critical

fabrication key factors of the compression molding process that affect the interfacial contact in all-thermoplastic sandwich panels [32,33].

The unique characteristic of uninterrupted manufacturing presents the double-belt method as a financially practical continuous operation technique, which is capable of laminating thermoplastic-based composites on large scales. In addition to the oven temperature and applied roller pressure, production speed plays an important role in the adequate impregnation of thermoplastic laminates since it directly affects the residence time and cooling rate [7,34–36,117,118]. Liu et al. studied the impact of production rate on the mechanical properties of carbon fiber phenylene sulfide, revealing its substantial influence on the microstructural characteristics of composite laminates [38]. Furthermore, it was proven by Ishida et al. that maintaining a consistent pressure level during fabrication enhances the laminate impregnation [119].

In the current study, aiming to enhance environmental sustainability, 100 percent recycled closed-cell PET foam material, made of post-consumer plastic water bottles, was considered as the core. Unlike traditional methods, no adhesive layer was applied between the composite facesheets and the core, offering a simpler, more sustainable fabrication process. Furthermore, because of the relatively high viscosity of Polypropylene thermoplastic resin in the composite facesheets, specific challenges such as proper skin impregnation and interfacial adhesion should be resolved during the fabrication process; therefore, precise assessments were performed to optimize the lamination parameters involved in both the double-belt and compression molding techniques. By eliminating any additional adherent layers, a comparative analysis was performed to determine the effects of the modified manufacturing process on sandwich panel properties. Moreover, a comprehensive empirical evaluation, including microscopic evaluations, tensile, and compression tests for composite plates, as well as peel-off and flatwise tests for sandwich panels, were carried out to validate the laminates' in-plane mechanical properties and interfacial bonding characteristics of the recycled PET foam core panels. Finally, since any qualitative properties variation related to the manufacturing process is reflected in the panels' performance, a series of three-point bending tests were conducted, which provides critical information on the sandwich panels' structural behavior.

4.3 Material and manufacturing process

Environmentally friendly 100% recycled closed-cell Polyethylene Terephthalate (PET) foam panels have been used as the core material. Three different core thicknesses of 10, and 20 mm with respective densities of 80 kg/m^3, and 50 mm thick PET core with the corresponding density of 100 kg/m^3 (ArmaPET Struct GR80, GR100) were selected for the current research. The PET foam material used in this study is entirely made from post-consumer recycled plastic bottles by a patented procedure. This innovative process uses a foaming agent to convert waste bottles into granules that are subsequently extruded into continuous foam boards, subsequently cut and welded into the required dimensions [27,120]. The facesheet composite laminates consist of one layer of 2/2 twill weave E-Glass/Polypropylene (Glass/PP), with commingled yarn and a nominal thickness of 1 mm. In this study, G represents the Glass/PP layer with the fiber weight fraction of 60 percent. Moreover, for the PET foam core material, the upper-case number shows the nominal core thickness in millimeters (for instance, PET^{50} represents PET foam core with thickness of 50 mm). In the present research, in addition to the [G/PET/G] sandwich panel, [G$_2$] composite laminates were produced to ensure the facesheets quality and performance. Further information on the mechanical properties of the raw materials is also presented in Table 4.1.

Table 4.1.

Mechanical properties and dimensional characteristics of the raw materials.

Material	Type	Nominal thickness [mm]	Fiber weight fraction [%]	Tensile strength [MPa]	Compression strength [MPa]	PP resin melting temperature [°C]	
E-Glass/PP	2/2 twill weave commingled cloth	1.00	60	203.8	60.2	160-165	
		Nominal thickness [mm]	Density [kg/m^3]	Tensile strength [MPa]	Compression strength [MPa]	Shear strength [MPa]	Melting temperature [°C]
100% recycled PET foam	ArmaPET struc GR80 & GR100 [120]	10	80	2.0	1.0	0.6	240-250
		20					
		50	100	2.5	1.5	0.75	

In order to fabricate the composite sandwich panels, two different techniques of compression molding and double-belt lamination were used. Since the current chapter is an attempt to evaluate the influence of modifications made on these two fabrication methods, the manufacturing

parameters require precise verification. Both methods involve subjecting stacked layers of dry weave glass/PP and PET foam core to the elevated temperature and pressure, effectively bonding them together using the fusion bonding approach. Because no additional adhesive layer is used, the manufacturing process of these thermoplastic composite sandwich panels entails a thorough assessment of the temperature, pressure, and processing time as these parameters significantly impact the appearance and integrity of the final products. A comprehensive parametric study was crucial to ensure the optimal quality, proper adhesion of the layers and absence of in-plane fiber waviness. Therefore, a sequence of iterative experiments was conducted for each manufacturing method to determine the optimal set of input parameters.

4.3.1 *Double-belt lamination process*

The automated roll-forming procedure is designed to produce large panels with a maximum width of 1.5 meters. The glass/PP rolled cloths and solid PET core panels were continuously fed into the machine. Rotation of the first forming roller set provides the force to automatically pull raw material into the machine. The production rate is regulated by adjusting the resistance force via the set screws located at the bearing supports of the input material rollers. Fiber alignment was maintained by the combined actions of the gripping force from the raw material rollers and the traction force applied by forming rollers. This configuration creates a tension force on the raw cloth which helps the fiber straightened before entering the primary ovens. Moreover, it will prevent the formation of defects such as wrinkles or overlaps in the facesheet composite layers [118,121].

Given the higher viscosity of thermoplastic PP resin, careful attention was devoted to the assigned temperature and pressure to achieve effective wetting and minimize void content. Collaborative efforts with Innovative Composite Product (ICP) Inc. were undertaken to execute optimal production parameters [122]. Passing through the primary ovens, the glass/PP sheets experienced a temperature range of 160-165°C. Subsequently, the first set of rollers applied pressure to form the facesheet composite laminates, being cooled in situ by the ambient airflow. Therefore, by placing two layers of raw cloth on top of each other, fabrication of [G_2] composite laminates could be finished in a single step.

Unlike composite laminates, manufacturing sandwich panels require additional steps, that demand meticulous attention to the process details to ensure adequate bonding between facesheet

and PET core. Following the consolidation of the composite facings in the initial step, facesheets are subjected to a second heating phase with a base temperature range of 160-165°C. Meanwhile, the PET foam core, overlaid with a 0.065 mm thick PP film was exposed to the oven temperature range of 200-205°C. It is worth noting that the PET core material did not reach its melting point passing through the secondary oven. Nevertheless, it is necessary to heat the PET core to mitigate any temperature loss before progressing to the next phase. Complementary evaluation of the PET foam core dimensional variations revealed that the thickness remained within a negligible variation range at the elevated temperature. Due to its insulating nature, the expansion of the foam core is known to be inherently small, especially at such a limited processing span and localized surface heating condition.

Preheating the core surfaces is essential for improving adhesion, particularly because of the abrupt cooling of melted thermoplastic PP resin touching the PET foam. The facesheets were pressed onto the PET core at the secondary set of rollers, with careful monitoring of roller gaps to prevent an unexpected core crush. The double-belt lamination method's cooling phase utilized air to cool the panels at room temperature conditions. Finally, an automatic circular saw was employed to trim and section the sandwich panels to the specified dimensions.

Figure 4.1 and Figure 4.2 provide detailed insights into the sequential steps of the manufacturing process, presenting pictures of the machine and schematic representations of the modified double-belt method.
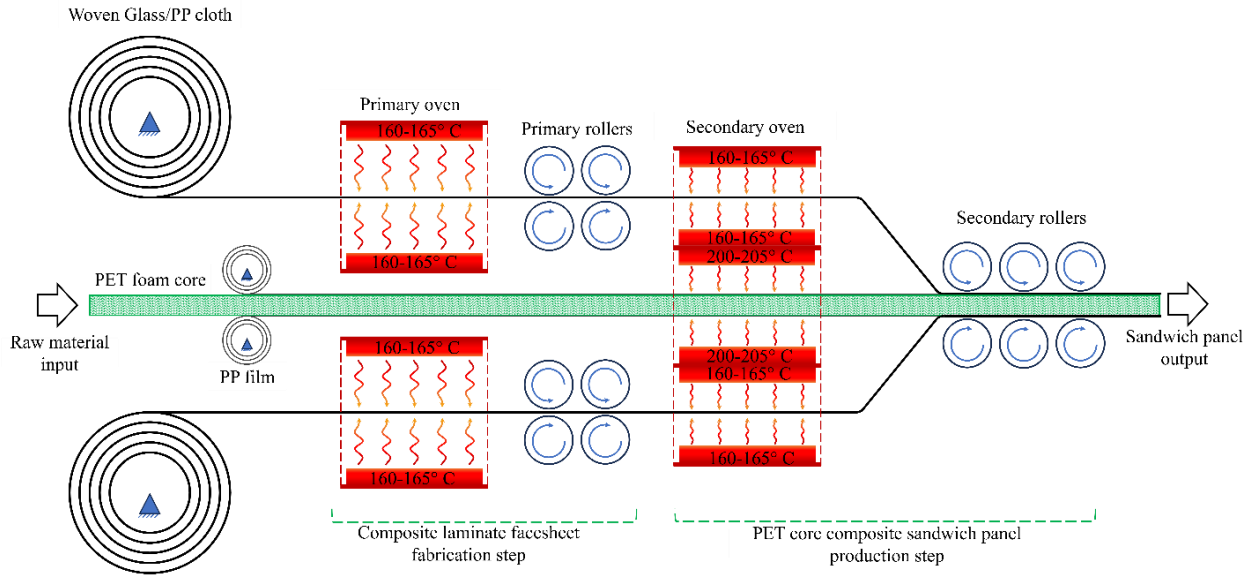
Figure 4.1. A schematic diagram of the double-belt lamination process used to manufacture glass/PP composite recycled PET core sandwich panels.
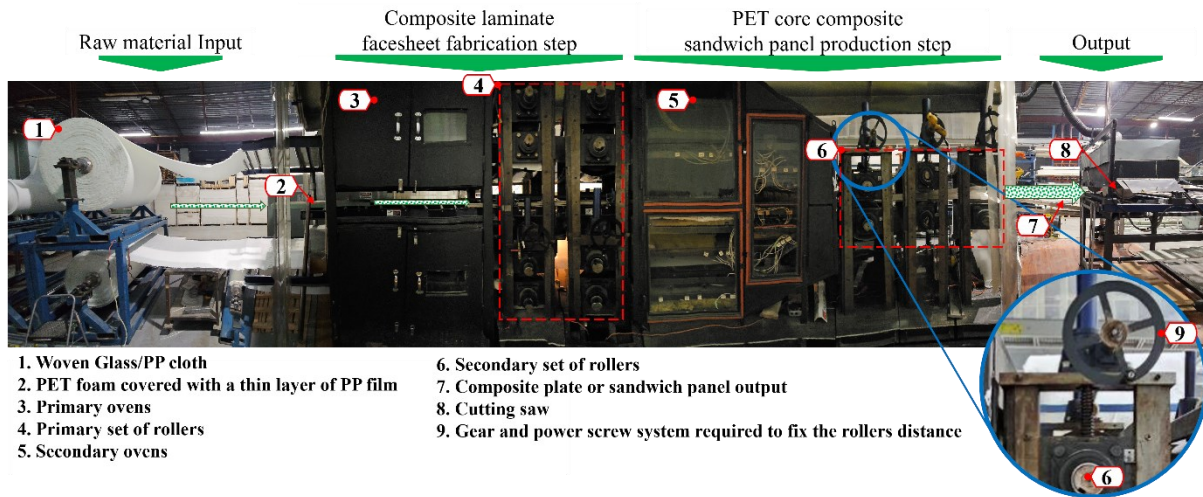
Figure 4.2. Double-belt laminating machine used to fabricate PP-based recycled PET foam core composite sandwich panels.

The optimization of the production process requires precise calibration of temperature and pressure to determine reasonably good product quality and economically efficient manufacturing rates. The pressure required to fabricate sandwich panels must be precisely controlled. Excessive

pressure can damage the core material, while insufficient pressure fails to provide adequate contact force required for the glass/PP skin to adhere to the core. This critical balance is essential, as it directly affects the feeding rate adjustments during production. Furthermore, lowering the production speed could cause a portion of melted PP resins to stick to the oven guiding rollers, negatively impacting panels' quality and production continuity. Nevertheless, an increase in production speed could compromise the impregnation of composite laminate skins or their adhesion to the PET foam. After running a series of trials and errors by ICP Inc, a production speed of 0.61 m/min was deemed suitable for glass/PP composite PET core sandwich panels with final thicknesses of 11.41 ± 0.04 mm, 20.46 ± 0.11 mm and 52.35 ± 0.12 mm. Finally, if the customer requests, a polyester veil cover layer is placed on the exterior surface of the composite sandwich panels to provide coverage. This ultimate visual aesthetics is not only for marketing purposes, but also improves the performance of the panels in humid environments.

4.3.2   Compression Molding

To laminate the composite PET foam core sandwich panels, layers of comingled raw glass/PP cloth and core were stacked in their order. Employing the hot press machine, the stacked layers and PET core were heated at a rate of 12°C/min reaching a controlled temperature range of 160-165°C when exposed to the pressure of 0.5 MPa. The consolidation period lasted for 1 minute, after which the hot press initiated a cooling cycle using water flow to gradually return to ambient temperature at the cooling rate of 15°C/min. However, for composite laminate production, 3 minutes of hold time under pressure of 1.5 MPa is required [123,124]. It is noteworthy that, contingent on the PET core thickness, a steel mold, closely matching the expected final sandwich panel thickness was used. The mold helps to control the resin flow, while maintaining the PET foam core configuration from being crushed under the compression loading of the hot press. Pressure and temperature should be kept at the specified range to prevent any fiber waviness induced by the flow of the melted PP resin during the manufacturing process. To facilitate a non-stick interface between the glass/PP composite facesheet and the heating elements, 0.08 mm thick Teflon sheets were employed. Figure 4.3 provides the schematic view of the hot press machine depicting more inclusive detail of the composite sandwich panel fabrication procedure. Employing the compression molding lamination process, a series of PP-based PET core sandwich panels with thicknesses of 12.30 ± 0.07 mm, 21.14 ± 0.06 mm and 52.36 ± 0.08 mm were fabricated.

1. Heating blocks
2. Non-stick Teflon sheet
3. Woven Glass/PP cloth
4. PET foam core
5. Mold
6. Hydraulic press
7. Pressure gauge
8. Thermocouple
9. Water cooling system
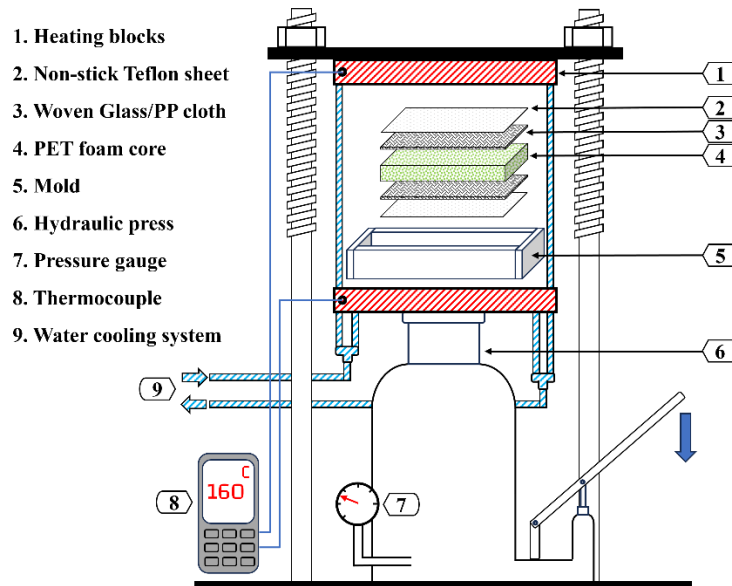
Figure 4.3. A schematic display of the sandwich panels lamination procedure with the hot press machine.

4.3.3   Empirical optimization procedure

Differential Scanning Calorimetry (DSC) tests were initially performed on the raw glass/PP cloth and the recycled PET foam core materials to precisely determine both thermoplastic PP and PET materials' behavior, particularly their exact melting temperature [125]. The programmed heating ramp of 10° C/min and Aluminium hermetic sample pans were used to run the tests in a TA Instrument Q200 DSC machine coupled with a Refrigerated Cooling System (RCS 90). Two repetitive heating and cooling cycles with the temperature range of -50° C to 250° C and -50° C to 300° C were considered for the glass/PP cloth and recycled PET foam, respectively. Finally, as recommended in DSC examinations, to ensure the reliability of the results, the initial heating and cooling cycle was excluded from the final data presented in Figure 4.4.
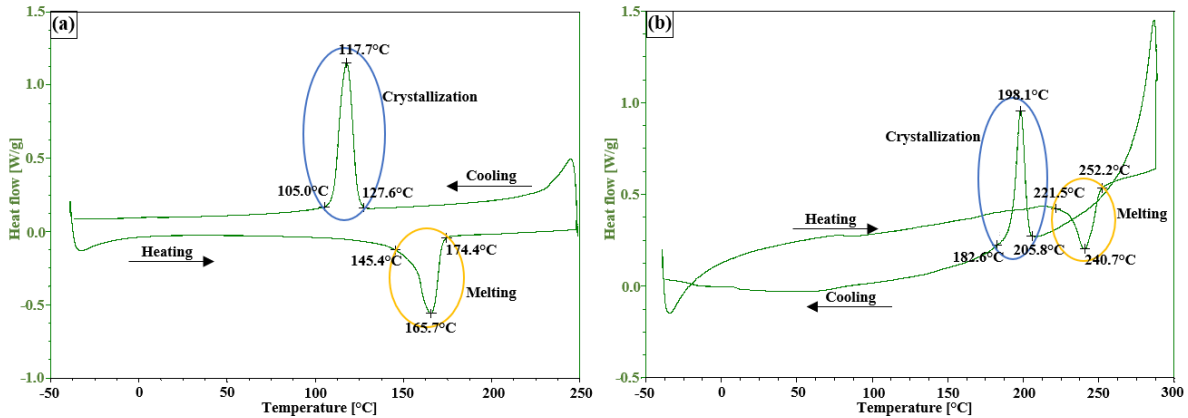
Figure 4.4. DSC heat cycle curves showing the melting and crystallization of (a). the PP resin within the glass/PP cloth, and (b) the recycled PET foam core material.

These DSC test data were used to determine the manufacturing temperature range. Several empirical trials and errors were conducted to optimize each manufacturing procedure separately. Based on the nature of the lamination techniques, certain parameters were required to be investigated; therefore, for each method, specific set values were selected, and a combination of these manufacturing parameters was evaluated. Table 4.2 presents the fabrication parameters and minimum number of manufacturing interactions performed in the current study to experimentally optimize the lamination processes. With respect to these influencing factors, a minimum number of tests were required to determine the optimized manufacturing parameters.

Table 4.2.

Manufacturing parameters and assessed range of each factor used to optimize the compression molding and double-belt method.

		Compression molding method			Double-belt lamination technique		
		Manufacturing parameters	Evaluated range of each fabrication factor	Minimum number of interactions	Manufacturing parameters	Evaluated range of each fabrication factor	Minimum number of interactions
[G₂] composite laminate		Mold thickness	2.46 mm 2.53 mm	24	1st rollers distance	Ranging between 2.3 mm to 2.5 mm	2
		Temperature	160-165° C 165-170° C		1st oven temperature	160-165° C	
		Process time	1 min 2 min 3 min		Feed rate	0.55 m/min 0.61 m/min	
		Pressure	1 MPa 1.5 MPa				
[G/PET/G] sandwich panel		Mold thickness	53.39 mm 53.96 mm	8	2nd rollers distance	Ranging between 53.0 mm to 54.0 mm	1
		Temperature	160-165° C		2nd oven temperature	160-165° C	
		Process time	1 min 2 min		Feed rate	0.61 m/min	
		Pressure	0.5 MPa 1 MPa				

The optimization process was initially focused on the parameters that governed the fabrication of composite facesheet laminates, with overlapping parameters subsequently being set for the panels' lamination step. Certain parameters like hot press temperature, oven temperature and feed rate in the double-belt method were set for sandwich panels' production based on the assessments done on laminates production. In addition to the 160-165° C temperature range, 165-170° C was examined during which the resin flow could not be well controlled, leading to the elimination of further iterations at this specific setting.

Since the recycled PET foam core materials were subjected to compression during the lamination process, it was essential to consider their compression strength prior to fabrication trials. Compression strengths of 1.0 MPa and 1.5 MPa were expected from the GR 80 and GR 100 recycled PET foam cores, respectively [120]. To verify these data, compression tests were

conducted in accordance with ASTM C 365/C 365M [126], the results for which were consistent with the catalog data. Figure 4.5 presented the compression test results performed at the head displacement rate of 2 mm/min using an MTS universal test machine equipped with a 25 kN load cell. It is known that elevated temperatures during the manufacturing stages can reduce the compression strength of these thermoplastic PET foam materials. Thus, in the current study, the lamination pressure was adjusted to remain within the safe range.
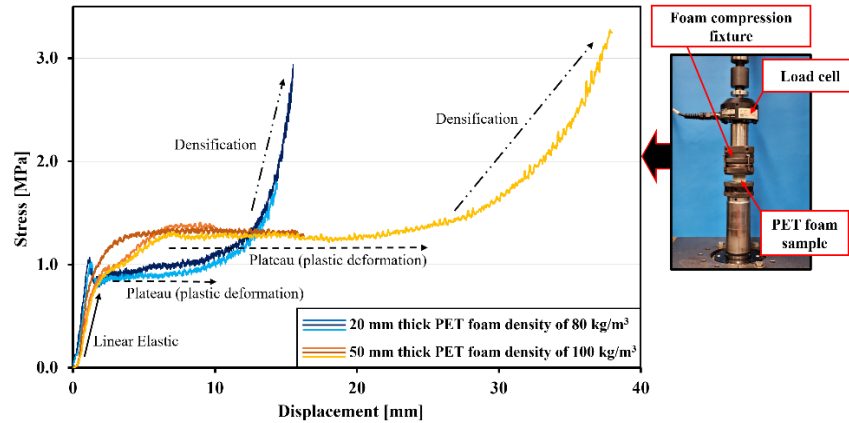
Figure 4.5. Compression test results of the recycled PET foam core samples with densities of 80 kg/m^3 (GR 80) and 100 kg/m^3 (GR 100).

To adjust the spacing between the rollers during the lamination process, a gear and power screw system was employed. This setup allows precise control over the rollers' distance, ensuring an accurate adjustment for different panel configurations. During the initial manufacturing phase, the machine was used to run a test production during which the optimal rollers' distance regarding the core thickness was determined to ensure the desired sandwich panels' quality and consistency. These trial and error iterations were initially conducted for the recycled PET foam core thickness of 50 mm. Thus, except for mold thickness and second roller modifications, which were tuned by a couple of new attempts, other parameters were maintained constant for thinner sandwich panels. This consistent approach helped ensure the reliability of both lamination processes, for which the final optimal manufacturing characteristics were presented in previous sections.

4.4 Experimental procedure

4.4.1 Laminate tensile test requirements

Under several loading conditions, such as tensile or bending, the sandwich panel's facesheet is known to serve as the load-bearing element. The performance of sandwich panels can be significantly altered by their facesheet mechanical properties. Hence, the properties of $[G_2]$ composite laminates fabricated with both methods require specific evaluation, while distinguishing their behavior under either tensile or compression loading. Using a diamond saw machine, specimens with dimensions of 110 mm × 25 mm were cut along the fiber directions. Lastly, quasi-static tensile tests were conducted at a rate of 2 mm/min in accordance with the ASTM D3039 standard [127].

4.4.2 Laminate compression test

As Figure 4.6. (a) represents, the upper skin of a sandwich panel experiences an in-plane compression load during a bending test. Thus, in accordance with ASTM D3410 [128] an anti-buckling fixture was employed to measure the compression strength of the composite laminates that serve as the sandwich panels facesheet. $[G_2]$ composite laminates were trimmed into 120 mm × 25 mm dimensions and examined at a displacement control compression loading with a head speed of 1.5 mm/min.

4.4.3 Flatwise tensile test

Flatwise tensile tests were performed to ensure the adhesion quality between the glass/PP composite skin and PET foam core material. These examinations were done on sandwich panels following the ASTM C297 guideline [94] at the standard displacement rate of 0.5 mm/min. Panels with the nominal core thickness of 10 mm and 20 mm were precisely cut into the dimensions of 1 inch × 1 inch, while the 50 mm thick PET core sandwich panels were cut into 2 inches × 2 inches. To guarantee the adhesion of the samples' skin to the fixture steel blocks, a coarse sanding process is done as part of the surfaces' preparation. DP 460 epoxy adhesive was used to affix the samples between the blocks shown in Figure 4.6. (d).

4.4.4   Peel-off test procedure

The adhesion formed between the composite facesheet and PET foam core can be evaluated by an alternative test method known as peel-off. In this paper, the roller drum peel-off fixture depicted in Figure 4.6. (c), was employed to evaluate the skin-to-core material has been assessed. A series of peel-off tests were conducted following the ASTM D3167 standard outline [95]. Because of the constraints of the drum peel-off fixture, where the rollers' maximum distance gap reaches 10 mm, samples with core thicknesses of 20 mm and 50 mm are required to be cut on one side to be compatible with the fixture limitations. Finally, the PET foam core sandwich panels were cut into 260 mm × 25.4 mm. A 35 mm long pre-existing crack was introduced to designate the non-adhered portion, effectively providing sufficient grip on the flexible skin during the test. Peel-off tests were operated at a head displacement rate of 25.4 mm/min. The peel strength determination involved normalizing the data to the specimen width, while recording measurements beyond the initial 25 mm of peel length. As the ASTM D3167 suggested, the average peel strength should be calculated by equation 4.1, and reported as a final determining factor for comparison studies [95].

Eq. 4.1. $$S = \frac{F}{w}$$

where S is the average peel-off strength, F and w represent the measured peel force and width of the sample, respectively.

4.4.5   Three-point bending

Flexural tests were performed on the sandwich panels to assess their performance under three-point bending conditions. PET foam core sandwich panels with lengths of 220 mm and 120mm were subjected to bending with support span lengths of 200 mm and 100 mm, respectively. In accordance with the ASTM C393 [96] standard, flexural experiments were done at a loading nose displacement rate of 2 mm/min.

All the tests were conducted using an MTS universal testing machine equipped with a maximum load cell capacity of either 5 kN or 100 kN depending on the expected load and fixture installation guides, distinctively depicted in Figure 4.6. To ensure the accuracy of the results, each test was meticulously repeated several times at a data sampling frequency of 2000 Hz.
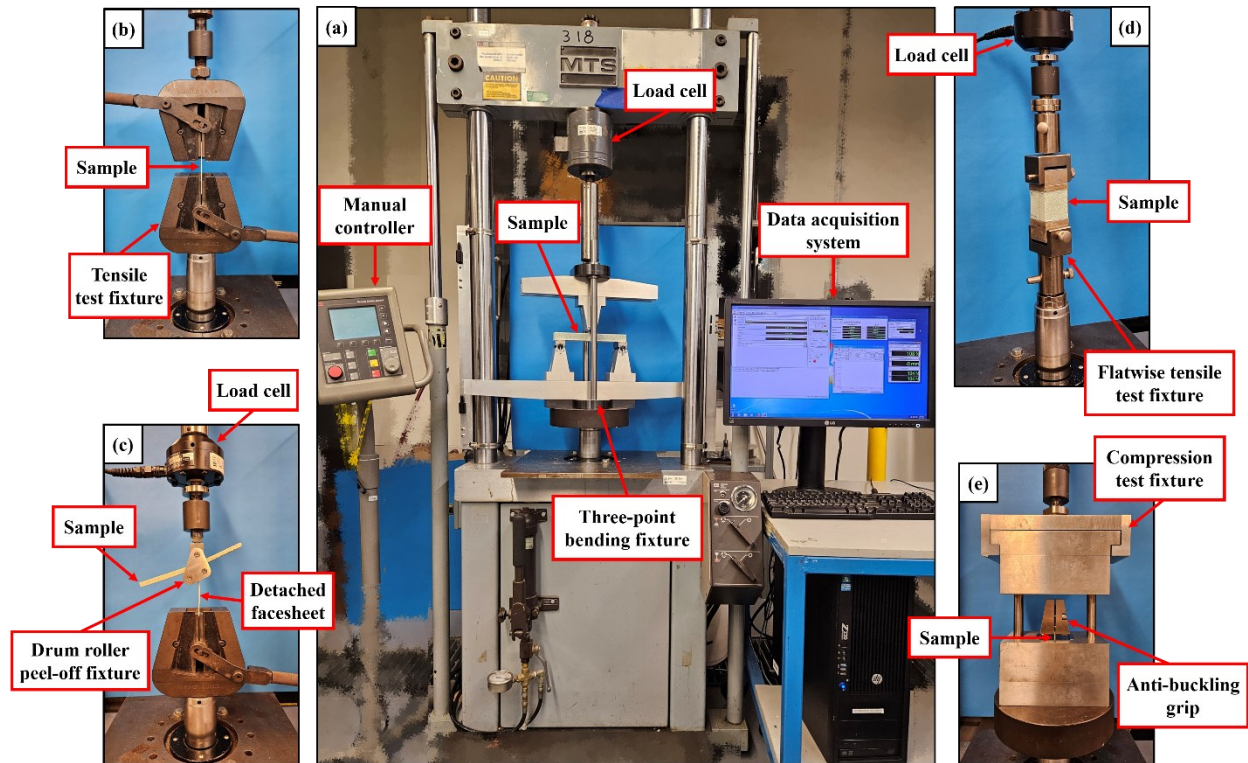
Figure 4.6. MTS universal testing machine equipped with the (a). three-point bending, (b). tensile test, (c). drum roller peel-off, (d). flatwise tensile test, and (e). compression test fixtures.

4.5 Results and discussion

Examinations were performed to evaluate the quality and performance of the thermoplastic sandwich panels. In both methods, the temperature was insufficient to melt the PET foam. Hence, the bonding mechanism between the PP-based composite facesheet and recycled PET foam core is primarily mechanical rather than molecular. For a proper molecular bonding to form between the two thermoplastics, both materials must first be melted, which was not the case in these processes. Thus, further investigation can potentially be done to measure and improve the level of entanglement between these materials. By optimizing the fabrication input parameters, both lamination techniques were capable of manufacturing PP-based composite sandwich panels with proper surface appearance and skin-to-core bonding. Figure 4.7 depicts the microscopic view of the [G_2] composite laminate and adhesion formed between the glass/PP facesheet and PET foam core.

Figure 4.7. Microscopic section views of the (a). [G_2] composite laminate, and skin-to-core bonding of panels with PET foam thicknesses of (b). 10 mm, (c). 20 mm, and (d). 50 mm.

The quality of the fabricated glass/PP composite laminate itself, which constitutes the skin of sandwich panels, was satisfactory for both fabrication methods. Even though voids can be depicted in the samples fabricated with either of the two approaches, they can develop more easily during the double-belt process. This increased incidence of voids can be attributed to the nature of the double-belt technique, where the laminate experiences a sudden release of pressure as it passes through the rollers. In contrast, the compression molding lamination method maintains a constant pressure at a controlled cooling rate, which helps in preventing the formation of unexpected voids within the composite laminates and sandwich panel facesheets during the cooling phase.

42

As presented in Table 4.3, the tensile and compression strength of [G₂] composite laminates made with both methods were proximately matched. Nevertheless, applying tension force on the raw woven cloth during the feeding stage reduces the chance of fiber waviness which results in a marginal improvement of the laminate's mechanical properties for composite plates made with the double-belt procedure.

The precision in manufacturing parameters is critical since a minor deviation from the optimized settings can drastically reduce the quality of the final product. Using the double-belt process to laminate the sandwich panels doubles down the effect of key variables such as temperature, pressure, and production speed. For instance, an increased feeding rate results in an improper impregnation of the composite facesheet or adhering surface. Consequently, reducing the gap between rollers causes undesirable permanent deformation or crushing of the PET core. A slight modification in temperature not only can drastically affect the quality, but also has a major influence on the continuity of the production. To elaborate further on this point, it has been observed that increasing the temperature of the secondary oven will cause considerably large macroscopic voids. Furthermore, melted PP resin will stick to the guiding rollers of the double-belt machine which leads to accidental fire and a full oppression halt. Hence, the optimized manufacturing parameters were selected after several trial series conducted by ICP Inc. to fabricate glass/pp composite laminate and PET foam core sandwich panels.

A parametrical study was precisely performed for the compression molding procedure to optimize the temperature, heating idle time and applied pressure, effectively eliminating potential defects. During the fabrication process, common imperfections such as resin washout, fiber waviness and permanent core deformation were anticipated. These issues were prevented by employing a precise mold, controlling temperature, pressure and idle time. Continuous and effective bonding between the composite skin and PET foam was established using both manufacturing techniques.

The use of closed-cell PET foam as the sandwich structure core material can result in the entrapment of air bubbles within the adhering surface. Additionally, defects commonly associated with the manufacturing process, such as facesheet voids and foam deformation, were observed. As discussed earlier, maintaining constant pressure through the rollers during the cooling stage is challenging, which leads to higher void formation in the composite facesheets of panels made with

the double-belt process. Reheating the consolidated composite facesheets during the bonding phase causes the trapped air in composite to expand which forms multiple voids within the structure. Furthermore, regional permanent deformation was depicted in cell walls where high roller pressure was applied over a limited surface area. Nevertheless, during the compression molding process, pressure was distributed over a relatively larger area, and the final thickness of the panels was also restricted by the mold tolerances. These adjustments in the production states resulted in moderately reduced void content in the composite facesheets and the elimination of permanent foam core deformations.

The magnified regions adjacent to the PET foam surface show a satisfactory adhesion of the glass/PP composite skin to the core. Yet, complementary examinations are necessary to assess the robustness of this connection. It is well-known that proper bonding between the layers is crucial for effective load transfer, whereas inadequate bonding causes premature damage or delamination [110]. Hence, peel-off and flatwise tensile tests were conducted in the current study to assess the integrity of these bonds, for which the measured strengths are presented in Table **4.3**. A slight improvement is achieved by manufacturing the samples with the hot press machine. The reason for that lies in the ability to sustain the production parameters that favorably influence the adhesion of the PP-based facesheet to PET foam. As a comparative baseline, the bonding between two layers of glass/PP composite laminates made by the double-belt method was assessed, for which the average peel strength of 3423.9 N/m was measured. Furthermore, the tensile strength of each PET foam core, presented in Table **4.1**, is the maximum expected value that happens in a flatwise test if the connection is good enough leading to full core failure at the midsection.

Moreover, compared to the [G/PET^{50}/G] sandwich panel, thinner panels offer a reduced available bonding surface. This reduction in the available bonding interface consequently leads to diminished adhesion properties between the PET core and facesheet in samples with lower core density. This phenomenon is attributed to the inherently limited contact points and interactions between the core and the melted adhered facesheet resin, which results in a noticeable decline in bonding strength.

Table 4.3.
Tensile, compression, peel-off, and flatwise tensile strength of Glass/PP composite laminates and composite PET foam core sandwich panels.

Fabrication technique	Stacking sequence	Sandwich panel PET core thickness [mm]	Tensile strength [MPa]	Compression strength [MPa]	Peel strength [N/m]	Flatwise tensile strength [MPa]
Double-belt lamination	[G$_2$]	-	231.9	61.6	3423.9	-
	[G/PET/G]	10	-	-	2810.6	0.76
		20	-	-	2869.9	0.81
		50	-	-	3364.6	1.08 [118]
Hot press lamination	[G$_2$]	-	203.8 [123]	60.2	-	-
	[G/PET/G]	10	-	-	2975.5	0.85
		20	-	-	3021.4	0.88
		50	-	-	3368.4	1.05

In addition to the ultimate bonding strength, the failure modes and post-failure appearance of the facing and core surfaces need thorough assessments. Figure 4.8 depicts the surface of the detached composite skin from the PET foam core after the peel-off tests. The presence of clustered greenish PET foam material adhered to the peeled composite skin indicates a substrate failure. Although the white-colored glass/PP facesheet suggests an adhesion failure, numerous core cells remain linked to the skin demonstrate a mixed failure mode. Sandwich panels made with both lamination methods exhibited a combination of the discussed failure modes. Nevertheless, an analysis of the peel surface from panels manufactured by the hot press machine revealed a predominantly substrate failure over a larger area. This transition in failure mode accounts for the variations in measured peel strength between samples produced using the two lamination methods.
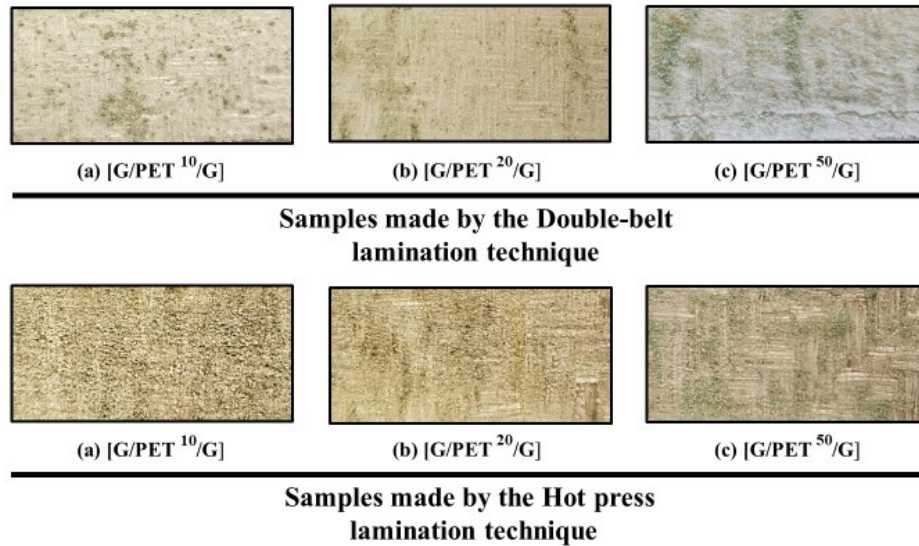
Figure 4.8. Composite facesheet surface appearance of (a) 10 mm, (b) 20 mm, and (c) 50 mm thick recycled PET foam core sandwich panels after the peel-off tests.

As mentioned, variations of the PET foam material density can affect the establishment of adhesion between the composite skin and core. A higher foam density provides relatively more accessible bonding points, thereby enhancing adhesion strength. The surface failure patterns of samples after running flatwise tests, presented in Figure 4.9, depict a combination of adhesion and substrate failure. The appearance of such a failure mode proves the robustness of the bond established between the skin and PET foam. Evaluations revealed that by employing either of the two manufacturing techniques, an effectively integrated attachment was developed between the layers. Higher foam densities offer a more exposed surface, which facilitates the bonding of the PP resin. This is evidenced by the increased flatwise tensile strength in [G/PET^{50}/G] sandwich panels with 100 kg/m^3 PET foam density compared to those with 80 kg/m^3 foam density. Finally, since results of both peel-off and flatwise tensile tests for samples made by either technique were closely aligned, both were considered capable of fabricating PET foam core composite panels with proper quality.
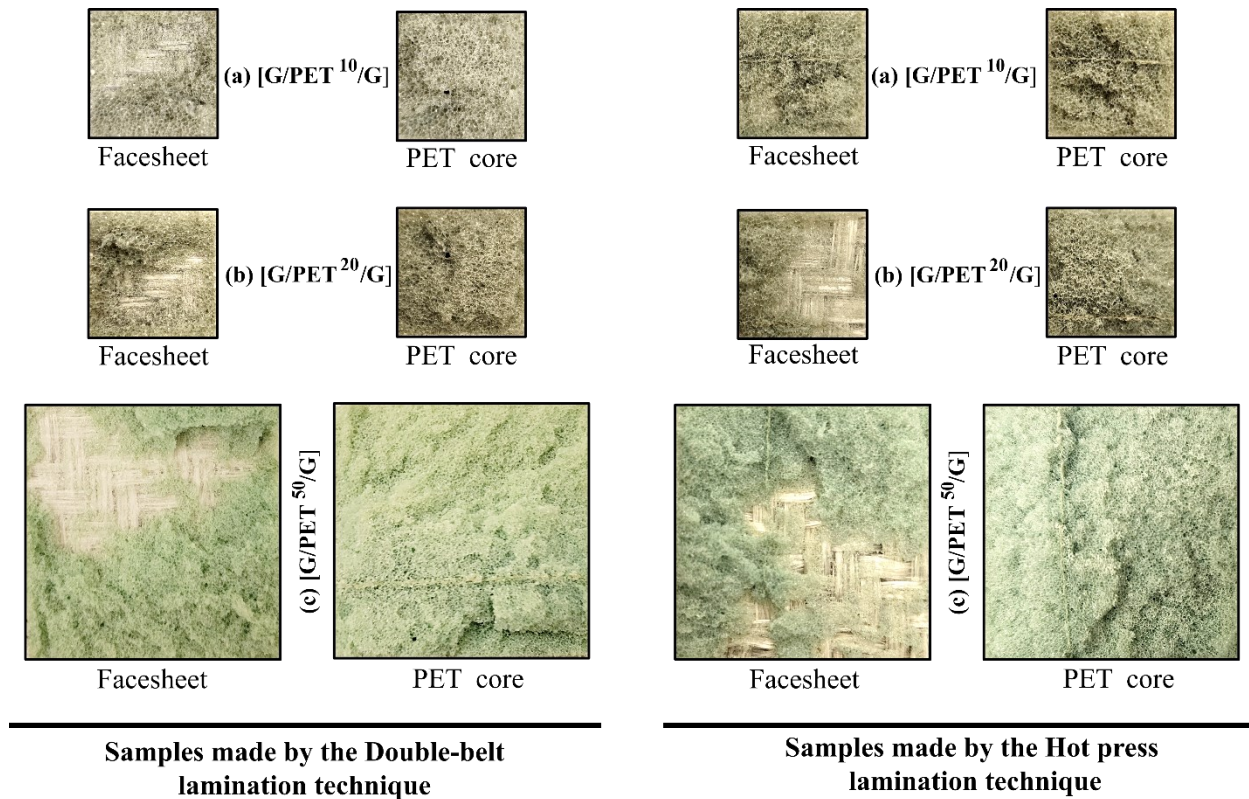
Figure 4.9. Composite facesheet and PET foam failure pattern under flatwise tensile tests for sandwich panels with (a) 10 mm, (b) 20 mm, and (c) 50 mm thick core.

One of the primary motivations for introducing sandwich panels to the industry is to improve the bending performance of structures by distancing the load-bearing composite laminates from the neutral axis; therefore, alongside the skin-to-core bonding, the mechanical properties of the laminated composite facesheets require specific examinations. Former analyses were conducted on several governing properties that can significantly affect the overall performance of sandwich panels. To examine them, the manufactured recycled PET foam core composite sandwich panels were subjected to three-point bending conditions. While the composite foam core sandwich panels' behavior has been studied under bending conditions [103,107,113], this research mainly investigates the manufacturing method's influence on these panels.

The flexural response of [G/PET^{20}/G] sandwich panels revealed a substantial difference between the samples made with each approach. Figure 4.10 presents a thorough inspection of the force-displacement behavior of [G/PET^{20}/G] sandwich panels and their failure modes under the 200 mm span length. A distinguished difference in maximum load-bearing capacity level was

observed, consequently leading to different failure modes. The panels made with the double-belt method experienced facesheet buckling failure, respective to which the skin separates from the PET core. Nevertheless, the samples manufactured with the hot press could withstand 76.7% higher loads, experiencing either compression failure of the top facesheet or core shear failure.
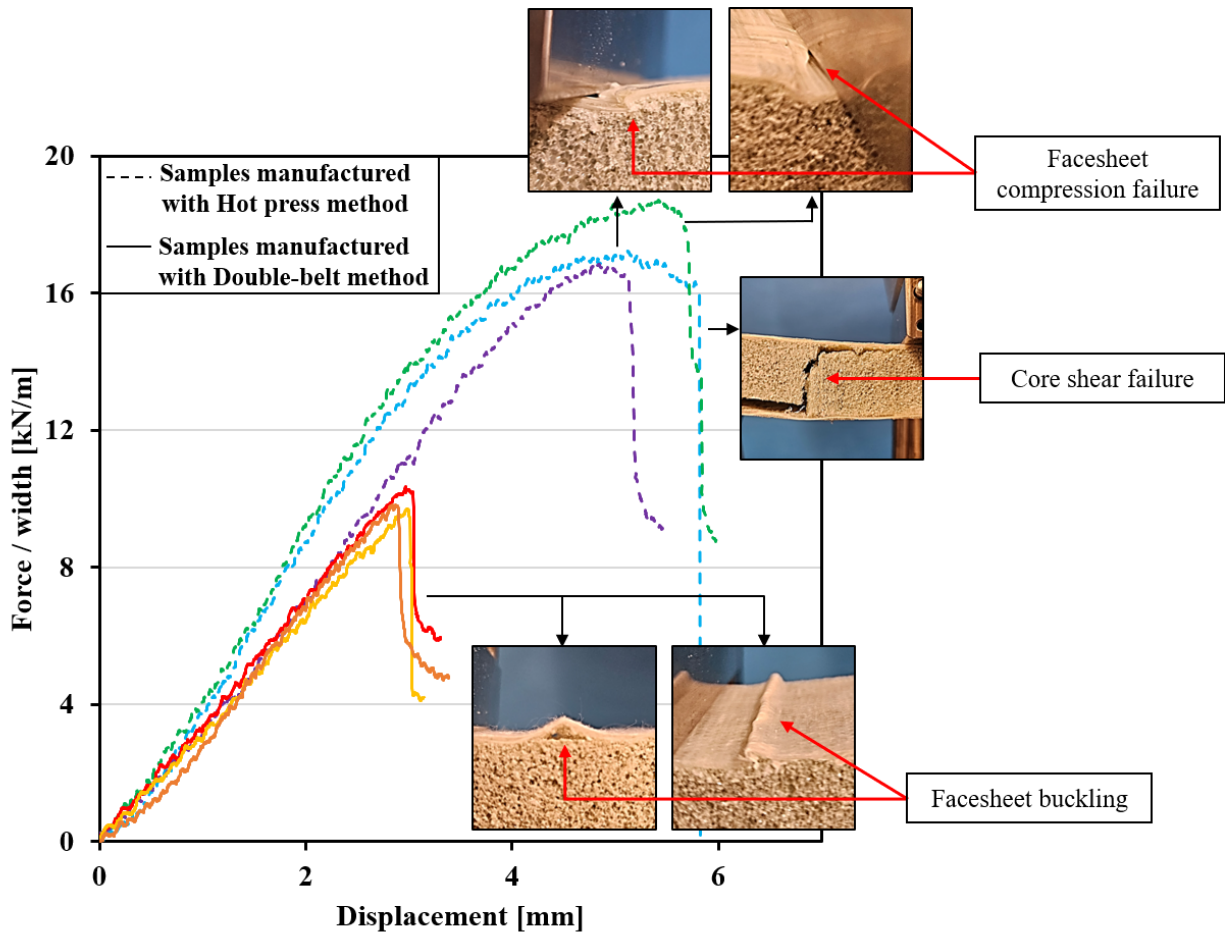
Figure 4.10. Three-point bending response of [G/PET^{20}/G] recycled PET core composite sandwich panels under the span length of 200 mm.

The noticeable variation in flexural response can be attributed to the impacts of the production procedure on the quality of the sandwich panels. Because of the superiority of the compression molding technique in forging a relatively superior connection between the PET foam core and PP-based composite, these samples are expected to resist skin delamination. In samples made with this approach, the skin remained adhered to the PET foam even after the facesheet compression failure, signifying robust adhesion between the composite skin to the core. However,

the panels manufactured by the double-belt method exhibited different behavior; the top facesheet buckled under the compression load, which caused a consecutive separation of the composite facesheet from the PET foam core.

In addition to the discussed relatively inferior cohesion between the layers observed in panels produced by the double-belt machine, the sequential stages involved in this process can significantly affect the quality of PP-based composite facesheets. During the second stage of production, the already solidified thermoplastic-based laminates are reheated to the melting temperature of PP resin. Passing through the second roller sets, the pressure applied to the panels is bounded by the recycled PET foam material limits, because of which certain defects were introduced to the composite facesheets. This assertion was also confirmed by the increase in the number of detected voids formed in the composite facesheet of sandwich panels made with the double-belt technique, also detected in the former microscopic evaluations. These determined defects can directly deteriorate the mechanical compression properties of the composite laminates leading to lower load-bearing capacity of the sandwich panels.

To assess the severity of the properties' degradation during the secondary lamination stage, compression tests were performed for the single layer of composite glass/PP laminates removed from the PET core sandwich panels. Before discussing the results, it is worth noting that the thickness of the specimen can affect the compression properties following the ASTM D3410 standard requirements [128]. Compared to the previously discussed [G_2] laminate properties, conducting compression tests on a single layer of composite facesheet leads to mixed-mode buckling and compression failure. Hence, these additional tests were primarily done to comparatively study the impact of sequential manufacturing procedures on the panels.

Because during the compression molding lamination process, consistent pressure was applied to the sandwich panel in a single step, fewer defects are expected to form. The measured compression strength of the composite facesheet made with the compression molding technique was around 36.0 MPa. Nevertheless, a drastic reduction of compression strength was seen for glass fiber composite facesheets of the sandwich panels made with the double-belt method, almost reaching 16.02 MPa. This marked decline in compression properties is related to the intensity of the unexpected defects such as voids being integrated after the second lamination step. Ultimately, the inferior compression characteristics of the upper composite facesheet, made by the double-belt

method, have led to buckling failure and subsequent separation of skin from the PET core under the three-point bending load.

According to ASTM C393 [96], the facesheet bending stress (σ) and the core shear stress (τ) can be calculated with equations 4.2 and 4.3.

Eq. 4.2.
$$\sigma = \frac{PL}{2t(d+c)b}$$

Eq. 4.3.
$$\tau = \frac{P}{(d+c)b}$$

where P is the measured load, L represents the span length, b, c, d, and t are the sandwich panel width, core thickness, panel thickness, and facesheet thickness, respectively.

Calculations have revealed that the average stress of the composite facesheets reached the maximum of 43.02 MPa for the sandwich panels made by compression molding, and 24.35 MPa for those made with the double-belt method. Here, slightly higher stress results can be explained by the additional constraints imposed on the composite skin, restricting it from the side that is adhered to the PET foam. Furthermore, it was noted that the facesheet failure stress threshold for the sandwich panels made with the compression molding process is almost twice the panels manufactured with the double-belt process. The stress analyses, compiled with the compression test results, verify the degrading impact of the sequential lamination procedure on the mechanical properties of the sandwich panels made by the double-belt method. The measured core shear stress in the sandwich panel that underwent the core shear failure reached 0.42 MPa, edging close to the 0.6 MPa shear strength of the recycled PET foam core (shared data by Armacell [120]). Because the shear stress of the PET core in samples manufactured with the double-belt method does not attain the documented shear strength, before experiencing facesheet catastrophic failure, no evidence of core shear was observed for these samples. In conclusion, the assessment findings strongly emphasize the importance of maintaining precise control over temperature and pressure during each manufacturing approach.
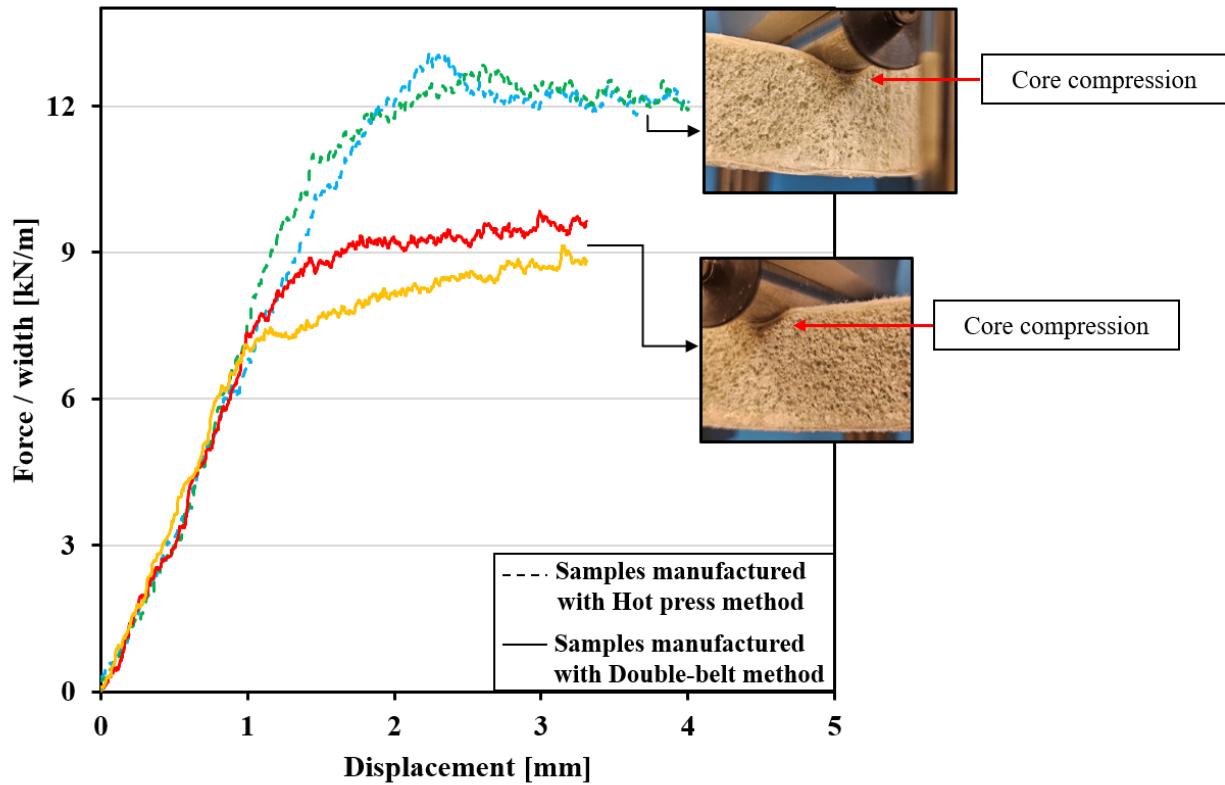
Figure 4.11. Three-point bending response of [G/PET^{20}/G] recycled PET core composite sandwich panels under the span length of 100 mm.

As depicted in Figure 4.11, at shorter span lengths, the PET foam core permanently deforms under the loading nose due to the intensity of vertical out-of-plane compression force. This localized deformation leads to a plateau in the force data during the three-point bending test. Even though the samples did not fail catastrophically, the PET foam core and glass fiber composite facesheet sustained local damages, affecting the overall performance of sandwich panels. Thus, the bending tests are terminated along the plateau. More than 30% increase in the maximum plateau load level was determined for the samples made by the hot press machine. For [G/PET^{20}/G] sandwich panels fabricated via compression molding, the maximum calculated compression stress experienced by the facesheets was determined to be 15.9 MPa, with a corresponding core shear stress of 0.32 MPa. In contrast, for panels manufactured using the double-belt method, these respective stress measurements reached 11.6 MPa and 0.23 MPa. This improvement is attributed to the superior mechanical properties of facesheet and the efficacy of skin-to-core adhesion in the compression molded panels, which benefits the load transfer between the layers.
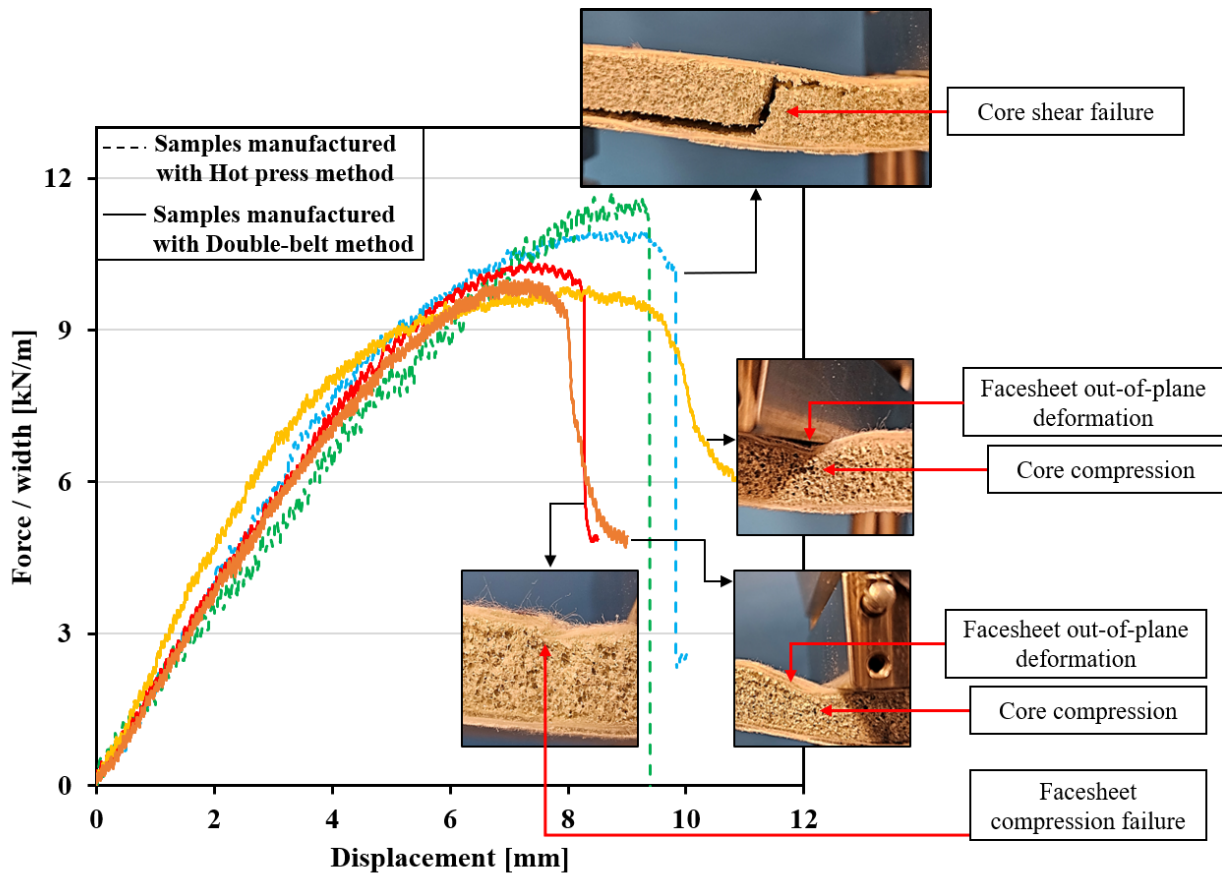
Figure 4.12. Flexural response of [G/PET^{10}/G] recycled PET core composite sandwich panels under three-point bending with 200 mm span length.

The bending tests were repeated for sandwich panels with 10 mm thick PET core under the span lengths of 200 mm and 100 mm which are presented in Figure 4.12, and Figure 4.13. Under a three-point loading condition, it is well-known that increased span lengths impose greater stress on the facesheets. The [G/PET^{10}/G] panels exhibited distinct failure modes attributable to variations in their properties inherited during the lamination process. As previously discussed, thermoplastic-based composite skins subjected to the secondary processing phase, that included reheating the already solidified composite facesheet, exhibit relatively diminished compression properties. [G/PET^{10}/G] sandwich panels experienced either a skin compression failure or facesheet out-of-plane deformation leading to permanent core compression. The bearable stress of the composite facesheet reached a maximum of 45.5 MPa, while the PET foam core experienced 0.45 MPa shear stress. On the other hand, the samples manufactured with the compression molding technique failed due to the PET core shear. Before these sandwich panels failed at the core shear stress of 0.54 MPa, the facesheet stress of sandwich panels made with compression molding touched the maximum of 54.2 MPa.
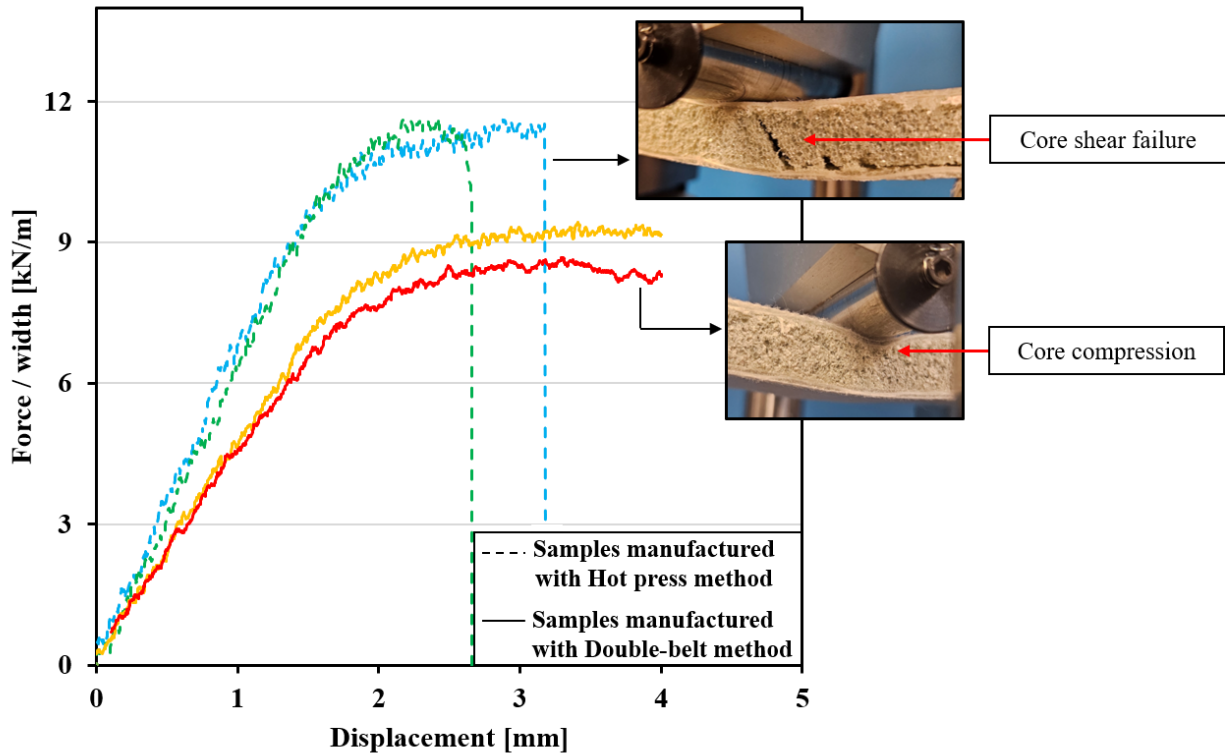
Figure 4.13. Three-point bending test results of [G/PET^{10}/G] recycled PET core composite sandwich panels under 100 mm span length.

The chance of core failures under either shear or compression stress is increased for the panels under 100 mm span length bending. Compared to the core compression and composite facesheet failures, the catastrophic breakage of the PET core can be distinguished by its specific sudden load drop to near zero. Notably, [G/PET^{10}/G] sandwich panels produced via the hot press machine failed at a core shear stress of 0.55 MPa under a 100 mm span length bending load. However, the panels made with the continuous double-belt process reached a plateau, during which the PET foam core permanently deformed under the localized compression force at the loading nose. These samples experienced facesheet stress of 21.7 MPa and core shear stress of 0.43 MPa at the maximum reached point within the plateau.

The conducted bending tests clearly distinguished the variations in qualitative mechanical properties introduced from the distinct manufacturing process of the PP-based PET core sandwich panels. In contrast to the double-belt method, the compression molding technique showed its superiority in the lamination of fully thermoplastic composite PET foam core sandwich panels.

The improved skin-to-core adhesion combined with higher in-plane compression properties of the composite facesheet achieved through a single-step process enhanced the load-bearing performance of such sandwich panels.

In addition to the quality of the final composite sandwich panels, the production time, expenses and size of the panels must align with the targeted market demands. The continuous manufacturing nature of the double-belt lamination method makes this approach a feasible production technique for thermoplastic-based composite in the industry [7,118]. Moreover, because the roller distance can be adjusted during the lamination procedure, this method offers an advantage in easier optimization. This adaptability helps achieve high-quality products, even in initial production runs, a feature that enhances the process's practicality. Its flexibility to incorporate additional layers based on customers' needs, such as water-repellent skin, mats, or colorful thermoplastic coverings, all of which can be integrated within the automated production line. Finally, by using alternative options as core materials, such as the thermoplastic PP honeycomb cores, there is a potential to heat the core separately, facilitating a molecular bonding between the molten layers, and further enhancing the structural integrity of the final product.

Taking advantage of this lamination procedure needs a careful evaluation of previously mentioned manufacturing parameters in each fabrication stage with respect to the properties of the input resin and core. Yet, one of the downsides of the double-belt machine used in this research was the inability to control these manufacturing parameters, often resulting in variability of the product's performance. Thus, the double-belt machine lamination process faces an important challenge which includes the heating and cooling rate in the process parameters. These trials have highlighted the need for more control strategies within the double-belt process, underscoring the importance of continued research in this area. Further investigation is required to closely monitor and evaluate these influential parameters during the continuous manufacturing of sandwich panels using the double-belt machine.

4.6 Conclusion

Due to its capacity to maintain continuous high-rate production, while minimizing manual labor, the double-belt lamination process was compared to the compression molding technique. In order to laminate environmentally sustainable thermoplastic sandwich panels, 100 percent recycled

PET foam material made of post-consumer plastic bottles was examined. The glass/PP composite facehseet experienced a degradation in properties going through the second lamination stage of the double-belt method, mainly due to reheating the solidified composite surface. Besides, the increase of void formation in the composite facesheet and permanent foam cell deformation represents the probable defects during this sequential fabrication process.

The peel-off and flatwise tensile tests evaluation showed that higher PET foam density facilitates the adhesion between the PP-based composite skin and core, owing to the increased available surface area. Moreover, it was discovered that the skin-to-core bonding can significantly depend on the employed fabrication method, consequently affecting the load distribution and bending performance of the sandwich panels. The flexural tests performed on the sandwich panels confirmed the deviation between the panels' performance caused by the manufacturing procedure. The presence of fewer defects introduced during the lamination phase directly influenced the flexural behavior of the panels, increasing their load-bearing capacity and changing their failure response. The dominant failure mechanisms under bending load conditions were core shear failure, compression failure, and buckling of the top facesheet. These catastrophic failures can be governed by the quality of samples inherited from the production techniques.

In conclusion, the optimization endeavors directed toward the double-belt lamination procedure and compression molding revealed their effectiveness in recycled PET foam core sandwich panels. Even though the double-belt lamination technique used in this research presents a continuous automatic production approach, the compression molding process offers considerably precise control of the lamination temperature and pressure. Despite slight potential quality degradation during the double-belt fabrication process, its adoption remains viable due to its cost efficiency and capability to produce large-scale panels with satisfactory quality, facilitated by precise control over manufacturing parameters.

Chapter 5:

Low-Velocity Impact Response of Hybrid Thermoplastic Glass Fiber Composites Reinforced with Stainless-Steel Mesh

5. Low-Velocity Impact Response of Hybrid Thermoplastic Glass Fiber Composites Reinforced with Stainless-Steel Mesh

This section which is also published as "Experimental Investigation on the Effects of Stainless-Steel Mesh Reinforcing Layers on Low-Velocity Impact Response of Hybrid Thermoplastic Glass Fiber Composites" is precisely done to assess the influence of several contributing factors on the LVI behavior of reinforced composite plates. In addition to the improvements that hybridization could offer to the composite structure, in this chapter more details about the extend of damages and perforation thresholds respective to each reinforced laminate were presented.

5.1 Abstract

This study aims to assess the hybridization effect on the perforation threshold of Low-Velocity Impact (LVI) in thermoplastic glass composite laminates, incorporating layers of resin-impregnated stainless-steel mesh. Reinforcing methodologies such as hybridization are recently being adopted as a practical approach to increasing the energy-absorbing capacity of polymer composites. In this chapter, a multi-step hot press lamination method has been employed to fabricate the hybrid composite laminates strengthened with stainless-steel mesh layers. Several stacking sequences, metal mesh wire sizes, orientation and position relative to the impactor have been examined under various LVI energies. It was revealed that the LVI penetration energy was increased for the thermoplastic-based composite laminates reinforced with stainless-steel mesh layers. Furthermore, the LVI penetration energy threshold was significantly influenced by the metal mesh wire size, orientation and stacking sequence. Finally, the backlight method capability was assessed to detect the after-impact interlaminar damages.

5.2 Introduction

Despite being used in advanced applications, fiber-reinforced composite materials are prone to impact damages, stemming from sources such as a hard projectile, runaway debris, hail or drop of a tool. Even barely visible indentations under specific impact energies can cause internal damages, including matrix cracking, delamination and fiber breakage, which drastically degrade

the performance of composite laminates. It has been revealed that the LVI behavior of composite structures is dependent on their fabrication, material system, geometry, impactor parameters and environmental conditions [5,129,130]. Furthermore, empirical studies have proven that the tup configuration, fiber volume fraction and laminate thickness can significantly affect the LVI perforation energy of composite laminates [2,3]. In the context of LVI loading, the importance of geometric factors is intensified due to their global target response [47]. In contrast to the impactor's mass and velocity, which have negligible effects on the penetration energy, the applied energy magnitude dominantly controls the LVI behavior [39,40]. In addition to the ambient temperature, fiber architecture and resin toughness can determine the outcomes of the LVI tests [6,131].

Woven composite laminates have higher toughness than the unidirectional ones, experiencing an unstable crack growth and crack jumps propagation pattern. Because of their enhanced toughness, the presence of woven layers suppresses the delamination initiation point, leading to lower Compression After Impact (CAI) properties [47,132–135]. Fiber composites reinforced with thermoplastic matrix are resistant to impact damages, in contrast to the thermoset based laminates which have inferior toughness properties [5,46,48,50,56]. Vieille et al. examined the influence of resin on the LVI behavior of carbon fiber composite laminates. Due to its specific energy absorption performance, the glass fiber composite laminates reinforced with the Polypropylene (PP) resin gained interest in recent research [136–138]. Boria et al. performed a thorough empirical investigation of the mechanical properties of a PP-based composite laminate under repeated LVI scenarios [139]. It was concluded that modifying the resin materials can govern the impact perforation energy, damage propagation, and permanent after-impact deformation of composite plates [51,140]. Moreover, inspecting the impacted samples introduces the matrix plasticization and straining of the whole yarn as the primary energy-absorbing mechanisms within the thermoplastic-based Glass composites [52]. Hence, not only the woven thermoplastic-based composites are the preferred choice withstanding higher impact energies, but also they are more sustainable due to their economical manufacturing process and recyclability [7].

Nowadays, hybrid metallic composites are increasingly acknowledged, mainly due to their elasto-plastic energy-absorbing characteristic, which improves impact penetration threshold 27–33. Aluminium layers and core structures used to manufacture hybrid composite laminates and sandwich panels showed their capability of improving the impact response even against high-speed

ballistic projectiles [146–148]. Using thin wire stainless-steel fibers can potentially reinforce the composite laminates under various loading scenarios. Furthermore, LVI tests revealed that hybridizing the composite laminate using metal fiber layers with larger wire diameters, increases the impact perforation energy [11,68,69,73]. A few scholars also studied the effect of metal mesh layers as the strengthening component of hybrid composite plates. The mesh size and stacking sequence effect of hybrid laminates were examined under tensile loading conditions, which resulted in increased stiffness and ultimate strain of these samples. Moreover, it was noted that in addition to the stacking sequence of reinforcing metal mesh layers, fiber direction and fabrication process pressure can affect the laminates' tensile and flexural performance [9,10,75,149].

Wang et al. designed a special clamping fixture to perform LVI on neat stainless-steel mesh at various impact conditions [150,151]. To the best of the authors' knowledge, there is a limited number of studies on hybridizations using metal mesh as the reinforcing layer. It was depicted that strengthening the composite laminates with steel mesh enhances the impact perforation energy threshold. Moreover, it was understood that the position of the mesh layer relative to the indenter plays a significant role in the damage extent of thermoset composite laminates [71,72]. In a previous study, the influence of hybridization on thermoplastic samples manufactured by the double-belt lamination method has been studied [117]. However, due to the fabrication procedure limitations, composite layers with low fiber content were selected, providing excess thermoplastic resin to improve the adherence between the composite layers and reinforcing metal mesh.

In the current research, a multistage approach is considered to fabricate the hybrid thermoplastic laminates using a hot press machine. Because of the relatively higher viscosity of thermoplastic PP resin, introducing it to this application required specific assessments. Since the lamination procedure includes pre-impregnation of stainless-steel mesh layers, glass composite layers with 60 % fiber weight fractions were used. Incorporating the impregnated metal mesh layers with PP resin allows the use of composite layers with higher fiber contents, while improving the layers' adhesion. Lastly, the main focus is to evaluate the effect of stainless-steel mesh size, stacking sequence, orientation, and layer count on hybrid thermoplastic-based composites under various LVI loading energies. The effect of these factors needed to be determined for the thermoplastic-based composite laminates; therefore, a wide range of LVI tests were performed to assess the influence of hybridization on these plates. In addition to the perforation impact energy

threshold, laminates were closely examined to assess their LVI response, after-impact deformation and the extent of damage.

5.3 Experimental procedures

5.3.1 Materials and fabrication process

Composite laminates were fabricated using 2/2 twill weave E-Glass/Polypropylene (E-Glass/PP) layers with a fiber weight fraction of 60%, which were donated by Innovative Composite Products (ICP) Inc. The hybrid laminates contain three different 304 stainless-steel plain weave meshes with wire diameters of 0.70 mm ($M^{0.70}$), 0.35 mm ($M^{0.35}$), and 0.165 mm ($M^{0.16}$). Specific details of the mentioned materials used in this study are distinctly presented in Table 5.1. Several permutations of stacking sequences, with or without mesh, were fabricated to evaluate the effects of metal mesh diameter, layup sequence and orientation. $[G_2]$, $[G_3]$, $[G/M^{0.16}/G]$, $[G_2/M^{0.16}]$, $[M^{0.16}/G_2]$, $[G/M^{0.16}]_s$, $[M^{0.16}/G]_s$, $[G/M^{0.35}/G]$, $[G_2/M^{0.35}]$, $[M^{0.35}/G_2]$, $[G/M^{0.70}/G]$, $[G_2/M^{0.70}]$, $[M^{0.70}/G_2]$ and $[G/M^{0.70}_{45°}/G]$ present the variation of composite layups studied in the current research. In order to produce the $[G/M^{0.70}_{45°}/G]$ hybrid laminates, metal mesh is rotated by 45 degrees relative to the orientation of the woven Glass/PP layers. Laminates were made using a hot press technique, during which stacked layers of dry weave Glass/PP and pre-impregnated stainless-steel mesh were subjected to elevated temperature and pressure, effectively binding them together. The current methodology considers the fabrication of hybrid laminates as a sequential two-step process, wherein the initial step entails the impregnation of metal mesh with PP sheets.

The PP sheets were heated up to 160-165° C and pressed into the stainless-steel mesh under pressure of 1.5 MPa. After maintaining the configuration for 3 minutes, the hot press uses water, gradually reaching the ambient temperature at the cooling rate of 15° C/min. To achieve the proper laminate quality, the selected cooling temperature rate was chosen through trial and error. Different thicknesses of PP sheets were considered for impregnating the stainless-steel mesh while any excess PP was trimmed post-process. On the other hand, to fabricate the composite laminates, the stacked layers were subjected to a temperature of 160-165° C, under 0.5 MPa pressure for a duration of 1 minute. It is worth mentioning that in each step, a steel mold closely matching the expected final laminate thickness has been used to control the resin flow. Due to the dimensional constraints of the hot press and enhanced control over resin flow, laminates were fabricated in 120

mm × 120 mm square shapes. Table 5.2 presents detailed information about the dimensional characteristics of the fabricated laminates. It is worth noting that the laminates with different mesh layup sequences or directions almost have the same dimensions.

Table 5.1.

Mechanical properties of the materials

Material	Type	Nominal thickness [mm]	Wire diameter [mm]	Mesh size	Opening size [mm]	Open area
Metal mesh	304 stainless-steel	0.33	0.165	70 × 70	0.20	30%
		0.70	0.35	24 × 24	0.70	44%
		1.40	0.70	12 × 12	1.40	44%

		Nominal thickness [mm]	Density [kg/m^3]	Tensile strength [MPa]	Melting temperature [°C]	
PP sheet	100% Polypropylene	0.406 0.508 1.588	0.913	27.58	160-165	

The cross section of the fabricated laminates was examined under an optical microscope to assess the impregnation of layers. As Figure 5.1 presents, the open areas of stainless-steel mesh were adequately filled with PP, which formed a robust interlayer connection, particularly in hybrid laminate. The magnified regions adjacent to the stainless-steel wires depict a satisfactory impregnation of the metal mesh with PP resin.

Table 5.2.

Dimensional characteristics of fabricated laminates.

Laminate stacking sequence	Stainless-steel mesh wire diameter [mm]	Impregnated mesh layer thickness [mm]	Laminate thickness [mm]	Areal density [kg/m²]
[G$_2$]	-	-	2.18 ± 0.03	2.95
[G$_3$]	-	-	3.32 ± 0.02	4.47
[G/M$^{0.16}$/G]	0.165	0.455 ± 0.01	2.58 ± 0.02	4.04
[G/M$^{0.16}$]$_s$			3.02 ± 0.01	5.24
[G/M$^{0.35}$/G]	0.35	0.66 ± 0.02	2.66 ± 0.02	4.52
[G/M$^{0.35}$]$_s$			3.60 ± 0.03	6.40
[G/M$^{0.70}$/G]	0.70	1.60 ± 0.01	3.50 ± 0.02	6.29
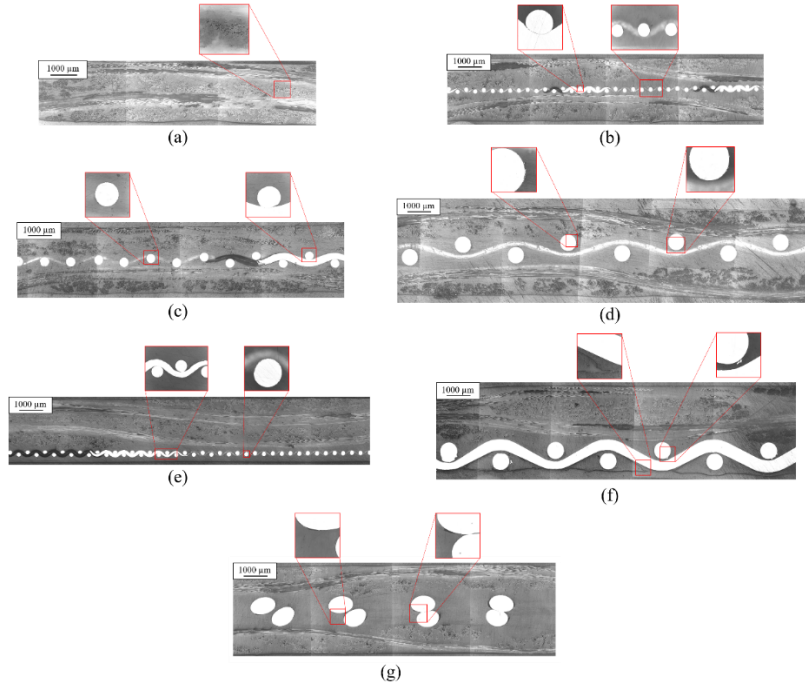
Figure 5.1. Microscopic picture of the non-hybrid and hybrid composite plates, (a) [G$_2$], (b) [G/M$^{0.16}$/G], (c) [G/M$^{0.35}$/G], (d) [G/M$^{0.70}$/G], (e) [G$_2$/M$^{0.16}$], (f) [G$_2$/M$^{0.70}$], and (g) [G/M$^{0.70}_{45°}$/G].

5.3.2   Tensile properties of laminates

Composite laminates and impregnated stainless-steel mesh were individually subjected to quasi-static tensile tests in accordance with ASTM D3039 [127,152]. Specimens were cut along the fiber directions with dimensions of 110 mm × 25 mm utilizing a diamond saw machine. Tensile

tests were conducted under the standard rate of 2 mm/min, employing an MTS testing machine equipped with a 100 kN load cell. To better evaluate the tensile behavior of the laminates, all collected data are translated into stress-strain curves, and the final measured data are presented in Table 5.3.

Table 5.3.
Mechanical tensile properties of impregnated stainless-steel mesh, hybrid and non-hybrid composite laminates.

Laminate stacking sequence	Strength [MPa]	Ultimate strain [%]	Stiffness [GPa]
$[M^{0.16}]$	122.49	10.55	6.32
$[M^{0.35}]$	123.39	10.04	7.15
$[M^{0.70}]$	135.25	7.08	7.28
$[M^{0.70}_{45°}]$	96.26	37.52	1.01
$[G_2]$	203.98	2.91	8.54
$[G_3]$	197.95	3.50	7.66
$[G/M^{0.16}/G]$	198.04	3.26	7.82
$[G/M^{0.16}]_s$	179.01	3.21	7.75
$[G/M^{0.35}/G]$	203.27	3.43	8.44
$[G/M^{0.35}]_s$	166.82	3.50	7.27
$[G/M^{0.70}/G]$	153.59	3.39	6.59
$[G/M^{0.70}_{45°}/G]$	142.18	3.17	6.00

Hasselbruch et al. investigated the influence of hybridization on the mechanical properties of thermoplastic Carbon/PPS composites reinforced with steel wire mesh [75]. After a linear elastic phase, a non-linear plastic deformation followed by a stepwise consecutive failure of wires was observed in hybrid samples under quasi-static tensile loading. In the current study, an analysis was conducted on the impregnated metal meshes and hybrid composite laminates. Woven impregnated mesh layers followed the same elasto-plastic path, where wire failure happens in an incremental sequential manner. It is worth mentioning that the impregnated $[M^{0.70}_{45°}]$ mesh plate displays a significantly increased plastic response under tensile load, which is substantiated by its ultimate strain characteristic. Moreover, the ultimate strain and modulus are affected due to the capacity of woven metal mesh to stretch when pulled during the tensile test. The hybridized specimens did not undergo complete separation into two distinct pieces subsequent to the initial catastrophic failure, since some of the metal mesh wires remain connected to the composite layers. Furthermore, the

disparity in material properties between the impregnated metal mesh and Glass/PP layers caused a reduction in hybridized laminates strength under the tensile loading conditions.

5.3.3 Drop weight impact tests

The Instron 9340 drop tower impact machine, instrumented with a 22 kN load cell, is used to conduct LVI tests following the ASTM D7136 and D3763 [152,153] standard routines. The composite laminates were trimmed to the dimensions of 110 mm × 110 mm. A pneumatic circular clamp with 76 mm inner diameter secures the samples in place, being hit by a 16 mm diameter hemispheric tup, depicted in Figure 5.2. Multiple LVI tests with impact energies ranging from 15 J to 70 J were performed to examine the performance of both hybrid and non-hybrid composite laminates. In order to mitigate the influencing factors, impact velocity is maintained around 3.03 m/s to 3.11 m/s; therefore, LVI tests should be conducted within a controlled range of drop weight height, spanning from 468 mm to 493 mm. Considering the specified impact conditions, additional mass is incorporated to achieve a striker mass range of 3.265 kg to 14.765 kg. The impact machine's data acquisition system records the force-time data at a sampling frequency of 2000 kHz. Besides, a Piezoelectric sensor captures the striker's speed precisely at the impact initiation. These collected data have been used to calculate the impactor velocity, displacement, and energy responses [6,154].
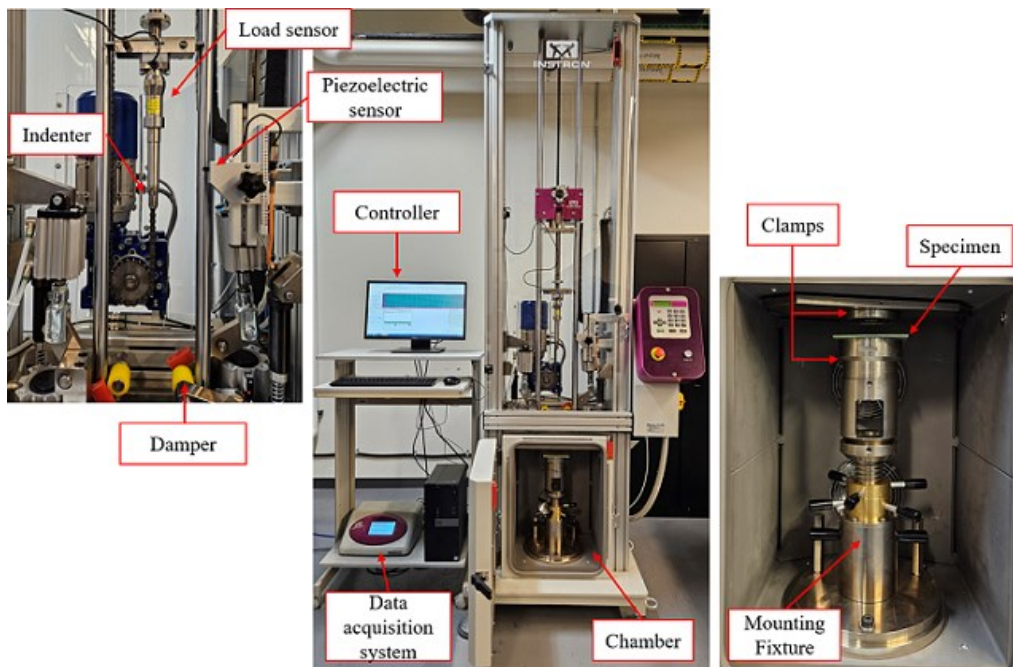
Figure 5.2. The Instron 9340 drop weight impact machine equipped with pneumatic circular clamps with an inner diameter of 76 mm.

The permanent indentation depth of the impacted samples was measured using a dial gauge with a precision of up to ± 0.01 inches. Furthermore, an assessment of the deformation of the impacted laminate is conducted in close proximity to the impact zone at a radius of 10 mm from the center. Finally, to elucidate the extent of damage after impact, supplementary photographic documentation is crucial. It was revealed that damages can negatively affect the translucency of the Glass/PP composite laminates [52,117]. Hence, the backlight method is considered to be a viable damage detection approach for the current investigation as well. Damages such as cracks and delamination can block the light from passing through, which creates a regional contrast variation. For the inspection, the samples were placed between a light source and imaging system. The specimens were illuminated with a quad-LED true tone flashlight placed in the center of a cylindrical stand. A triple camera system with a 50-megapixel primary shooter (12-megapixel ultrawide, and 10-megapixel telephoto) positioned horizontally above the samples was used to capture pictures of the impacted samples. Lastly, image processing was done to improve the detection of damage zones modifying the contrast and sharpness of the images.

5.4 Results and discussion

LVI behavior of composite laminates can be markedly influenced by multiple factors including striker dimensions, boundary conditions, laminate thickness, impact energy, reinforcements and etc. [2,3,6,154][155]. Depending on the applied impact energy, composite laminates can show different responses. Under relatively low impact energies, a rebound situation is expected to happen. During this phenomenon, the striker bounces back upon hitting the laminate restoring the elastic energy portion of the laminate response. The remaining energy is absorbed by the laminate through a combination of plastic deformation, damage propagation and friction. Nevertheless, if the impact energy exceeds the perforation threshold, the applied energy is entirely absorbed during the impact process.

The current study focuses on the influence of hybridization on the LVI behavior of Glass/PP composites. At an industrial level, these laminates are ultimately expected to be used as the structural parts in prefabricated cabins commonly found in housing, cargo, or refrigerated trucks.

These composite plates are exposed to impact events during their work life, or even within the installation and maintenance process. Therefore, hybridization could be presented as a valuable solution method capable of delaying the penetration of the structure's composite surface under impact conditions. Three distinct stainless-steel mesh wire sizes were used in this project to determine the hybridization effect in contrast to the non-hybrid composite laminates. Ahmed et al. demonstrated that the position of metal mesh regarding the impactor can alter the perforation energy of hybrid glass/epoxy laminates [72]. Thus, three permutations of stacking sequences for hybrid laminates have been examined to evaluate their performance under LVI conditions. Furthermore, an assessment has been conducted on several laminates with different metal mesh layers' count and orientation, aiming to identify the hybrid composite lamination which exhibits superior response. More details regarding the aforementioned tests are presented in the subsequent subsections.

5.4.1 *Influence of stainless-steel mesh wire diameter*

In addition to the general rebound or perforating response of the laminates, force-displacement curves serve as a means to determine the bending stiffness, maximum force, and displacement. A series of LVI tests is performed to capture the exact required energy for laminates to reach the full plate perforation state. A comparison of LVI response of hybrid and non-hybrid $[G_2]$, $[G_3]$, $[G/M^{0.16}/G]$, $[G/M^{0.35}/G]$, $[G/M^{0.70}/G]$ laminates under various impact energies is done. Besides the hybridization influence, $[G_2]$, and $[G_3]$ non-hybrid composite laminates are examined in this research to evaluate the effect of laminate thickness as presented in Figure 5.3.

If the applied impact energy is insufficient for the striker to perforate the sample, the energy curve descends to the absorption energy level after touching the peak. In an impact test, a combination of energy-absorbing phenomena, including damage and plastic deformation can occur alongside friction. Within the force-displacement diagram, the samples' deformation recovers at a point where the tup rebounds from the laminate. Thus, in rebound impact conditions the absorbed energy is a fraction of the total applied LVI energy since elastic energy is required to throw the tup back up. The dissipated energy is expected to reach the impact energy in a contact response, closely preceding the occurrence of the perforation phenomenon [6]. On the other hand, under a perforation impact energy, the striker penetrates the sample until being halted either by the machine's dampers or becoming wedged into the sample.
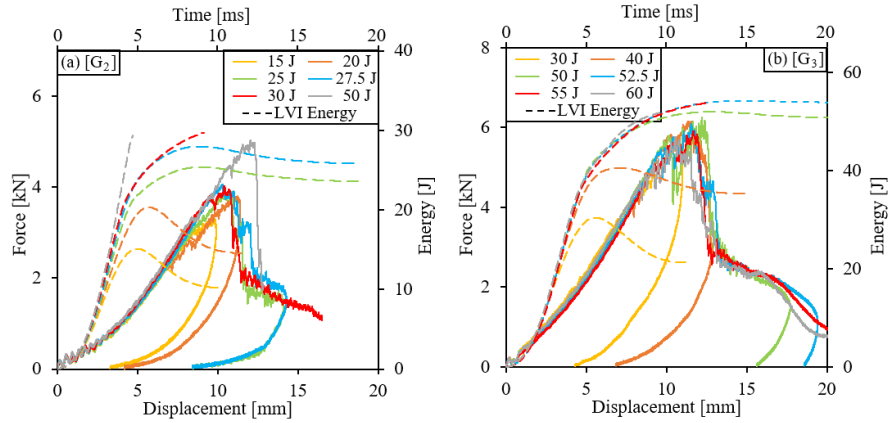
Figure 5.3. Force-displacement, and energy-time response of the non-hybrid Glass/PP, (a) [G_2], and (b) [G_3] laminates under different impact energies.

Caprino et al. noticed that composite laminate thickness plays a significant role in the LVI perforation energy [2,3]. As expected, the perforation energy of the [G_3] laminate increased by 75 % compared to the [G_2] composite samples. Moreover, the average bending stiffness under LVI loading conditions for [G_3] composites is 34.0 % higher than the [G_2] laminates, which resulted in relatively reduced deformability of the [G_3] plates. The noticed stiffness increase can be attributed to the thickness of the samples and fiber distance from the neutral middle plane. Consequently, the measured deformation in the vicinity of the impact site showed higher values for [G_2] laminates, under lower impact energies. The difference between the samples' deformation close to the impact site specifies that the state of damage is considerably localized for the [G_3] laminates.

Hybridization is generally shown to be capable of improving the impact behavior of fiber reinforced composites [58]. Because of their elasto-plastic response, the metallic layers are capable of improving the energy absorption capacity of composite plates. Thus, in the current research, focus is drawn to the LVI behavior of composite laminates strengthened with stainless-steel mesh layers. Even though Ahmed et al. reported that hybridizing thermoset composite laminates using metal mesh effectively changes their LVI response, the effect of mesh size, particularly on the hybrid thermoplastic Glass/PP plates, is not well understood [72]. Due to the geometrical properties of the metal mesh, certain manufacturing obstacles were resolved, particularly during the impregnation of these layers. Unlike fibers, the metal mesh resists deformation during the manufacturing process, effectively preventing the resin washout. This is a substantial aspect that can significantly affect the overall performance of the hybrid composite laminates. Comprehensive

data collected from the LVI tests on the hybrid composite plates has been presented in Figure 5.4 and Table 5.4 for various mesh wire sizes.
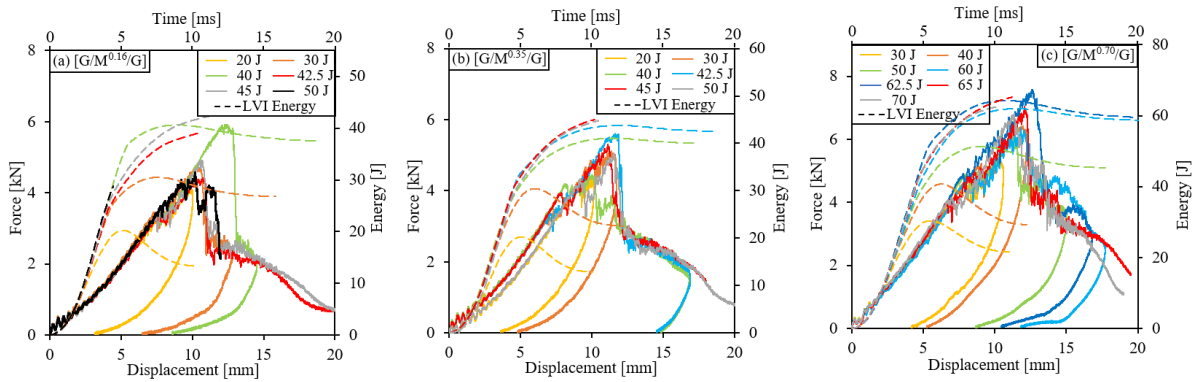
Figure 5.4. Force-displacement and energy-time behavior of hybrid laminates under various impact energies, (a) $[G/M^{0.16}/G]$, (b) $[G/M^{0.35}/G]$, (c) $[G/M^{0.70}/G]$.

Compared to the non-hybrid $[G_2]$ laminates, the perforation energy of $[G/M^{0.16}/G]$, $[G/M^{0.35}/G]$ and $[G/M^{0.70}/G]$ hybrid ones increased 41.7 %, 50 %, and 117.7 %, respectively. The energy absorption improvement in the hybrid laminates is attributed to a combination of damage and plastic deformation of the reinforcing metallic layer. Furthermore, the presence of the impregnated metal mesh layer recedes the Glass-PP layer further from the neutral line. Assuming the LVI loading imitates a semi-dynamic flexural condition, distancing the composite layer from its original location improves its impact performance. Hence, in contrast to the $[G_2]$ plate, the stiffness of the hybrid samples rises by 28.1 %, 30.8 % and 53.8 % with respect to the stainless-steel wire diameter increase. Table 5.4 summarizes the LVI results on hybrid and non-hybrid composite laminates subjected to various impact energies. It is worth mentioning that, the letter "P" determines the measured penetration energy thresholds under the LVI loading conditions in all the tables.

68

Table 5.4.
Summary of the LVI experiments on hybrid and non-hybrid composite laminates under various impact energies.

Laminate stacking sequence	Impact energy [J]	Peak force [kN]	Disp. at peak force [mm]	Max. displacement [mm]	After-impact dent depth [mm]	After-impact dent's edge depth [mm]	Dissipated energy [J]
[G$_2$]	15	3.32	9.56	9.90	0.46	0.12	10.07
	20	3.81	10.95	11.40	0.86	0.38	14.19
	25	3.93	10.66	14.10	3.94	1.14	23.20
	27.5	4.06	10.26	14.30	3.28	1.14	25.35
	30	4.02	10.40	-	P	0.33	29.71
	50	5.03	12.03	-	P	0.97	29.32
[G$_3$]	30	5.53	10.58	11.00	0.97	0.30	20.85
	40	6.16	11.33	12.86	2.64	0.58	34.74
	50	6.25	12.20	17.72	6.60	0.64	48.84
	52.5	6.09	11.53	19.42	6.83-P	0.89	53.74
	55	5.91	11.63	-	P	0.69	53.84
	60	5.77	10.54	-	P	0.28	51.75
[G/M$^{0.16}$/G]	20	4.12	9.89	10.04	0.74	0.36	13.06
	30	4.73	10.44	12.84	2.82	1.04	26.32
	35	4.53	10.61	15.73	4.32	1.12	33.15
	40	5.92	12.34	14.53	3.81	1.19	36.92
	42.5	4.42	10.73	-	P	0.69	39.06
	45	4.91	10.66	-	P	0.71	42.50
	50	4.58	10.19	-	P	0.46	28.75
[G/M$^{0.35}$/G]	20	4.38	10.01	10.17	0.89	0.30	12.60
	30	5.11	11.37	11.75	1.09	0.48	22.14
	40	4.44	10.00	16.81	5.61	1.41	38.95
	42.5	5.60	11.62	16.90	5.03	1.27	41.23
	45	5.31	11.12	-	P	0.97	45.02
	50	5.06	11.53	-	P	0.41	44.79
[G/M$^{0.70}$/G]	30	5.37	10.27	10.61	1.70	0.56	21.22
	40	6.41	11.96	12.25	1.83	1.02	28.58
	50	6.09	11.17	15.04	4.95	1.91	43.99
	55	6.38	11.72	16.22	6.05	2.03	49.93
	57.5	6.62	11.44	16.19	5.13	1.65	51.97
	60	6.38	11.81	17.72	7.21	2.26	56.50
	62.5	7.58	12.61	16.80	6.20	1.57	57.56
	65	7.04	12.08	-	P	1.46	65.22
	70	6.71	11.35	-	P	0.71	62.55

It is a well-established fact that damages occurring during the impact loading condition can deteriorate the load bearing capacity of the laminate; therefore, the first detectable drop in the force data is the representative of plate damage initiation [6]. Analyses revealed that damage initiation force directly correlates with the reinforcing wire mesh diameter. Furthermore, compared to the [G$_2$] laminates, hybridization improved the composite laminate performance, experiencing higher force values before the first sign of the damage.

As previously mentioned, in a rebound LVI condition, a certain portion of the applied energy is recovered by the striker during the bounce back phenomenon. Yet, upon reaching the perforation state, the impact energy is fully absorbed by the laminate [6]; therefore, after the perforation initiation, the absorbed energy value recedes from the diagonal line within the energy profile diagram. In other words, the state at which the applied impact energy intersects with the absorbed energy along the diagonal line can be considered as the LVI perforation energy threshold. Figure 5.5 presents the various energy profiles for non-hybrid and hybrid composite laminates, simplifying the detection of perforation point.
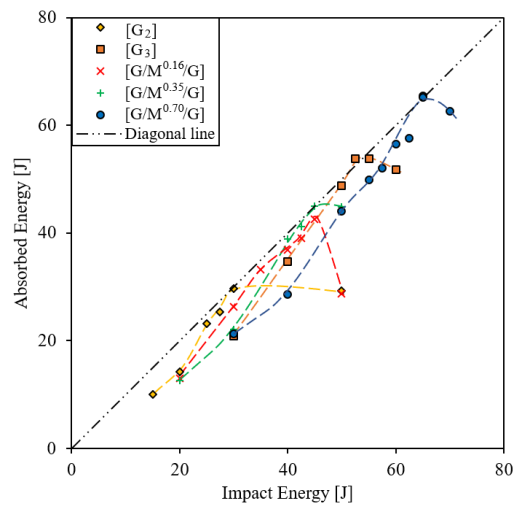
Figure 5.5. Energy profile of the hybrid and non-hybrid composite laminates.

Capturing damage details in photographs for reflective pale surfaces such as Glass/PP composites, under normal light conditions is challenging. Nonetheless, since damages affect the transparency of the composite plate, they appear as dimmed areas when illuminated from the rear. By employing the backlight method, the extent of damage has been depicted in Figure 5.6 to examine the effect of hybridization, while the damaged zone is distinguished with dotted red lines. Being illuminated with a light source from the distal side, damage zones were clearly distinguished. Hence, this photography approach proved its capability to effectively emphasize the damaged regions in such thin transparent composite plates.
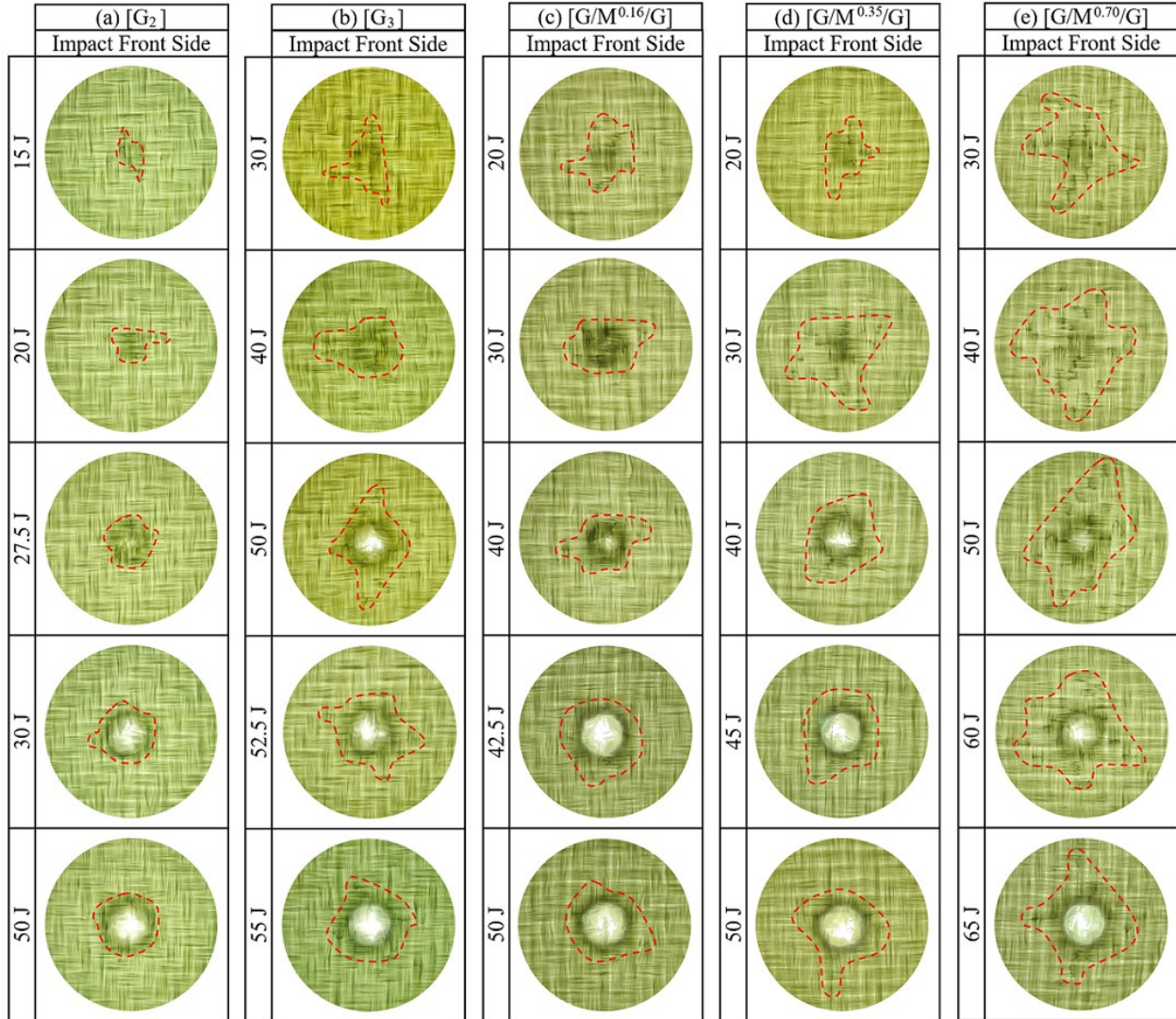
Figure 5.6. The extent of damage under various LVI energies captured with backlight technique (impact side).

Shah et al. identified a range of damage mechanisms including matrix plastic deformation, matrix cracking, localized fiber breakage and fiber pull-out of glass thermoplastic composites under LVI loading [52]. In this research, laminates subjected to relatively low impact energies show a small indentation where the indenter contacts the sample. Using the backlight method, matrix cracks, delamination and damages that occurred in these laminates have been highlighted. Since the level of damage expands by increasing the impact energy, it is expected to see wider darkened regions using the backlight technique. Furthermore, other types of damage like fiber breakage and fiber pull-out form at the rear impact site. Compared to the non-hybrid laminate,

damages emerge out of the indent zone for the laminates strengthened with stainless-steel mesh. Experiencing damage within a wider range from the impact point allows these hybrid laminates to absorb higher energies without reaching their penetration limits. Therefore, more extensive damage could be detected at a distance from the impact point, particularly for [G/M$^{0.70}$/G] laminate, which exhibits permanent global deformation.

To ensure the thickness resemblance, the hybrid laminates were compared to the [G$_3$] plates as well. Among the hybrid composite laminates, only the [G/M$^{0.70}$/G] one outperformed the non-hybrid [G$_3$] by 23.8 percent rise in the perforation energy. It has been observed that the laminate strengthened with 0.7 mm wire diameter mesh deforms globally due to its plastic behavior, while the [G$_3$] laminates experience more localized damage. Here, the extent of damage at a point that the indenter touches serves as an indicator of localized damage, while the after-impact dent's edge deformation is caused due to the structural plastic response. For instance, when subjected to a 50 J impact energy, the after-impact dent depth of [G$_3$] sample reached 6.60 mm, exhibiting a near dent permanent deformation of 0.64 mm. Nonetheless, the hybrid [G/M$^{0.70}$/G] laminate responded in a totally opposite manner under the same LVI conditions. The [G/M$^{0.70}$/G] sample's exact collision spot and its edge deformed 4.95 mm and 1.91 mm, respectively. Therefore, hybridizing the composite laminate with stainless-steel mesh layers proves advantageous to the structural energy absorption capacity under the LVI loading conditions.

Figure 5.7 provides a comparative analysis of [G$_3$], and [G/M$^{0.70}$/G] laminates under certain impact energies. Both laminates experience nearly identical maximum force, with the recorded force data experiencing a sudden decline when surpasses the maximum bearable load threshold. Yet, under high impact energies, force reduces more drastically for non-hybrid composite laminates, while the hybrid ones can deform without significantly losing their strength. Because hybrid laminates experience higher force values at the same deflection levels, they can absorb higher impact energies. This specific behavior is attributed to the presence of stainless-steel mesh layer, which shows an elasto-plastic response causing permanent deformations further from the impact zone. The process of hybridization appears to involve a broader engagement of sample areas within the LVI response, which results in a complex performance causing damage and plastic deformation.
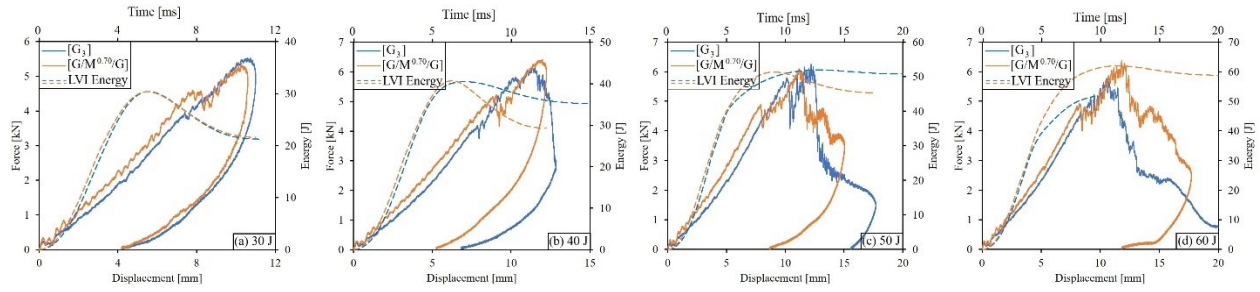
Figure 5.7. A comparison of hybrid [G/M$^{0.70}$/G] laminates responses versus the non-hybrid [G$_3$] subjected to (a) 30 J, (b) 40 J, (c) 50 J, (d) 60 J impact energies.

Research in the field of LVI has introduced the concept of global deformation in laminates as an energy-absorbing mechanism. Analysis of the post impact dent deformations has shown that laminates with lower penetration thresholds experience more localized damage, while those capable of withstanding higher impact energies exhibit global deformation [51,72,156]. While the examined thermoplastic composite laminates exhibited a localized damage response, hybridization positively modified their LVI behavior. In other words, in contrast to the non-hybrid laminates, the hybrid ones undergo permanent deformation showing damages extending to the outer impact zone. Thus, in addition to their higher energy absorption capacity, composite laminates strengthened with metal mesh layers restore a certain portion of the plate's deformation. In a rebound condition, the displacement at which the collected force data drops to zero represents the detachment of the indenter from the plate after striking the plate. Since hybridizing composite laminates changes the level of material's engagement and response, the indenter separates at relatively lower displacements under rebound LVI loading. This specific performance accounts for the observed difference between the after-impact's exact collision point and near dent deformations for [G/M$^{0.70}$/G] and [G$_3$] laminates, also shown in Figure 5.8.
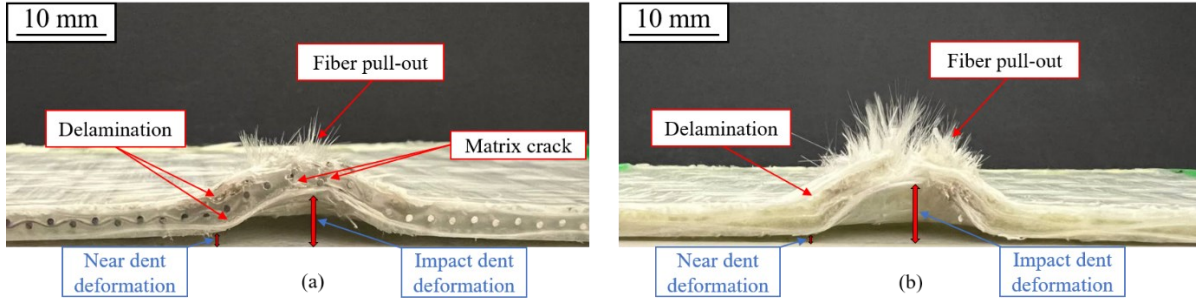
Figure 5.8. Section view of (a) $[G/M^{0.70}/G]$, (b) $[G_3]$ composite laminates after 50 J impact energy, illustrating the global and local deformations of impacted samples.

5.4.2 Stacking sequence effect

Ahmed et al. noticed that the position of the steel mesh layer can influence the LVI perforation energy of the hybrid thermoset Glass/Epoxy laminates [72]. In the current research, three different stacking sequences of hybrid composite laminates were analyzed in order to assess the effect of stainless-steel mesh layer position relative to the impactor. Although the LVI response of hybrid composite plates with a mesh layer placed at the mid-plane was studied in the previous sub-section, the influence of positioning this reinforcing layer either in front or rear impact side required more attention. It has been revealed that modifying the stacking sequence had a minor effect on the hybrid laminates behavior under LVI, particularly for small mesh sizes. Nevertheless, as Figure 5.9 illustrates, alterations were made to examine the reinforcing layup sequence of hybrid laminates strengthened with the 0.7 mm mesh wire diameter.
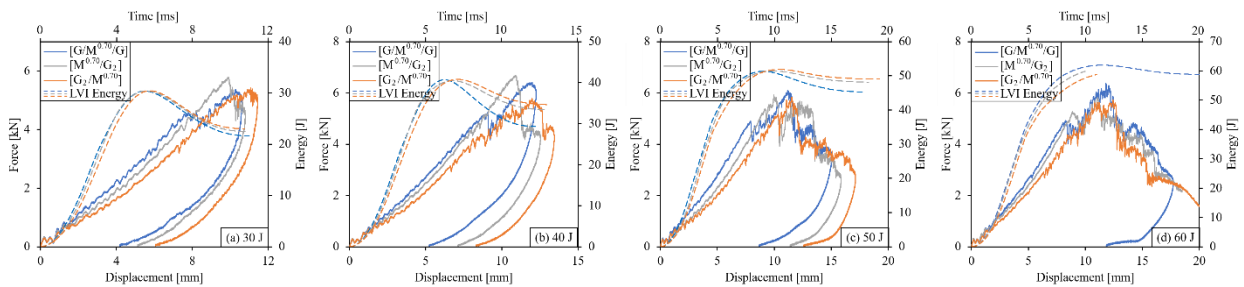
Figure 5.9. A comparison of stacking sequence effect of the hybrid composite laminates reinforced with $M^{0.70}$ mesh layer at (a) 30 J, (b) 40 J, (c) 50 J, and (d) 60 J impact energies.

Placing the metal mesh layer at the mid-plane, the Glass/PP layers were distanced from the neutral line, which resulted in the $[G/M^{0.70}/G]$ stiffness exceeding the other stacking sequences.

Due to their relatively higher bending stiffness, the [G/M$^{0.70}$/G] laminates restore more displacement after being hit by the striker. Even though the level of bearable force is almost the same, [G/M$^{0.70}$/G] hybrid composite plates outperform the alternative layup options under LVI loading conditions in terms of perforation energy threshold. Evaluations depicted that the perforation energy of the [G/M$^{0.70}$/G] laminate is 8.3 % higher than [M$^{0.70}$/G$_2$], and 13 % higher than [G$_2$/M$^{0.70}$]. To better assess the influence of mesh layer position relative to the tup, test details were presented in Table 5.5.

Table 5.5.
Summary of the LVI test results of [M$^{0.70}$/G$_2$] and [G$_2$/M$^{0.70}$] hybrid composite laminates at certain impact energies.

Laminate stacking sequence	Impact energy [J]	Peak force [kN]	Disp. at peak force [mm]	Max. displacement [mm]	After-impact dent depth [mm]	After-impact dent's edge depth [mm]	Dissipated energy [J]
[M$^{0.70}$/G$_2$]	30	5.79	9.86	10.80	2.59	1.27	22.08
	40	6.68	10.86	12.54	4.60	2.18	32.95
	50	5.92	9.97	15.86	9.40	2.54	46.73
	55	5.31	10.36	17.45	9.70	3.05	52.58
	57.5	6.39	10.33	16.77	9.98	3.35	54.14
	60	5.83	11.08	-	P	2.26	59.89
[G$_2$/M$^{0.70}$]	30	5.42	11.08	11.44	2.67	1.63	22.57
	40	5.79	11.97	13.45	4.78	1.85	33.85
	50	5.83	11.54	17.13	7.24	1.91	47.15
	55	5.77	11.46	19.73	7.75	2.18	54.31
	57.5	6.16	10.15	-	P	2.74	58.30
	60	5.72	12.43	-	P	2.03	58.80

The backlight technique was found to be inadequate to examine the damage extent of [M$^{0.70}$/G$_2$] samples in which the stainless-steel mesh layer comes into contact with the indenter. When illuminated from behind, the current method effectively highlights cracks in the front layer. However, since the metal mesh itself significantly affects the transparency of the laminate, placing it on the impact side doesn't assist with the exposure of damage details. Figure 5.10 illustrates the extent of damage for the selected stacking sequences at various LVI energies. Finally, analyzing the post impact behavior of the laminates showed that [M$^{0.70}$/G$_2$] laminates undergo substantial permanent deformation in contrast to the other two alternative layup options. It is evident that, due to its elasto-plastic response, the metal mesh layers can push the relatively stiff Glass/PP layers back.

For [G$_2$/M$^{0.70}$] laminates, where the reinforcing metal layer experiences tension load, cracks occur within the PP material. Under higher impact energies, the enlarged cracks result in a fully

visible debonding between the stainless-steel mesh wire and PP resin. Furthermore, after a certain level of plastic deformation, the metal wires snapped in 0 or 90 degrees with respect to the fiber orientations. Necking, which is a signature of plastic deformation of metallic parts under tensile loading, was also depicted at the tip of the mesh wire breaking points.
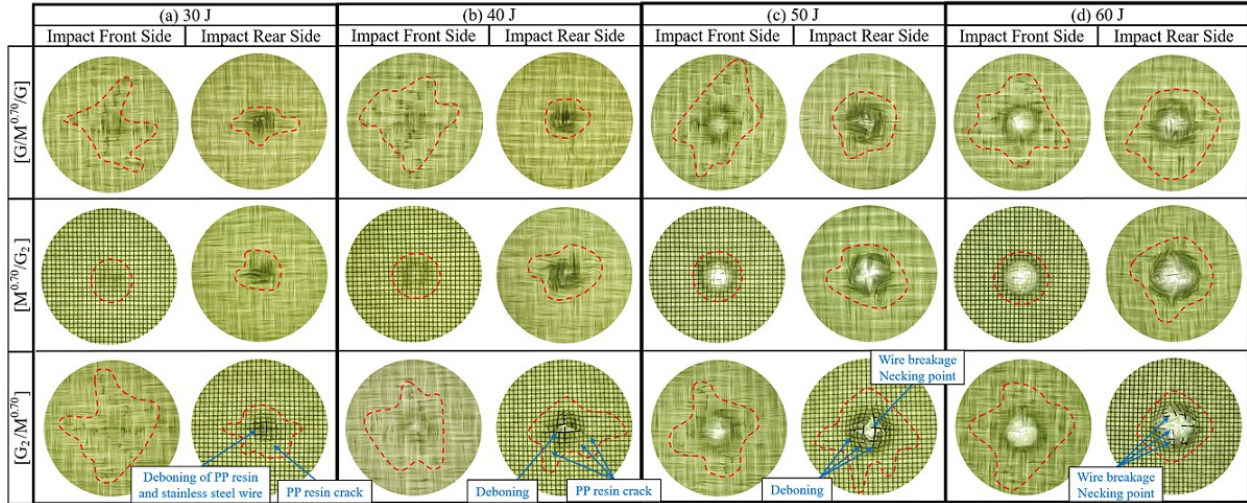
Figure 5.10. Comparison of the damage extent of $[G/M^{0.70}/G]$, $[M^{0.70}/G_2]$, and $[G_2/M^{0.70}]$ hybrid composite laminates under various LVI energies.

5.4.3   Layers' orientation effect

In order to address the effect of layup orientation on the penetration energy threshold, the reinforcing mesh layer was reoriented by 45 degrees with respect to the Glass fiber direction. Although hybridization in general causes mechanical property deviation, rotating the stainless-steel mesh layer develops the mentioned property mismatch. Consequently, the $[G/M^{0.70}_{45°}/G]$ hybrid composite plates show proportionally lower initial failure forces, as displayed in Figure 5.11. Besides, $[G/M^{0.70}_{45°}/G]$ laminates reach a semi-plateau state, where the force resonates around the maximum bearable value for a reasonable displacement before the rebound or penetration. On the other hand, the load carrying capacity of $[G/M^{0.70}/G]$ sample notably drops after touching the maximum force limit; therefore, the maximum load threshold is reduced in contrast to the hybrid laminates in which woven metal mesh wire orientation aligns with the fibers of the composite layer.
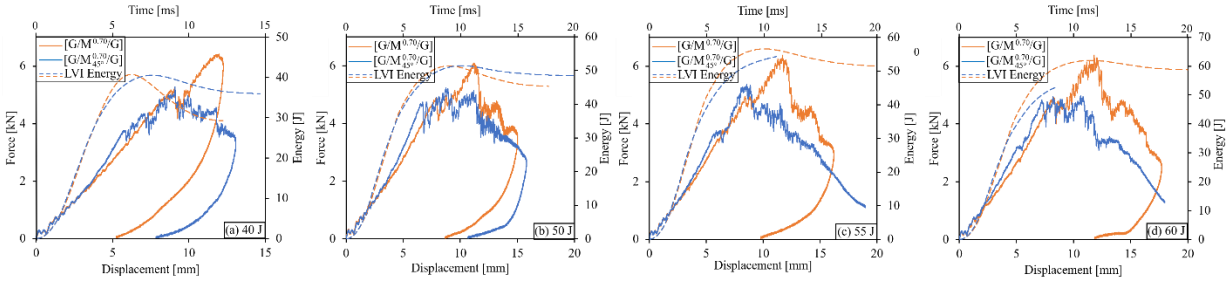
Figure 5.11. Assessment of metal mesh orientation effect on LVI behavior of hybrid composite laminates subjected to (a) 40 J, (b) 50 J, (c) 55 J, and 60 J impact energies.

Table 5.6.
Summary of LVI recorded data for $[G/M^{0.70}_{45°}/G]$ hybrid composite laminate under various impact energies.

Laminate stacking sequence	Impact energy [J]	Peak force [kN]	Disp. at peak force [mm]	Max. displacement [mm]	After-impact dent depth [mm]	After-impact dent's edge depth [mm]	Dissipated energy [J]
$[G/M^{0.70}_{45°}/G]$	40	5.27	9.09	13.07	4.67	1.47	35.46
	50	5.23	8.76	15.81	6.83	2.11	47.05
	55	5.38	8.58	-	P	1.57	54.32
	60	4.97	10.62	-	P	1.42	52.92

It has been empirically proven that positioning the reinforcing stainless-steel mesh layer with an angle to the Glass fibers increases the severity of damage at the exact impact zone. More information about the effect of layer orientation on the LVI performance of the hybrid laminates was provided in Table 5.6. While the $[G/M^{0.70}_{45°}/G]$ laminates undergo localized damage, the $[G/M^{0.70}/G]$ ones experience damage in a broader zone. The higher the mismatch between the layers' material properties gets, the more delamination is expected to grow. Thus, reorienting the strengthening metal mesh layer in a way that wires align with the Glass fibers suppresses the interlaminar damages in comparison to the $[G/M^{0.70}_{45°}/G]$ laminates. Moreover, the evaluation of damage extent in Figure 5.12 revealed that damages propagate within a relatively limited vicinity of the impact zone. Lastly, the LVI test results confirmed that the impact energy required for the indenter to fully perforate the $[G/M^{0.70}/G]$ samples is 15.4 % higher than the $[G/M^{0.70}_{45°}/G]$ laminates.
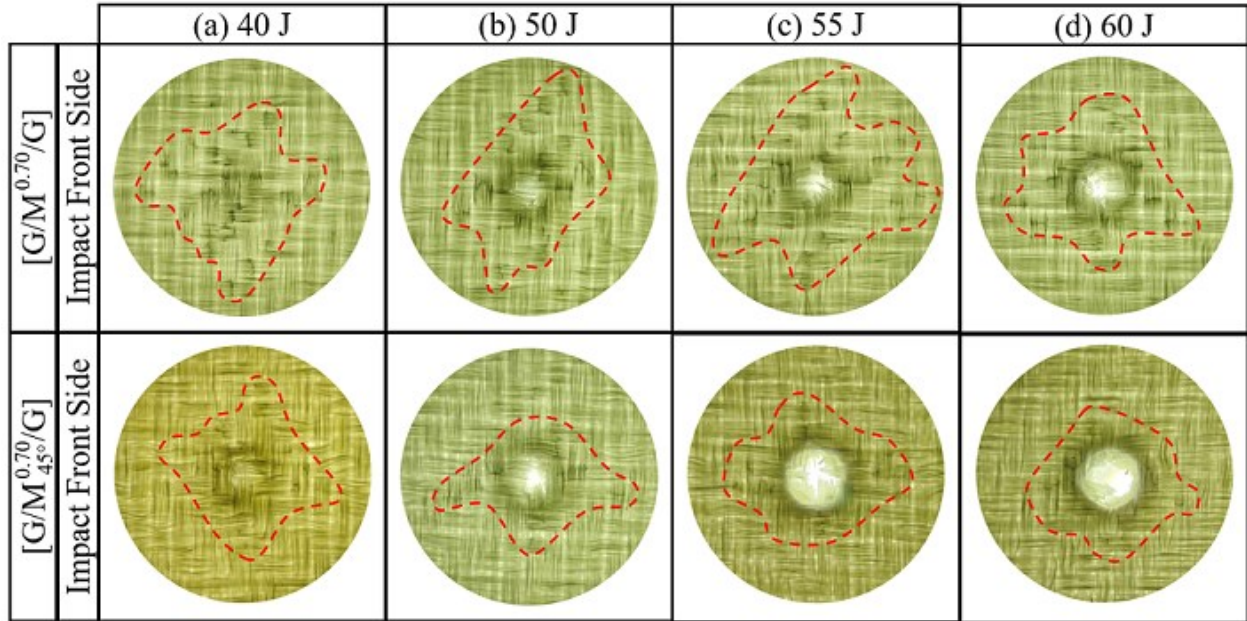
Figure 5.12. Damage extent of [G/M$^{0.70}$/G], and [G/M$^{0.70}_{45°}$/G] hybrid laminates under (a) 40 J, (b) 50 J, (c) 55 J and (d) 60 J impact energies.

5.4.4 Effect of metal mesh layer counts

It has been observed that hybridization can positively improve the perforation energy threshold under LVI loading conditions. Yet, the effect of replacing the single stainless-steel mesh reinforcement layer with a number of stacked thinner ones has remained unknown. In the current research, since the studied mesh wire diameters are double the size of the thinner ones, two layup sequences of [G/M]$_s$ and [M/G]$_s$ were also investigated. The LVI perforation energy for [G/M$^{0.16}$]$_s$ and [M$^{0.16}$/G]$_s$ laminates didn't experience a notable deviation from the [G/M$^{0.35}$/G] plate. Nevertheless, the [M$^{0.35}$/G]$_s$ and [G/M$^{0.35}$]$_s$ hybrid laminates respectively withstand 15.3 % and 7.7 % lower LVI energies compared to the [G/M$^{0.75}$/G], before the indenter fully penetrates the samples. In the previous sub-sections, it has been determined that the [G/M/G] is the optimal lamination sequence scenario among the possible options. Shifting the metal mesh to the mid-plane recedes the Glass/PP layers further from the neutral line, which is beneficial to the LVI response of the hybrid laminates. Thus, as expected, lower impact energy is required to perforate the [M$^{0.35}$/G]$_s$ laminate.

Table 5.7.
Summary of LVI test results of $[G/M^{0.35}]_s$ and $[M^{0.35}/G]_s$ plates at different impact energies.

Laminate stacking sequence	Impact energy [J]	Peak force [kN]	Disp. at peak force [mm]	Max. displacement [mm]	After-impact dent depth [mm]	After-impact dent's edge depth [mm]	Dissipated energy [J]
$[M^{0.35}/G]_s$	30	4.55	10.47	11.95	0.86	0.51	24.72
	40	5.37	12.20	13.99	6.43	2.18	34.41
	50	4.64	9.92	20.53	10.03	2.29	49.79
	52.5	5.57	12.37	18.28	8.53	3.40	50.73
	55	4.67	9.24	-	P	2.13	53.81
	60	5.67	10.43	-	P	1.19	56.13
$[G/M^{0.35}]_s$	30	5.17	10.74	11.14	1.40	0.56	21.53
	40	5.73	11.53	13.09	2.90	0.89	32.95
	50	6.17	12.16	16.05	4.57	1.02	45.04
	55	6.36	12.66	17.69	6.30	1.17	51.54
	57.5	6.34	12.18	18.37	5.44	1.65	54.26
	60	5.87	11.81	-	P	0.89	60.48

As demonstrated in Figure 5.13, $[G/M^{0.35}]_s$ laminates, featuring two layers of stacked impregnated mesh located at the mid-plane, mimic the force-displacement pattern of $[G/M^{0.70}/G]$ plates below the impact perforation level. However, $[G/M^{0.35}]_s$ composite laminates are more susceptible to penetration if struck by a projectile. This vulnerability is attributed to the manufacturing procedure of the woven metal mesh layers, which involves relatively more cold work to shape the wires. Hence, the mesh layers with the wire diameter of 0.35 mm undergo less plastic deformation, absorbing considerably smaller portion of the applied energy during an LVI test.
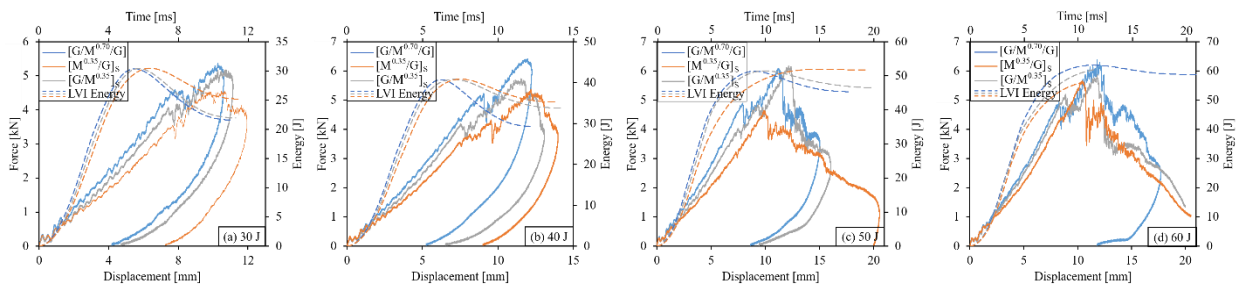
Figure 5.13. Evaluation of the LVI response of $[G/M^{0.70}/G]$, $[G/M^{0.35}]_s$ and $[M^{0.35}/G]_s$ laminates under (a) 30 J, (b) 40 J, (c) 50 J and (d) 60 J impact energies.

Indentation correlates with the absorbed energy during the LVI loading and can serve as a quantitative indicator of the severity of laminate damage. Specifically, the depth of indentation presented in Table 5.7 provides insights into the hybrid laminate's capacity to absorb and dissipate

impact energy. Despite the improvement in damage detection using the backlight method, its functionality is reduced, particularly when examining the hybrid laminates strengthened with mesh layers located externally. Yet, the backlight method remains a reliable technique for initial damage assessment, even though it lacks precision in quantifying these regions. Its ability to identify damaged areas helps in directing further analysis and facilitates a comprehensive understanding of laminate's response to the LVI loading. Figure 5.14 shows that a combination of compression failure, delamination, and PP cracks within the tensile loading side are the initial damages of $[M^{0.35}/G]_s$ laminates. These damages grow with increasing impact energy, which ultimately leads to the breakage of the reinforcing mesh wires in both warp and weft directions.

The extent of damage is quite different for the laminates with metal mesh layers positioned in the middle. In addition to the damage at the collision zone, cracks occurred in the composite layers can be easily detected. Since cracks significantly alter the local transparency of the sample, they have been darkened, making them clearly noticeable when illuminated from behind. Although both the $[G/M^{0.35}]_s$ and $[G/M^{0.70}/G]$ laminate have been reinforced with a 0.7 mm thick impregnated metal mesh layer, they do not show identical LVI responses. In contrast to the $[G/M^{0.35}]_s$, $[G/M^{0.70}/G]$ hybrid composite samples experienced more extensive permanent deformation, distancing from the impact point. Because during the manufacturing procedure of mesh, more cold work is done forming the 0.35 mm metal wires, their plastic behavior is less than the 0.7 mm ones; therefore, damages do not propagate in $[G/M^{0.35}]_s$ as easily as they do in the $[G/M^{0.70}/G]$ samples, which is also confirmed by the impact dent and near dent permanent deformations after running the LVI tests.
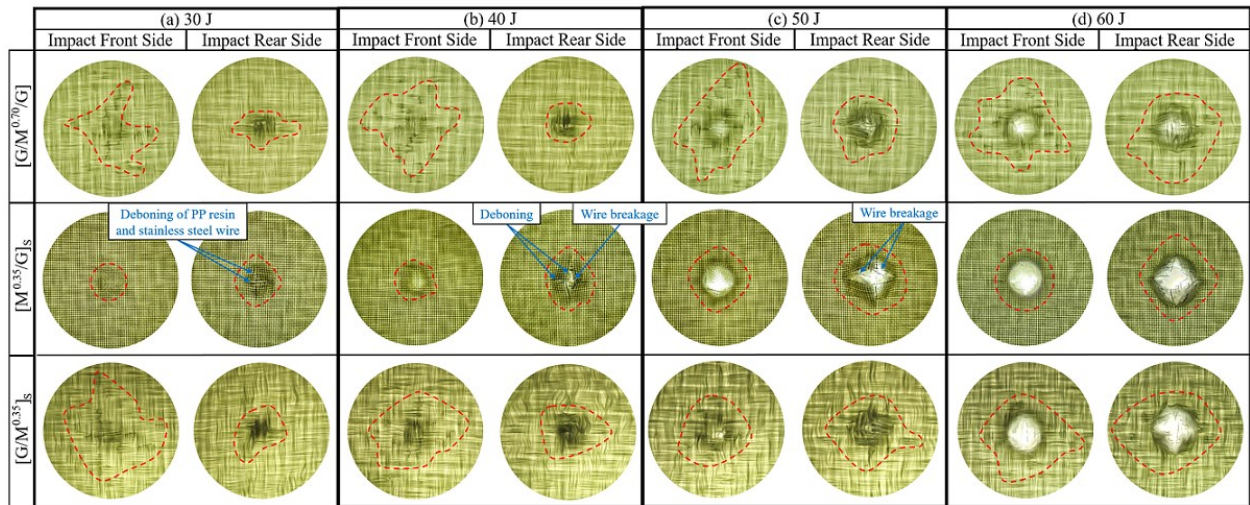
Figure 5.14. Examination of the damage response of the [G/M$^{0.70}$/G], [G/M$^{0.35}$]$_s$ and [M$^{0.35}$/G]$_s$ hybrid composites subjected to (a) 30 J, (b) 40 J, (c) 50 J and (d) 60 J impact energies.

In conclusion, hybridization has proven to be positively effective in the LVI response of thermoplastic composite plates. Due to the elasto-plastic response of the strengthening stainless-steel mesh layers, the hybrid composite laminates' energy-absorbing behavior has been improved. Figure 5.15 provides a comprehensive comparison of the LVI energy required for the indenter to fully penetrate through the laminate. Among all the stacking sequences investigated in this chapter, the [G/M$^{0.70}$/G] hybrid composite laminate demonstrated the ability to withstand higher impact energies. Finally, Finite Element Modeling (FEM) is outlined to comprehensively explore and optimize the outcomes of this study, thereby maximizing its potential contribution to further research in the field.
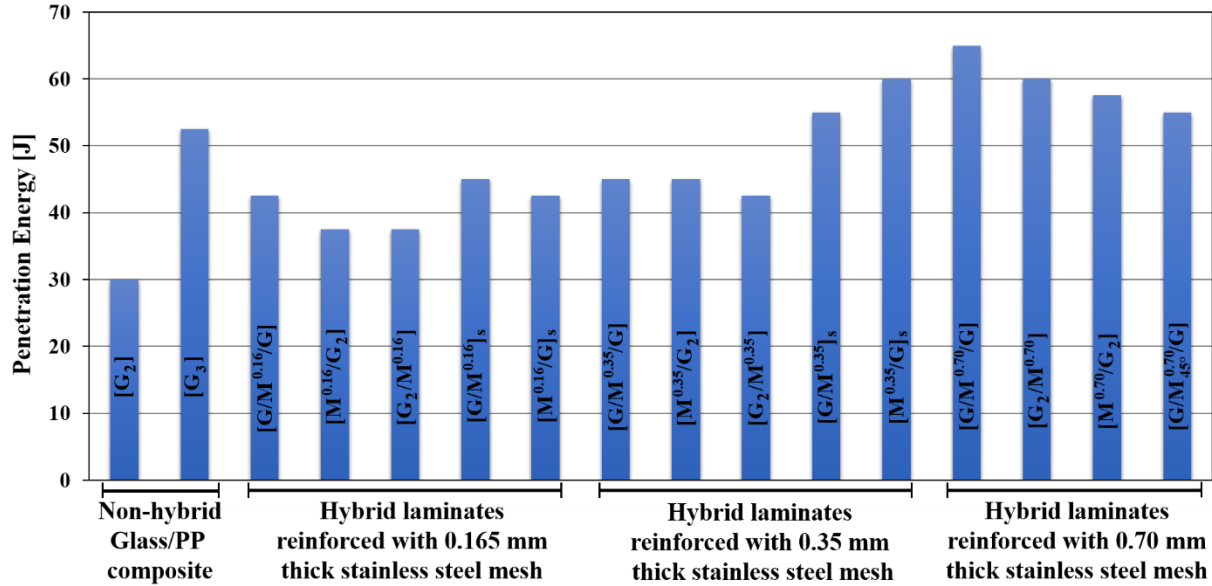
Figure 5.15. A comparison of the LVI perforation energy threshold of various hybrid composite laminates.

5.5 Conclusion

A new multi-step fabrication method was considered in this study to fabricate hybrid Glass/PP thermoplastic composites strengthened with stainless-steel mesh layers. The current multi-step hot press procedure established a bonding between the impregnated metal mesh and composite layers. In this research, the effect of hybridization of thermoplastic composite laminate reinforced with stainless-steel mesh has been thoroughly examined under the LVI loading. Additionally, various factors such as metal mesh wire diameter size, stacking sequence, layup orientation and number of reinforcing layers were investigated. The backlight method was used to evaluate the damage formation in these hybrid laminates.

It was revealed that the hybrid composite laminates outperform the non-hybrid laminates, exhibiting a greater ability to withstand higher impact energies before reaching the perforation state. Specifically, the $[G/M^{0.70}/G]$ hybrid composite laminate demonstrates superior energy absorption compared to both $[G_2]$ and $[G_3]$ non-hybrid laminates. Furthermore, post-impact damage assessments depicted that the hybrid laminates absorb energy through plastic deformation and damage mechanisms, resulting a global response.

Even though the variations of the LVI penetration energy threshold are relatively small, placing the reinforcing stainless-steel mesh layer at the mid-plane improved the laminates' performance. Besides, layup orientation can considerably influence the LVI response of the laminates. In contrast to [G/M$^{0.70}_{45°}$/G], the [G/M$^{0.70}$/G] hybrid composite laminates not only withstand higher forces, but also behave differently after reaching the maximum bearable force. Finally, assessing the LVI behavior of hybrid laminates with different numbers of mesh layers revealed that the laminates with thicker mesh wires require higher impact energies to penetrate. The [G/M$^{0.70}$/G] hybrid composite laminate outperformed all the permutations examined in the current research. These laminates absorb impact energy due to the specific elasto-plastic response of the reinforcing layer. Hence, because of the energy-absorbing behavior of stainless-steel mesh layer, hybridizing the thermoplastic-based composite laminates with metal mesh improved the penetration energy threshold under LVI loading conditions.

Chapter 6:

Effect of Hybridization on the Low-Velocity Impact Behavior of Reinforced PET Foam Core Sandwich Panels

6. Effect of Hybridization on the Low-Velocity Impact Behavior of Reinforced PET Foam Core Sandwich Panels

This chapter, published with the title of "Recycled PET Foam Core Sandwich Panels with Reinforced Hybrid Composite Facesheets: A Sustainable Approach for Enhanced Impact Resistance" takes advantage of the selected metal mesh size in previous research to reinforce composite PET foam core sandwich panels. With respect to this choice, the LVI behavior and perforation threshold of such hybrid composite sandwich panels were studied. Moreover, the type of failures and extend of after impact damages were defined by taking pictures of the cross-section of the panels showing damages, particularly those related to the reinforcing metallic layers.

6.1 Abstract

This research explores the Low-Velocity Impact behavior of thermoplastic composite sandwich panels with 100 % recycled Polyethylene Terephthalate (PET) foam sourced from post-consumer plastic water bottles. Being recognized as a reliable technique, hybridization using stainless-steel mesh layers was employed to reinforce the panels' composite facesheets of sandwich panels accessible for modular housing, cold storage rooms and cargo trucks. Adequate impregnation of the reinforcement metallic mesh layer alongside proper skin-to-core adhesion was accomplished by optimizing a two-phase compression molding method. The effect of hybridization on impact response of sandwich panels with two different PET foam core thicknesses, and stacking sequence were evaluated. It was revealed that reinforcing the impacted surface of the composite sandwich panels significantly increased the perforation threshold. Moreover, analyzing the post-impact section view of the samples indicated that hybridization modified the damage propagation response of the PET foam core sandwich composites, through which the energy absorption capacity was improved.

6.2 Introduction

Composite sandwich panels have been engineered to meet the demand for lightweight structures with superior flexural performance. The performance of sandwich panels with various combinations of skin, core material, and adhesive layer has been investigated for decades

[97,98,101,106,108]. It has been revealed that enhancing the bonding between the layers has a crucial role in load distribution, altering or delaying the expected failure mechanisms under bending conditions [103,105,110]. PET foam core sandwich panels, reinforced with Glass fiber composite facesheets, were extensively used in certain industrial applications such as wind turbines, and modular prefabricated building structures [24,104,111].

Moreover, thermoplastic composites are becoming a trend, particularly valued for their outstanding mechanical properties, manufacturability, and environmental sustainability. The recyclability potential of PET materials proposed a growing shift towards incorporating eco-friendly PET foam, which was recycled from bottle caps [25–29]. The feasibility of fabrication and recycling of Glass fiber composite sandwich panels with PET foam core has been studied by Kang et al., who designed a specific extraction mold for this purpose [31]. Moreover, several research studies were conducted to evaluate the impact of PET foam core thickness, composite skin, manufacturing techniques and parameters on the quality and failure sequence of these sandwich panels [93,112,113].

Despite the composites' outstanding properties, which makes them a reliable choice for various industrial cases, they are susceptible to impact damages occurring during installation, maintenance, and working life. In addition to the striking object's physical and geometrical properties, the behavior of composite laminates under Low-Velocity Impact (LVI) loading can be significantly influenced by the resin and fiber material, volume fraction, direction, stacking sequence, and fiber architecture. The LVI test was designed and performed to assess these mentioned factors while controlling the temperature, environmental and boundary conditions [2,3,6,39,130,131,136,154]. Reinforcing techniques such as the integration of carbon nanotubes into the fabrication procedure of glass fiber composites have proven to be beneficial to the impact behavior of these structures [157,158].

Mines et al. investigate the impact response, and damage sequence of the composite sandwich panels with different core materials, experiencing two separated peaks during the LVI tests [8]. Furthermore, numerical and experimental investigations were performed for composite sandwich panels, where impact damages were mostly observed and governed by the top face sheet and core [57,98,159–162]. Respectively, a comprehensive comparison of sandwich structures with different core configurations has been performed by Gua et al. [162]. Thermoplastic-based composite

laminates have shown a superior impact resistance, because of their specific higher toughness [52,138,139]. Dogan and Arikan exhibited that foam core sandwich panels with thermoplastic-based composite skin outperform the thermoset ones, particularly in terms of energy absorption [56].

On the other hand, the hybridization of composite laminates, using metallic reinforcement wires or layers, had proven to improve the elasto-plastic response of the plates. It has been shown that strengthening the composite plate with layers of resin-impregnated metallic mesh can improve the impact perforation threshold [11,68,69,71–73,148]. Under low-velocity and high-speed ballistic impacts, hybrid composite plates and sandwich structures either with metallic cores or reinforced skin depicted a notably enhanced resistance [146,148,163]. Moreover, these hybrid laminates experienced increased stiffness and ultimate strain properties, consequently affecting their tensile, flexural and LVI performance [9,10,75,149]. Examinations revealed that the metal mesh wire diameter, stacking sequence and orientation significantly affect the LVI response of composites [117,123]. Yet, there are certain research gaps when it comes to sandwich panels with hybrid composite facesheets.

In the present study, 100 % eco-friendly closed-cell PET foam, recycled from post-consumer plastic water bottles, was chosen as the sandwich structure core material. By integrating recycled materials into high-performance composites, this research demonstrates the feasibility of sustainable manufacturing without compromising mechanical performance. Eliminating the need for an adhesive layer in bonding the reinforced composite skin to the PET core offered a more sustainable lamination process. Due to the high viscosity of thermoplastic Polypropylene resin, a two-step compression molding lamination technique has been introduced and optimized to fabricate hybrid composite facesheets. Since the lamination process requires proper impregnation of stainless-steel mesh before the final manufacturing step, microscopic evaluation and flatwise tensile tests were performed to ensure the quality of impregnation, and adhesion between the layers.

Furthermore, this research mainly focused on the effect of hybridizing full-thermoplastic PET foam core sandwich composites with layers of stainless-steel mesh under LVI loading conditions. In addition to the hybridization, the influence of recycled PET foam core, skin thickness, and impactor collision sequence have been assessed. Hence, a series of LVI tests were conducted to examine the impact behavior and perforation energy threshold of the hybrid

composite PET core sandwich panels. Lastly, a comprehensive visual evaluation of the sectioned view of panels, microscopic assessments of metal wire breakage and measurement of permanent dents which are reflective of damages and plastic deformations were performed. Getting deep into these results significantly helped capture the damage propagation of hybrid and non-hybrid panels subjected to various impact energies.

6.3 Materials and fabrication process

In the present study, fully recycled closed-cell PET foam material with thicknesses of 10 mm and 20 mm has been used as the core. A novel patented process introduced by Armacell Co. was used to manufacture the PET foam material entirely from post-consumer recycled plastic bottles [27,120]. By employing a foaming agent on the PET granules, the waste water bottles were transformed into PET foam and extruded to continuous foam boards. These foam boards are subsequently cut and welded to the required dimensions by the thermoplastic materials welding procedure. In this manuscript, the uppercase numeral on the PET foam core indicates the nominal core thickness in millimeters. The selection of these PET foam cores was made not only to evaluate the effect of thickness on the LVI results of sandwich panels but also to assess the influences of reinforcing mesh layer relative distance to the neutral line under impact conditions.

The composite laminate used as the facesheet of the sandwich panels consisted of a single layer of 2/2 twill weave E-Glass/Polypropylene (Glass/PP). The notation "G" was used to denote the 1 mm thick commingled Glass/PP layer with a fiber weight fraction of 60 percent. The hybrid laminates incorporate a plain weave mesh made of 304 stainless-steel, featuring a wire diameter of 0.7 mm, which was designated as "M". A compression molding technique was used to fabricate the sandwich panels. As depicted in Figure 6.1, stacked layers of dry weave Glass/PP, pre-impregnated stainless-steel mesh and recycled PET foam material were effectively bonded under an optimized condition. It is worth noting that the lamination of hybrid sandwich panels is a sequential two-step process, where the metal mesh layers were initially impregnated with PP resin during the initial phase.

1. Heating blocks
2. Teflon sheet
3. Impregnated metal mesh with PP resin
4. PET foam core
5. Woven Glass/PP cloth
6. Mold
7. Hydraulic press
8. Pressure gauge
9. Thermocouple
10. Water cooling system
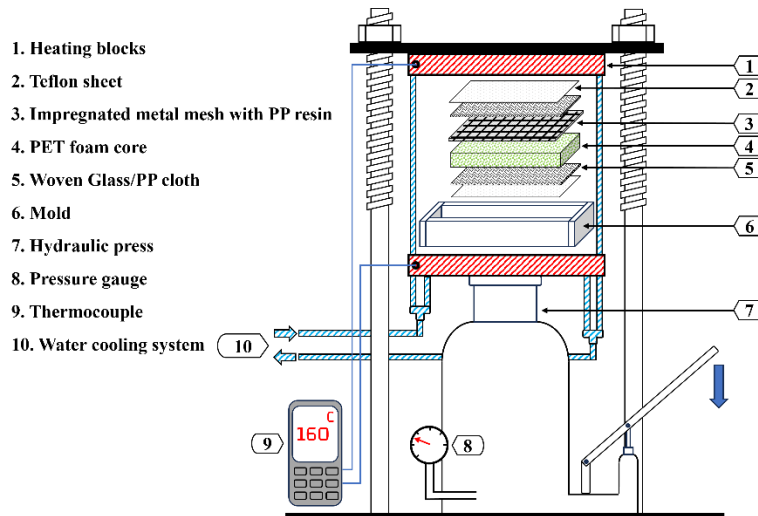
Figure 6.1. Schematic display of the hot press machine used to manufacture hybrid PET core composite sandwich panels.

Primarily, the metal mesh layers were properly impregnated with PP resin, where 1.6 mm thick PP sheets were heated to a temperature range of 160-165°C and pressed into the metal mesh under a constant pressure of 1.5 MPa for 3 minutes. The hot press molding plates were cooled by water flow, gradually returning to room temperature at a cooling rate of 15°C/min. Lastly, the excess PP resin was trimmed to be prepared for the production of the hybrid sandwich panels.

In order to laminate the PET foam core sandwich panels, the stacked layers of raw material were subjected to a controlled temperature of 160-165°C. This specific temperature is required to completely melt the PP resin in the commingled Glass/PP cloth. The consolidation phase lasted for 1 minute under a maintained pressure of 0.5 MPa, and a steel mold closely matching the final panels' thickness. The selection of proper mold thickness is significantly important and governed by the PET core thickness, and the number of facesheets considered for sandwich panels' lamination. The mold generally helps with control over the resin flow while preventing the PET foam crush under the compression loading during the fabrication procedure. Furthermore, 0.08 mm thick Teflon films were employed to ensure a non-stick interface between the composite skin and heating elements. Finally, the PET core sandwich panels were cooled down at the rate of 15°C/min to the ambient temperature.

The capability of the compression molding technique in manufacturing fully thermoplastic PP-based composite sandwich panels with PET foam core was previously investigated. Even though the adhesion film was eliminated, sandwich panels with proper facesheet quality and skin-to-core bonding were manufactured by this fusion bonding technique [118,124,164]. Yet, introducing a resin-rich impregnated mesh layer to the stacking sequence, required additional assessment steps to ensure manufacturing parameters for hybrid sandwich panels. The optimized parameters, particularly the mold thickness, were precisely determined by a series of trials and errors. Specific details of the raw materials used in the current study and the final dimensions of hybrid and non-hybrid sandwich panels were presented in Table 6.1.

Table 6.1.

Mechanical properties and dimensional characteristics of the raw materials and final sandwich panels.

Material	Type	Nominal thickness [mm]	Wire diameter [mm]	Mesh size	Opening size [mm]	Open area
Metal mesh	304 stainless-steel	1.40	0.70	12 × 12	1.40	44%
		Nominal thickness [mm]	Density [kg/m^3]	Tensile strength [MPa]		Melting temperature [°C]
PP sheet	100% Polypropylene	1.588	0.913	27.58		160-165
		Nominal thickness [mm]	Fiber weight fraction [%]	Tensile strength [MPa]		Compression strength [MPa]
E-Glass/PP	2/2 twill weave commingled cloth	1.00	60	203.8 [123]		60.2 [164]
		Nominal thickness [mm]	Density [kg/m^3]	Compression strength [MPa]	Shear strength [MPa]	Melting temperature [°C]
100% recycled PET foam	ArmaPET struc GR80	10 20	80	1.0 [120]	0.6 [120]	240-250

Panels stacking sequence	Sandwich panel thickness [mm]	Areal density [kg/m^2]
[G/PET^{10}/G]	12.30 ± 0.07	3.76 ± 0.05
[G/M/PET^{10}/G]	13.64 ± 0.03	6.55 ± 0.02
[G/PET^{20}/G]	21.14 ± 0.06	4.42 ± 0.06
[G$_2$/PET^{20}/G]	22.24 ± 0.08	6.04 ± 0.06
[G/M/PET^{20}/G]	22.47 ± 0.11	8.14 ± 0.04

6.4 Experimental procedures

6.4.1 Microscopic study

Because of the high viscosity nature of the thermoplastic PP resin, the fabrication parameters should be optimized to prevent unexpected defects such as fiber washout, leading to undesirable in-plane fiber waviness and resin reach regions. These defects deteriorate the quality of the composite skin, negatively affecting the performance of sandwich panels. Furthermore, the fabrication key parameters should be set carefully for the PP resin to fully impregnate the metal mesh open areas without any voids or trapped air within the hybrid composite facesheets. Previous evaluation has shown that not-optimized manufacturing parameters could cause improper impregnation for composite skin which can be resolved through fabrication method optimizations. It is worth noting that several assessments of the manufacturing process were conducted to minimize the potential for defects and voids during lamination [123,164].

As presented in Figure 6.2, microscopic evaluations were performed on the cross-section of the hybrid sandwich panels to ensure the quality of lamination. Within this visual inspection, it was revealed that with this two-step compression molding process, the open areas of the stainless-steel mesh were effectively filled with PP resin. In hybrid laminates reinforced with layers of metal mesh, trapped air bubbles or voids were most likely expected close to the metal mesh wires. Nevertheless, the magnified parts depict a thorough impregnation of metal wires' open areas with the PP resin ensuring a void-free structure and a robust interlayer connection. Moreover, there was no evidence of detectable voids in the composite facesheet. A close assessment of the interface of the PET foam and hybrid skin depicted a properly formed adhesion which is an indication of the reliability of the employed fabrication procedure.
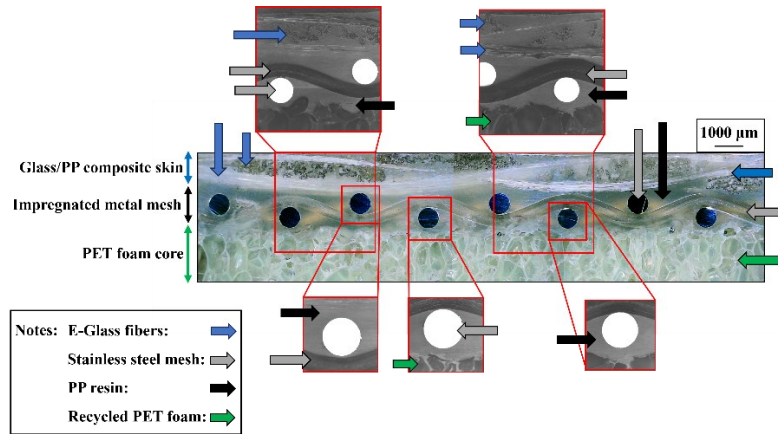
Figure 6.2. Microscopic section view of the manufactured hybrid composite PET core sandwich panel.

6.4.2 Flatwise tensile test

The hybrid laminate's skin-to-core bonding has been evaluated by conducting flatwise tensile tests, comparing the results to the non-hybrid sandwich panel test results. These tests were performed in accordance with the ASTM C297 standards [94]. Samples of 1 inch × 1 inch were cut out of the sandwich panels and glued to the steel fixture blocks using DP 460 epoxy adhesive. The blocks are secured within the moving heads of the MTS universal testing machine instrumented with a 5 kN load cell, running the test at a head displacement rate of 0.5 mm/min. The data acquisition system collects the force and displacement at the frequency of 2000 Hz. The average measured flatwise strength of the hybrid composite panels was 0.96 MPa, closely following the previous studies on non-hybrid samples [164]. Thus, the two-step compression molding method has proven its capability of fabricating hybrid composite sandwich panels with proper skin-to-core adhesion.

6.4.3 Low-Velocity Impact tests

LVI tests were performed using the Instron 9340 drop tower impact machine with respect to ASTM D7136 and D3763 standards [152,153]. Sandwich panels were cut into dimensions of 110 mm × 110 mm, to be secured in place by a pneumatic circular clamp with an inner diameter of 76 mm. Figure 6.3 demonstrated details of the impact tests machine with a 16 mm diameter hemispheric tup. LVI tests were performed at the impact energy range of 15 J to 90 J. The impactor

velocity and drop weight height were maintained in a determined range, respectively from 3.03 m/s to 3.11 ms, and 468 mm to 493 mm. Because of that, additional weights were required to increase the striker's total weight from 3.265 kg to 19.265 kg. The striker's initial impact velocity was measured by the Piezoelectric sensor detecting the flag point passing by it. The force-time data were recorded at the sampling frequency of 2000 kHz, employing a 22 kN load cell. The impactor velocity, displacement and energy were finally calculated by the collected data [6,154].
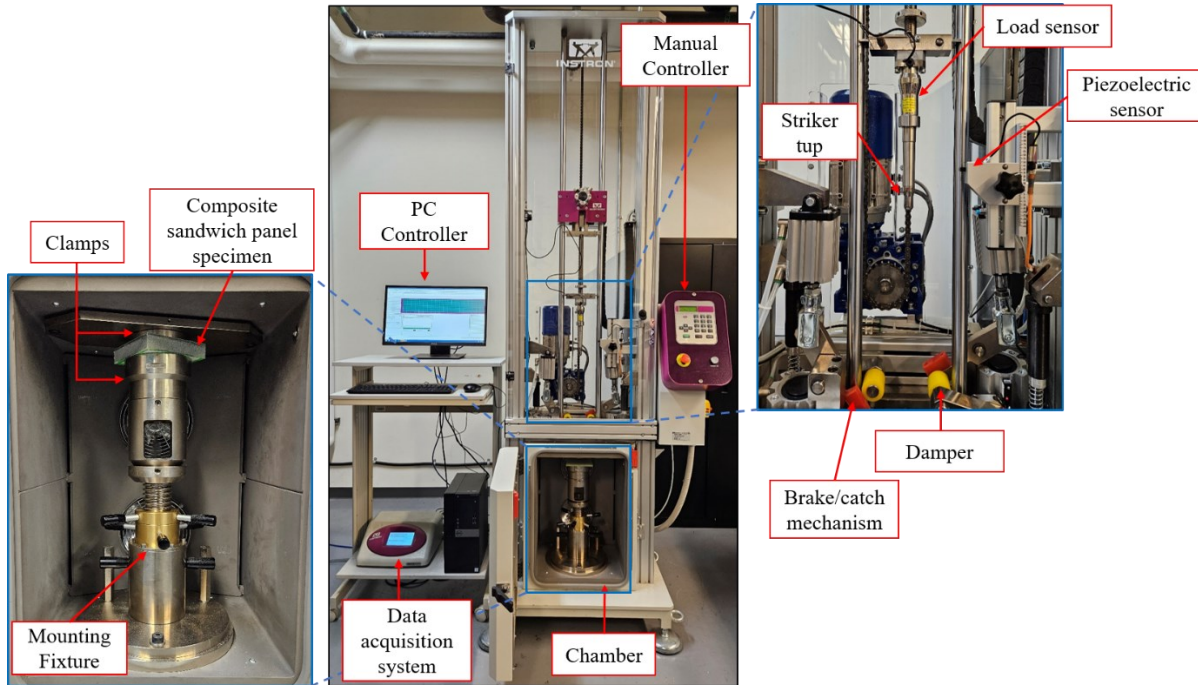
Figure 6.3. Instron 9340 drop weight impact test machine equipped with 16 mm diameter hemispheric tup and 76 mm inner diameter circular clamp.

To assess the permanent deformation and damage, the impacted sandwich panels' indentations were measured using a dial gauge with a precision of 0.001 inches. Moreover, the deformation of the surrounding impact region, within a radius of 10 mm of the center point, was measured to evaluate the global deformation of the samples. Because the composite skin is white-colored, taking pictures of the impacted surface and rear view cannot illustrate the extent of damage in the structures' facesheets. Hence, using a water-cooled diamond saw, the samples were cut in half to assess the section view and examine the LVI damages.

6.5 Results and discussion

It has been noted that the sandwich panels' response to LVI is a combined reflection of skin performance, core material and their bonding. Mines et al. compared the quasi-static and LVI response of the foam core and honeycomb core sandwich panels [8], where a sequential failure pattern was determined for each sandwich panel. It was depicted that the propagation of damage within the panels was a complex sequence of local indentation of the collision side, leading to skin-to-core debonding, failure of rear composite skin and core crush. This specific response of sandwich panels leads to a unique LVI behavior where two force peaks can be recorded, which were separately related to each facesheet response. Furthermore, the flexural performance of sandwich panels will influence the impact results, which can be governed by the facesheet properties and core thickness. The influence of resin type has been well assessed showing a significant variation in the LVI diagram with two distinguished peak forces [56].

The 2 by 2 twill weave comingled E-Glass/PP materials are widely used in industrial applications due to their availability and relatively lower price. Although other alternatives such as Kevlar offer superior energy absorption properties, its higher cost makes glass fiber a practical choice [5]. Furthermore, textile fiber composites generally outperform unidirectional laminates because of their woven structure [133]. It is also easier to handle and manufacture, making it more suitable for applications where both impact resistance and manufacturability are important. In comparison to thermosets, thermoplastic composites offer enhanced toughness and energy absorption [5,48,50,56]. The examined material allows continuous production with fabrication techniques like the automated double-belt method, significantly reducing manufacturing time and costs [7,118,164]. Moreover, thermoplastics composites are well-known for their environmental sustainability which gives the manufacturers the recyclability option.

Reinforcing the glass fiber composite laminates with stainless-steel mesh has been proven to effectively increase their perforation threshold under LVI loading conditions [117,123]. Nevertheless, the effect of hybridization on the thermoplastic-based PET foam core sandwich panels needs further investigation. Stainless-steel mesh is commonly available in the industry for a relatively reasonable price, offering corrosion resistance properties in humidity. This paper was a trial attempt aimed to assess the feasibility of hybridization, focusing on the specific

manufacturing process in a two-step fabrication and reinforced panels' response to impact performance.

In addition to the sandwich panels' specific flexural load-bearing properties, PET foam panels offer acoustic and thermal isolation. Moreover, materials used in this study either metallic mesh, thermoplastic PP-based composite skin, and the already recycled PET foam cores present a specific value in terms of environmental sustainability. In industry, these sandwich panels are commonly used as prefabricated structural elements in fast-building modular houses, cold rooms for storage, refrigerated cargo trucks, mini-truck floor panels and impact resistance walls covering large electrical facilities. Throughout their service life, installation or maintenance, these PET core sandwich panels are exposed to various impact events, such as drop of a tool, hail, runaway debris, or unexpected collisions. To enhance their durability, hybridization can be proposed as an effective strategy to improve the impact resistance, thereby delaying penetration and extending the panels' lifespan. Therefore, this study attempted to evaluate the effect of hybridization on the LVI performance of sandwich panels using a fully recycled PET foam core.

To assess the top facesheet perforation and the effect of composite skin thickness on the LVI response, $[G/PET^{20}/G]$ and $[G_2/PET^{20}/G]$ non-hybrid PET core sandwich panels were subjected to various impact energies. The investigation of the $[G_2/PET^{20}/G]$ configuration was not only aimed at understanding the influence of composite facing thickness, but also at facilitating a better comparison between the hybrid and non-hybrid sandwich panels with analogous skin thickness. Rebound, top facesheet penetration and full perforation of the panel are the common response scenarios expected from the LVI tests. During the rebound, the striker bounced back after hitting the surface of the sandwich panels. A specific portion of the impact energy is recovered by the striker which is the equivalent of required energy for tup bounce back. The rest is either dissipated or absorbed through damage, permanent deformation and friction. This rebound response has been captured at lower impact energy levels, where a portion of the applied energy was recovered by the elastic behavior of the sandwich panel, particularly the impacted surface.

Increasing the applied energy, the top facesheet perforates which causes a sudden load drop followed by a relatively prolonged steady load plateau. The load drop occurs since the facesheet composite material experiences a catastrophic damage state, locally losing its load-bearing capacity. In this study, the perforation of the top facesheet was considered the threshold where the

panel loses its structural integrity. At this point, the panel has absorbed all the impacting energy without any rebound detected after the strike. Nevertheless, the plateau is the reaction of core materials to being compressed or crushed under the striker force. Figure 6.4 presents the LVI response of [G/PET^{20}/G] sandwich panels, where the color red defines the perforation threshold of the top facesheet, clearly showing the mentioned plateau. Upon the striker penetrating the impact surface and being embedded in the PET core, all the impact energy is absorbed by the sample.
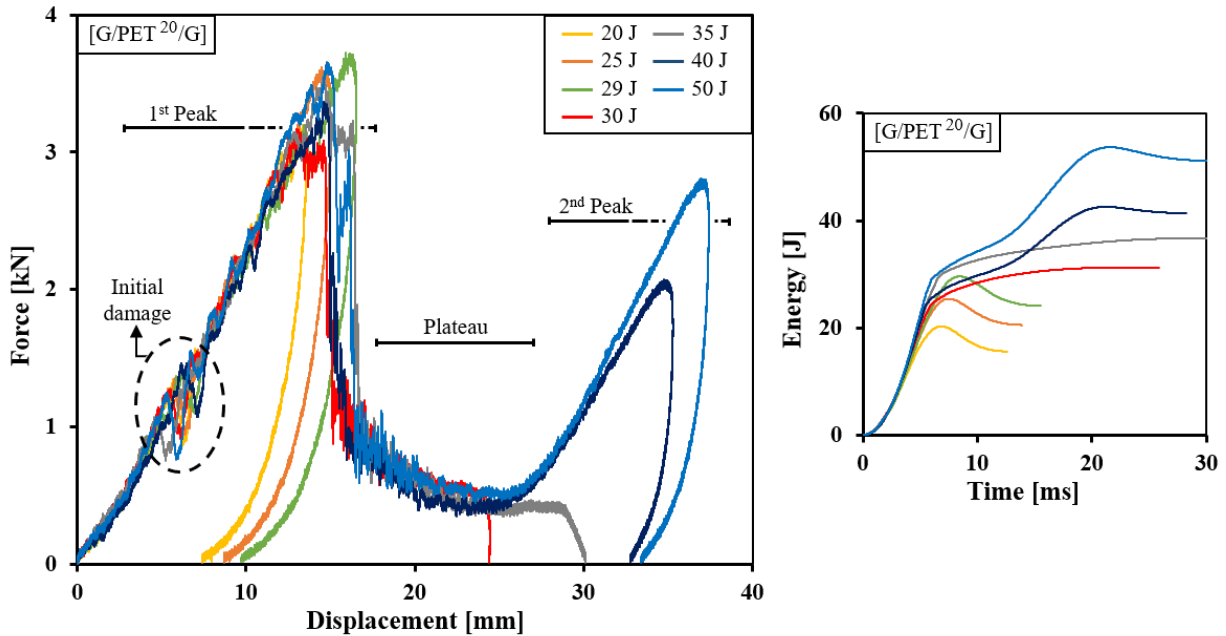
Figure 6.4. Force-displacement, and energy-time response of the non-hybrid [G/PET^{20}/G] composite sandwich panel under different impact energies.

The perforation of the top laminate was considered the sandwich panel perforation energy threshold. Although the rear facesheet may remain intact, the sandwich panel at this stage has lost its full performance. Moreover, in order to assess the post-perforation response and damage mechanisms of sandwich panels to the full puncture condition, LVI tests were continued at higher energies. It was revealed that under high-impact energies, the load increases once again experiencing a second peak following the plateau. Due to the elastic response of the rear composite skin, a small share of the energy can be returned to the striker, which leads to a displacement retraction in the diagrams. Nonetheless, if the energy is high enough, the striker fully perforates the panel, resulting in a secondary sudden load drop with no deformation recovery.

In addition to the mentioned general LVI response of foam core sandwich panels, it was determined that the first moderate load drop can be related to the local rigidity variations introduced to the laminate because of localized initial damage [165]. Upon this point, the panels' responses were considered to be elastic and without any damage development. Within the LVI response diagrams, this point can be also determined as the elastic loading limits. However, the consecutive load drops, followed by a sudden sharp one, were recognized to be a reaction to the initiations and propagation of the catastrophic damages. At this phase, which occurs at the first loading peak, it is common for the composite laminate skin to undergo matrix cracking, fiber breakage, fiber pull out and delamination. These damage mechanisms have been further elaborated, where the difference between hybrid and non-hybrid sandwich panels is examined in detail.

As anticipated, adding a second composite layer to the PET foam core sandwich panels skin enhances their perforation threshold. Figure 6.5 depicts the LVI response of the $[G_2/PET^{20}/G]$ composite panels under different LVI energies. Even though the composite facesheet layer is doubled in thickness, the $[G_2/PET^{20}/G]$ panel can withstand 75 % higher impact energies compared to the $[G/PET^{20}/G]$ before the first skin gets penetrated. Incorporating thicker composite skins led to a notable increase in initial damage and first peak load levels. Table 6.2 provides detailed information on each conducted LVI test. The data revealed that increasing the load-bearing capacity of the impacting surface results in less permanent deformation of the $[G_2/PET^{20}/G]$ sandwich panels compared to the $[G/PET^{20}/G]$ under the same impact energies.
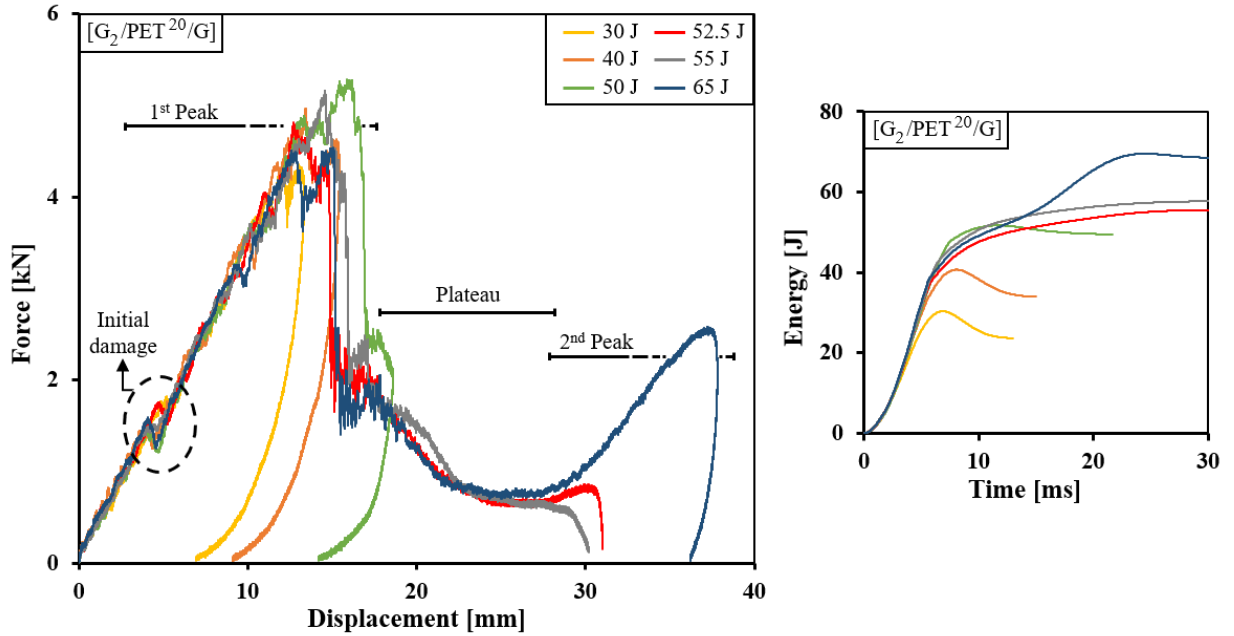
Figure 6.5. Force-displacement, and energy-time behavior of the non-hybrid [G$_2$/PET^{20}/G] composite sandwich panel at various LVI energies.

Table 6.2.

Summary of the LVI experiments on non-hybrid composite PET foam core sandwich panels under various impact energies.

Panels stacking sequence	Impact energy [J]	1st peak force [kN]	2nd peak force [kN]	Max. tup displacement [mm]	After-impact dent depth [mm]	After-impact dent's edge depth [mm]	After-impact rear side deformation [mm]	Dissipated energy [J]
[G/PET^{20}/G]	20	3.18	-	13.70	2.26	1.75	0.61	15.4
	25	3.61	-	14.99	3.05	2.36	1.04	20.5
	27.5	3.47	-	16.91	2.95	2.16	0.91	23.2
	29	3.73	-	16.53	3.35	2.54	1.02	24.1
	30	3.17	0.53	24.45	Top facesheet perforation	1.78	0.66	31.2
	35	3.57	0.45	30.12	Top facesheet perforation	2.03	0.91	36.7
	40	3.36	2.07	35.28	Top facesheet perforation	0.51	2.08	41.4
	50	3.66	2.80	37.40	Top facesheet perforation	0.25	2.29	51.6
[G$_2$/PET^{20}/G]	30	4.35	-	13.33	2.08	1.40	0.86	23.6
	40	4.97	-	15.42	2.69	1.68	1.70	34.0
	50	5.28	-	18.59	5.79	2.54	1.88	49.5
	52.5	4.81	0.86	30.98	Top facesheet perforation	1.60	1.19	55.5
	55	5.16	0.69	30.18	Top facesheet perforation	1.65	0.94	57.7
	65	4.53	2.57	37.80	Top facesheet perforation	0.69	3.12	69.5

98

Generally, the after-impact assessments of the section view of both non-hybrid sandwich panels, presented in

Figure 6.6 and Figure 6.7, depicted almost the same sequence of damage progression. Regardless of the sandwich panels' composite facesheet thickness, the damage behavior and propagation followed the same patterns. Nevertheless, each damage has occurred at significantly different LVI energy levels. Expectedly, it was determined that adding another layer of Glass/PP composite to the skin of the PET foam core sandwich panels can alter their LVI response. While the $[G/PET^{20}/G]$ sandwich panels experience top skin perforation, leading to catastrophic damages, the $[G_2/PET^{20}/G]$ panels merely experienced a limited extent of core crush and core shear under the same impact energy.
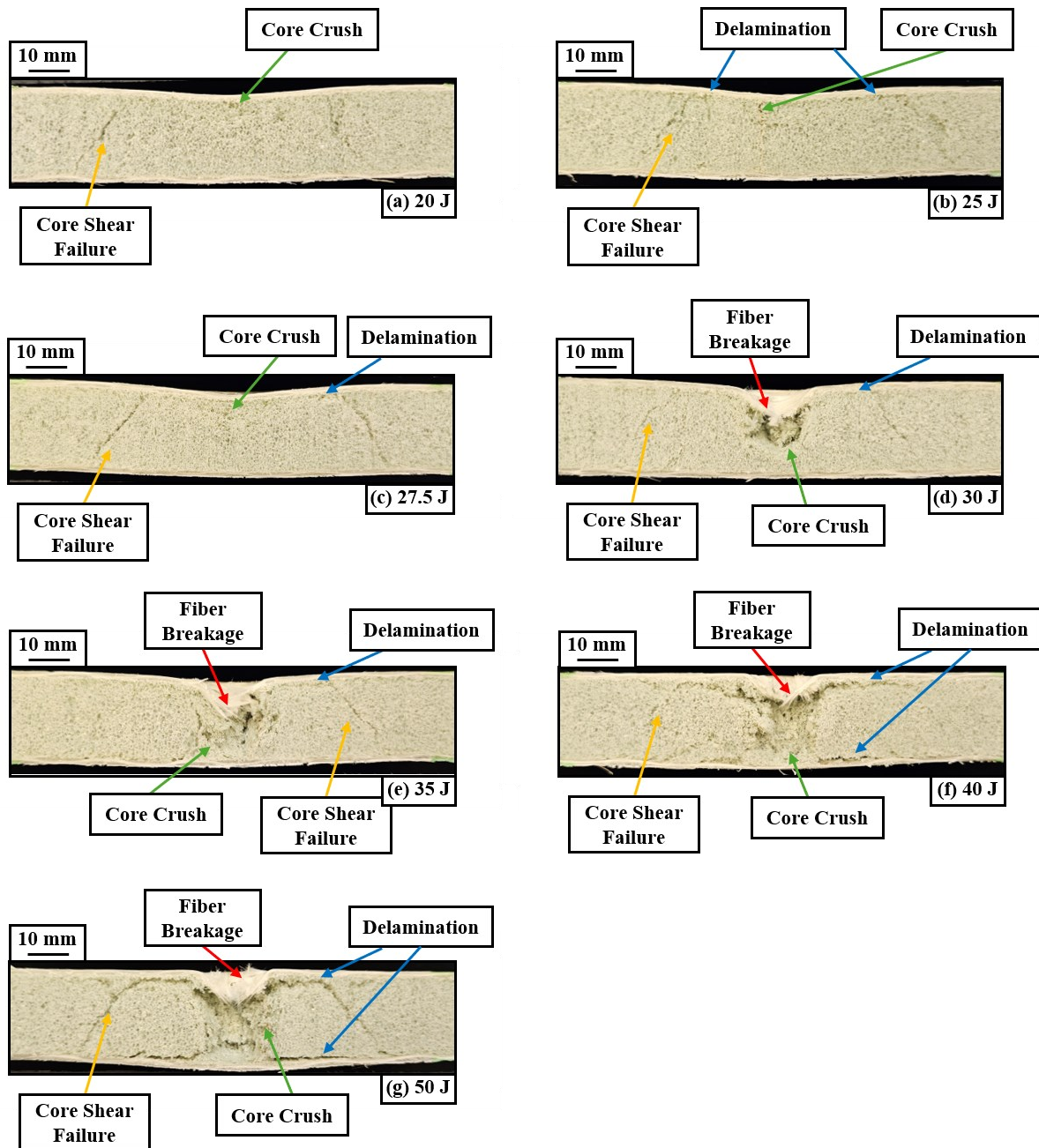
Figure 6.6. The after-impact section views of the non-hybrid [G/PET^{20}/G] composite sandwich panels under different impact energies.
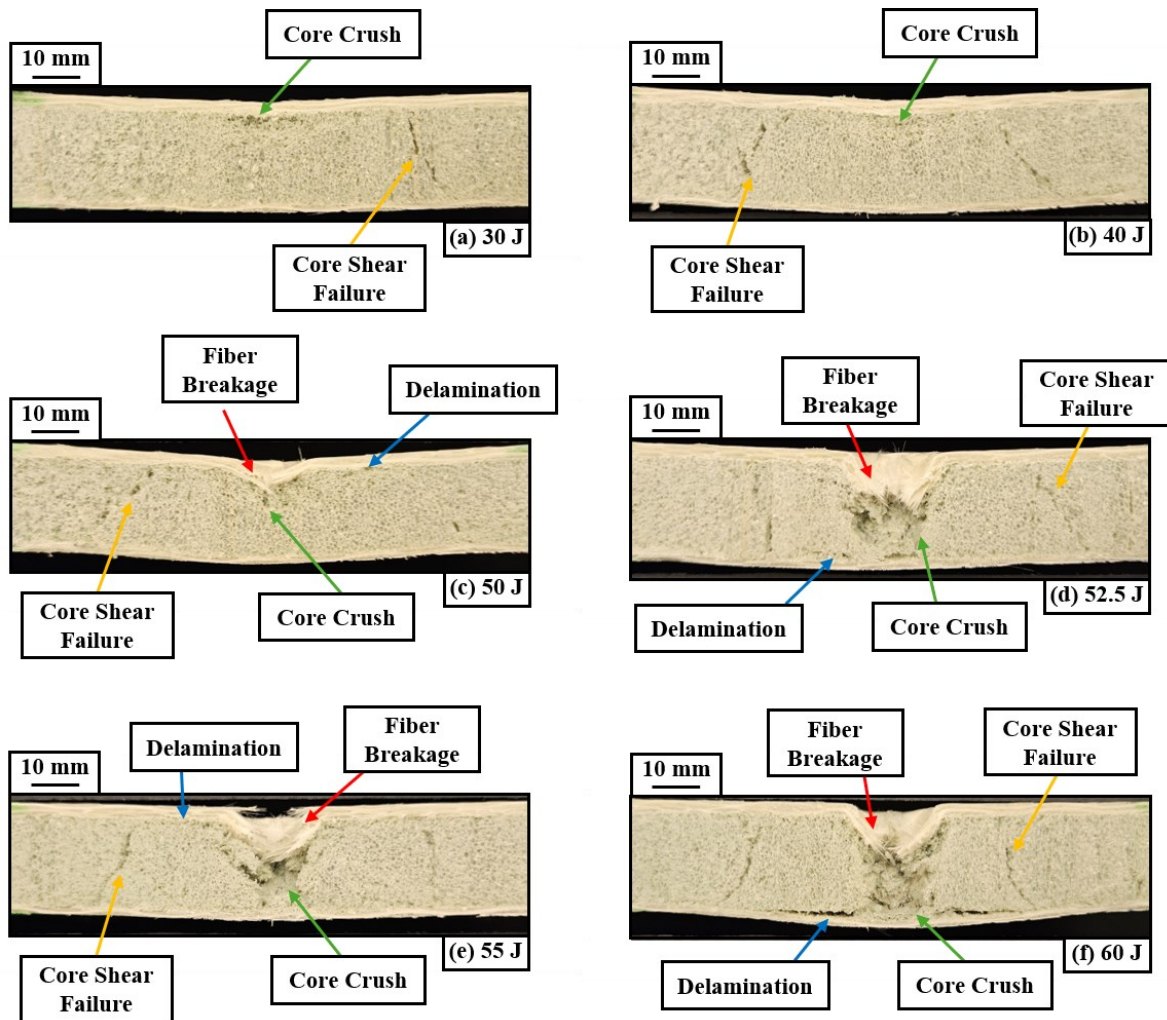
Figure 6.7. Damage progression of the non-hybrid [G$_2$/PET^{20}/G] composite sandwich panel under various impact energies.

At low impact energies, where the striker rebounds after hitting the surface, the [G/PET^{20}/G] sandwich panel undergoes core shear failure and localized permanent core crush beneath the collision point. The sandwich panel, particularly the impacted facesheet, can return some of the impact energy to the tup, recovering the elastic portion of the energy. However, the maximum movement of the tup in the panel caused compression loading on the core material which triggered the permanent core crush under the hemispheric impactor nose. Furthermore, stress can be transferred to the PET foam core due to the bending situation, which leads to core shear failure. Under higher impact energies, shear cracks in the PET foam propagate further and extend toward the facesheets, causing delamination between the PET core and composite skin.

By exceeding the penetration energy threshold, catastrophic levels of fiber breakage were reached, perforating the top facesheet and dramatically increasing the core crush. At this point, all the applied impact energy was absorbed, leading to permanent damage to the sandwich panel. In complementary tests at higher impact energies, the striker crushed the PET foam core and applied force to the rear composite skin. Despite surpassing the panels' penetration threshold, the LVI response of the intact rear facesheet allows the tup to recover a small portion of the energy, likely due to its elastic reaction. The limited rebound height triggers the break or catch mechanism, preventing secondary impacts. At this stage, widespread debonding between the composite skin and PET foam was noted.

As previously mentioned, the effect of hybridization on the sandwich panels with recycled PET foam core and reinforced composite facesheet requires further investigation. The current study evaluates the damage propagation of sandwich panels strengthened with a stainless-steel mesh. The LVI response of [G/M/PET^{20}/G] hybrid PET foam core sandwich panels is presented in Figure 6.8. A significant deviation in force-displacement behavior is demonstrated, accompanied by an improved penetration threshold. Comparing the top facesheet perforation threshold, the hybrid [G/M/PET^{20}/G] panels outperform the non-hybrid [G/PET^{20}/G] and [G$_2$/PET^{20}/G] ones by 108.3 % and 19 %, respectively.
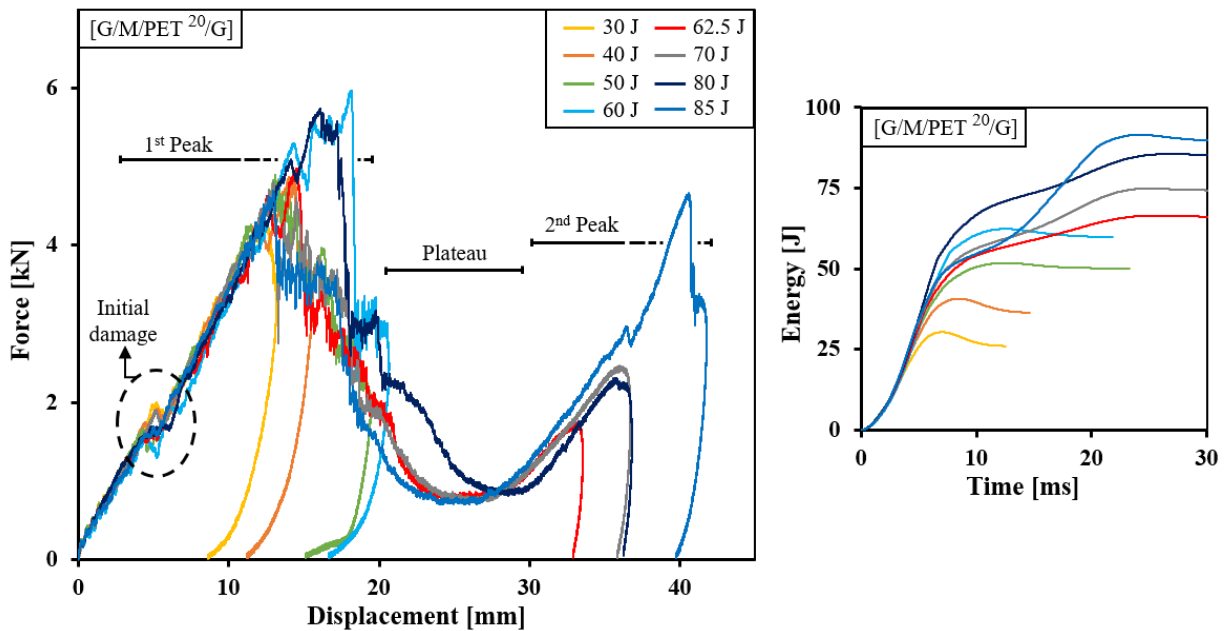
Figure 6.8. Force-displacement, and energy-time response of the hybrid [G/M/PET^{20}/G] composite PET core panel under different impact energy levels.

Table 6.3 provided detailed information on the LVI experiments conducted on hybrid samples, where the impacted surface was reinforced with a layer of stainless-steel mesh. The enhanced impact energy resistance was attributed to the elasto-plastic response of the metallic layer integrated into the composite laminate. In addition, the maximum load level at the first peak, which is governed by the impacting surface, increases compared to the non-hybrid samples. Moreover, after-impact dent depth analysis revealed that the newly introduced elasto-plastic energy-absorbing behavior results in relatively detectable permanent dents on the reinforced surface.

Table 6.3.

Summary of the LVI experiments on hybrid composite PET foam core sandwich panels under various impact energies.

Panels stacking sequence	Impact energy [J]	1st peak force [kN]	2nd peak force [kN]	Max. tup displacement [mm]	After-impact dent depth [mm]	After-impact dent's edge depth [mm]	After-impact rear side deformation [mm]	Dissipated energy [J]
[G/M/PET^{20}/G]	20	3.41	-	10.90	2.84	1.52	0.36	16.4
	30	4.26	-	13.19	5.08	2.41	0.58	26.0
	40	4.95	-	15.60	6.60	3.30	1.14	36.4
	50	4.89	-	19.46	8.03	3.18	1.98	50.0
	55	5.21	-	19.89	8.79	3.91	1.78	54.5
	60	5.96	-	20.66	8.13	4.32	1.91	59.8
	62.5	4.98	1.75	33.53	Top facesheet perforation	2.67	1.4	66.2
	65	5.15	1.21	32.21	Top facesheet perforation	2.79	1.5	68.8
	70	4.80	2.46	36.70	Top facesheet perforation	2.92	2.108	74.3
	80	5.73	2.31	36.80	Top facesheet perforation	4.57	2.41	85.3
	85	4.70	4.66	41.77	Top and rear facesheet perforation	-	-	89.8
	90	5.10	3.13	46.90	Top and rear facesheet perforation	-	-	97.6

It is well known that the glass fiber composite laminates exhibited an elasto-plastic response. The linear portion is distinguished from the non-linear section by the proportional stress limit (σ^{PL}). Nonetheless, the characteristics of this non-linear part can vary depending on the resin material, or reinforcements used in composite plates. Furthermore, it has been demonstrated that the non-linear stress-strain response can be modified by incorporating metallic layers into the composite laminate [75,123]. Figure 6.9 clearly illustrates this distinctive shift in behavior, highlighting the impact of stainless-steel mesh reinforcement on the overall mechanical response. In addition to increasing

the energy absorption because of plastic deformation, strengthening the plate with metallic mesh changes the catastrophic failure pattern of the glass/PP composite. Under a tensile loading condition, hybrid laminate experienced a sequential failure, where some of the metal wires remained connected after the maximum load [75,123].
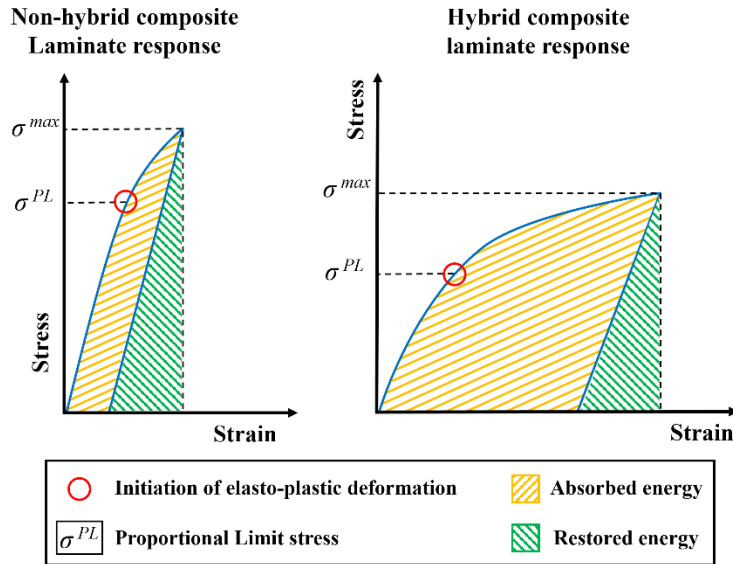
Figure 6.9. The schematic stress-strain diagram distinguishing the elasto-plastic behavior of the non-hybrid composite laminates versus the hybrid ones.

Hybridizing the composite laminate with impregnated steel mesh reduces the total elastic modulus and proportional stress limit, leading to greater plastic deformation of the sample skin. Due to this specific non-linear response, the reinforced composite facesheet can absorb higher energies. The absorbed energy has been distinguished from the restored energy portion presented in Figure 6.9. Thus, the improvement observed in the LVI perforation threshold of the sandwich panels' top facesheets can be attributed to this unique hybrid stacking sequence, which modifies the non-linear behavior to enhance the energy absorption capacity.

Evaluating the restored energy portion of the hybrid [G/M/PET[20]/G] composite panels further support this idea. Even before reaching the perforation state, the hybrid composite PET core sandwich panels absorbed a relatively higher share of the applied energy under the same impact energy. This phenomenon resulted in a noted increase in the permanent indentation depth of the impacted hybrid panels. Besides, this modification led to global deformation of the hybrid

composite panels compared to locally deformed non-hybrid ones. The after-impact measurements of the dents' edge depth confirm the mentioned deformation.

To examine the damage propagation in the hybrid [G/M/PET^{20}/G] sandwich panels, the section views were presented in Figure 6.10. Under low impact energies, core shear and localized PET foam crushing occurred upon collision. As mentioned, the presence of an additional metallic layer increased the absorption of energy. Fiber breakage and matrix cracks were observed as the primary non-catastrophic damages on the panel surfaces. In addition to that, matrix cracks can be distinguished in the impregnated reinforced metal mesh skin of the hybrid laminates. Moreover, the global deformation of the hybrid sandwich panels compared to the localized dent of the non-hybrid ones can be clearly distinguished in these section views.
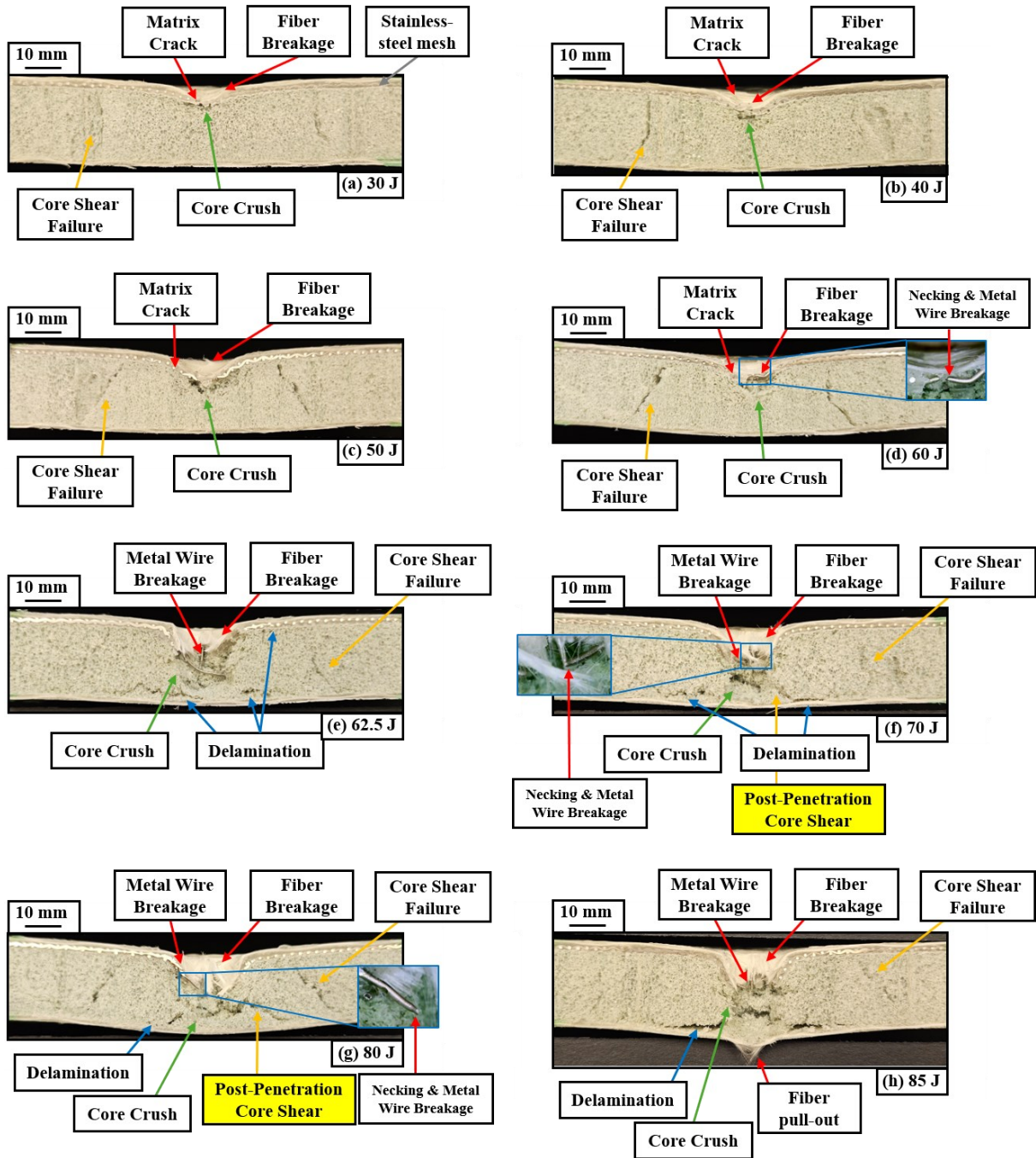
Figure 6.10. The section views of damage progression of the hybrid [G/M/PET^{20}/G] composite sandwich panel under various impact energies.

Upon reaching the upper facesheet perforation threshold, the metal wires experienced plastic deformation and exhibited signs of wire necking, followed by wire breakage. Consequently, the impactor penetrated the PET foam core, which led to a comparatively higher extent of core crushing

in these laminates compared to the non-hybrid ones. Moreover, delamination begins to propagate due to the core shear crack progress and the load applied to the rear composite facesheet from the compressed PET foam core. Most importantly, a new damage phenomenon has been observed for hybrid composite panels which were understood to be related to the deformed metallic mesh layer.

When the striker perforated the top skin and reshaped the structure, the load distribution was changed, which resulted in post-penetration shear cracks in the PET foam core. Since the upper composite facesheet was reinforced with a layer of stainless-steel mesh, the deformed metallic part can still bear load after perforation. Although the sample was damaged, the panel's strength was locally degraded merely at the impacted zone. This caused a reduction in strength at the impacted zone which can affect the overall response of the composite sandwich panels. However, even at the local levels below the collision zone, compared to the non-hybrid samples that were catastrophically damaged, the two sides of the broken wires in the metal mesh were still capable of bearing load. While the region near the fractured metal wires experienced plastic deformation and retained the ability to transfer load, the elements of the non-hybrid composite facesheet were damaged and eliminated from load bearing. This phenomenon can be related to a combination of plastic deformation and sequential material property degradation of the hybridized composite facesheet. This also directly affected the plateau load level differences between the hybrid and non-hybrid composite sandwich panels.

As discussed, the deformed parts of the reinforced hybrid composite facesheet are still capable of load bearing. Thus, the distribution of load to the lower layers resulted in forming inclined cracks in the PET foam core, being distinguished by post-penetration shear cracks. In other words, the transferred load can exert high shear force on the PET core, which increases the extent of crack formation in hybrid panels. These shear cracks differ in their propagation direction compared to the cracks known as delamination. The foam core shear cracks propagated in an inclined direction. Nevertheless, the delamination-related cracks were horizontal, which led to debonding of the PET foam core and facesheet. It is worth mentioning that delamination cracks can arise either from the extension of the core shear cracks or out-of-plane stresses applied to the rear skin. Overall, damage mechanisms and permanent deformations were defined to be the primary energy-absorbing phenomena under LVI loading conditions. Reinforcing with a layer of

metal mesh was revealed to be capable of altering these patterns and effectively increasing the energy absorption of the composite sandwich panels.

Even though hybridization was determined to be a valuable method for improving the energy absorption of sandwich panels, the stacking sequence effect on the LVI energies high enough to fully perforate the panels remains unknown. Therefore, complementary tests were performed, aiming to assess the sequence of the striker's collision with the hybrid and non-hybrid facesheets. It was generally expected that positioning the reinforcing stainless-steel layer on the impacting side is a reasonable option since the panel gets disqualified for further use after penetrating the top skin. Yet, more investigation was required for [G/M/PET^{20}/G] hybrid sandwich panels to examine their behavior under relatively high energies, during which the tup completely passes through the panels. Figure 6.11 presents the collected data comparing the [G/M/PET^{20}/G] versus the [G/PET^{20}/M/G] at impact energies exceeding 50 J, which was previously determined as the impact energy level capable of penetrating through the first skin and PET core of the non-hybrid panels.
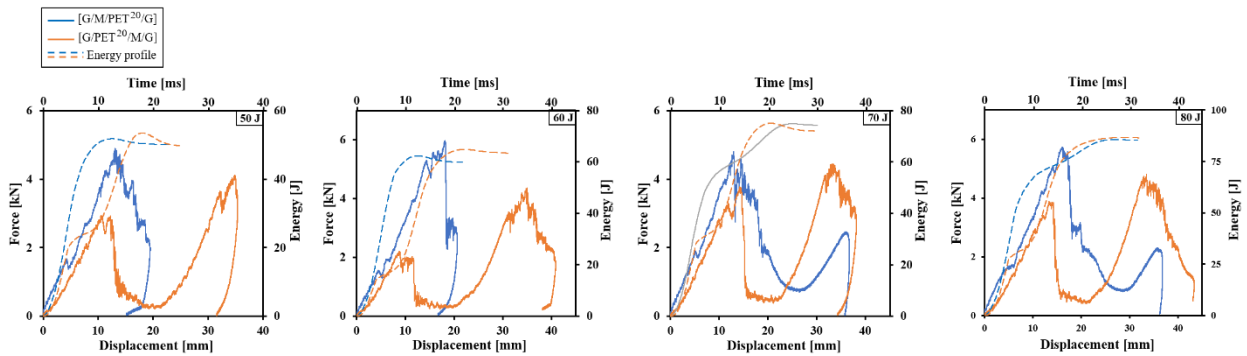
Figure 6.11. A comparison of LVI responses of [G/PET^{20}/M/G] and [G/M/PET^{20}/G] sandwich panels under (a) 50 J, (b) 60 J, (c) 70 J, and (d) 80 J impact energies.

Depending on the collision direction, these samples exhibit distinct behavior under impact. At 50 J impact energy, the striker penetrated the upper non-hybrid composite layer of [G/PET^{20}/M/G] panel, crushed the PET core, and hit the rear reinforced facesheet. This response is depicted in the force-displacement curve, where the orange curve shows two separate peaks. In contrast, the [G/M/PET^{20}/G] sandwich panels withstood the 50 J impact energy without perforating the reinforced hybrid composite skin. As a result, the force-displacement curve for the

[G/M/PET^{20}/G] sample shows a single force peak curve which is related to the top laminate response to the LVI test.

Exceeding the perforation threshold, a clear deviation in the LVI response has been observed for each stacking sequence. The [G/PET^{20}/M/G] samples reached the full perforation limit considerably sooner than the [G/M/PET^{20}/G] ones. Table 6.4 presents the detailed response of the conducted tests, supporting these statements. It was revealed that being supported by the PET foam core, the hybrid composite facesheet can withstand higher impact energies. Moreover, the elasto-plastic response is pronounced in the [G/M/PET^{20}/G] samples, which leads to higher impact energy required to fully perforate the sandwich panels.

Figure 6.12 shows the plastic deformation and damage propagation comparison, changing the sequence of reinforced skin being impacted. It was depicted that the introduction of post-perforation core shear damage and permanent plastic deformation of the hybrid facesheet results in significantly high LVI energies for the striker to pass through the panel.
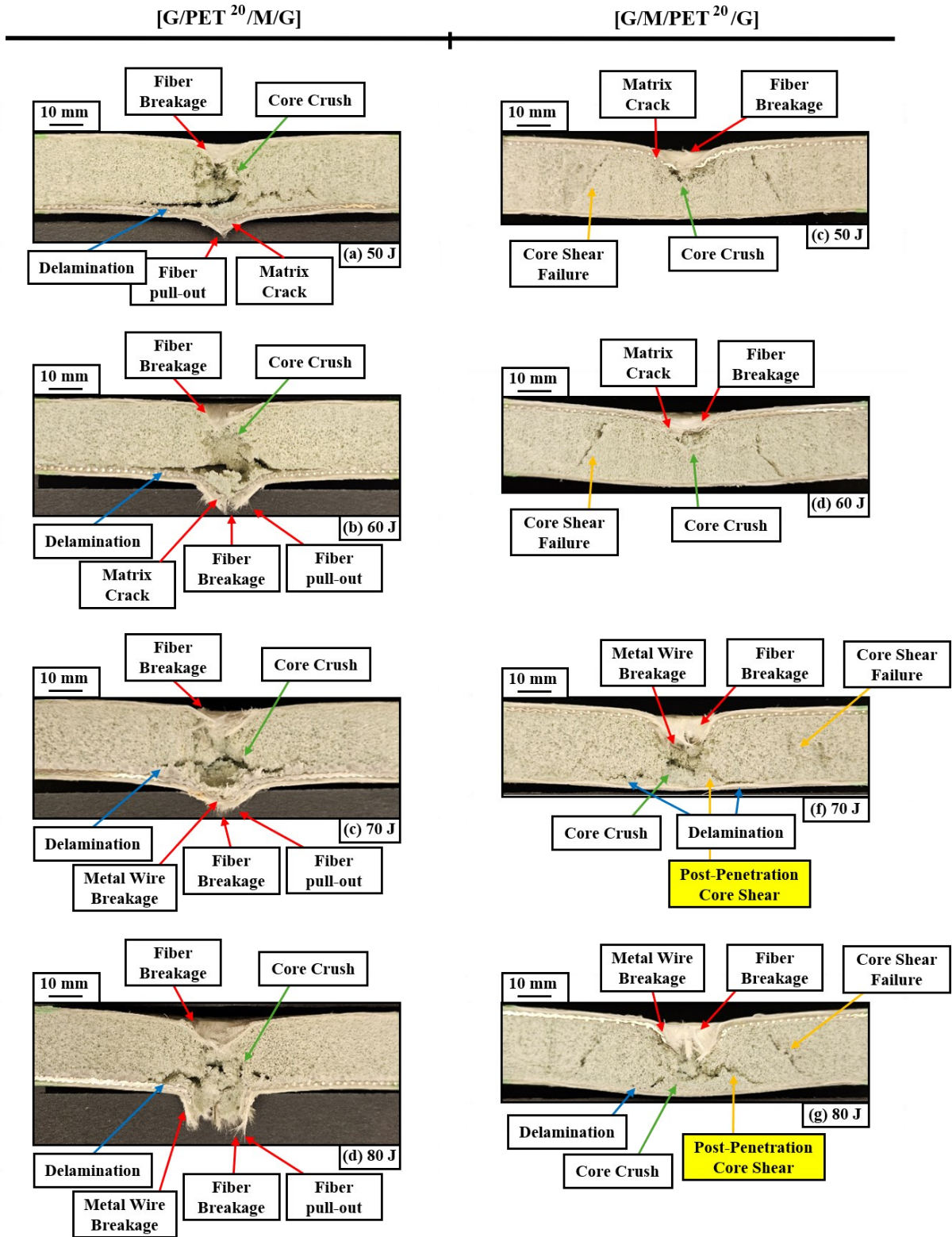
Figure 6.12. Comparison of damage propagation changing the impacting side of hybrid composite sandwich panels.

Table 6.4.
The LVI tests results on hybrid composite PET foam core sandwich panels with reinforced skin facing the rear collision side.

Panels stacking sequence	Impact energy [J]	1st peak force [kN]	2nd peak force [kN]	Max. tup displacement [mm]	After-impact dent depth [mm]	After-impact dent's edge depth [mm]	After-impact rear side deformation [mm]	Dissipated energy [J]
[G/PET^{20}/M/G]	50	2.94	4.12	35.38	Top facesheet perforation	1.91	-	49.8
	60	2.20	4.36	40.84	Top and rear facesheet perforation	1.78	-	63.4
	70	3.77	4.44	38.16	Top and rear facesheet perforation	2.03	-	72.0
	80	3.88	4.81	43.33	Top and rear facesheet perforation	3.51	-	86.4

The empirical study proved that strengthening the impacting surface of the PET foam core composite sandwich panels with a stainless-steel mesh layer can notably improve their LVI perforation threshold. It remains to be seen whether this improvement is replicated significantly enough in sandwich panels with reduced core thicknesses. Thus, in this part, hybrid and non-hybrid sandwich panels with nominal recycled PET foam thickness of 10 mm were subjected to various impact energies. Under LVI loading conditions, where the tup applies force at the center, a bending situation was simulated. The distance of the composite facesheets from the neutral axis is crucial for the flexural behavior of the sandwich panels, making the PET foam core thickness an important factor in LVI tests.

The LVI test results and the complementary measured data have been presented in Figure 6.13 and Table 6.5, respectively. It is well-known that lowering the distance between the skin and neutral axis leads to reduced load-bearing capacity of the sandwich panels. This reasoning supports the observed reduction in the measured load peaks within the LVI diagrams of [G/PET^{10}/G] compared to previously evaluated thicker panels. The perforation threshold was also reduced due to the diminished structural effect of the composite sandwich panels with thin PET foam cores.
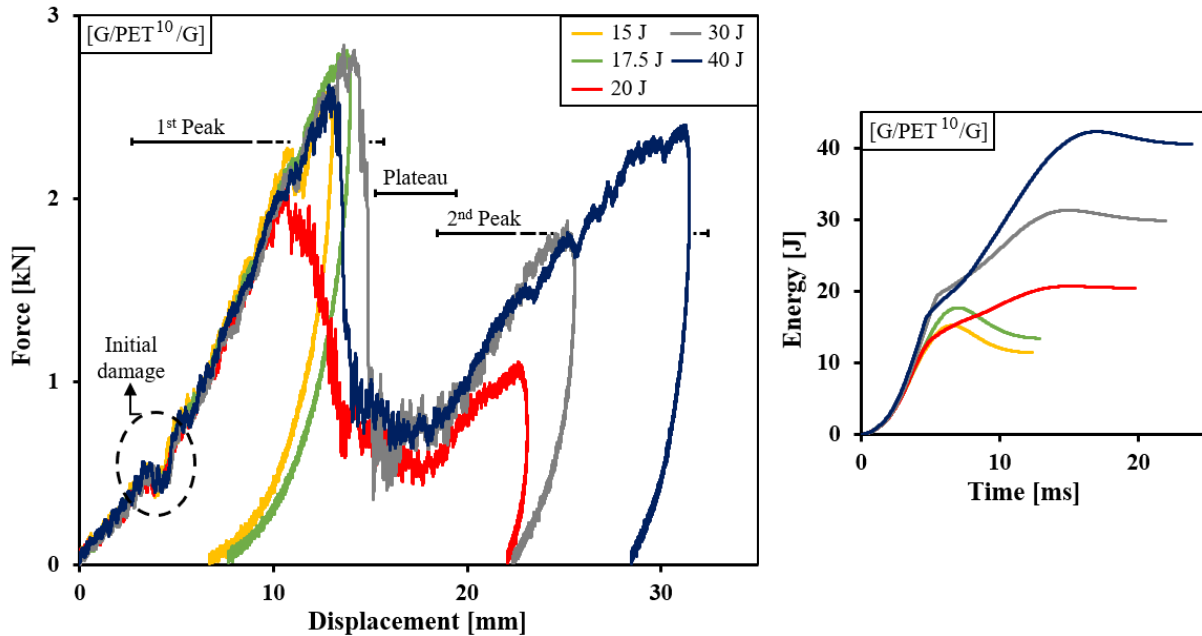
Figure 6.13. Force-displacement, and energy-time response of the non-hybrid [G/PET^{10}/G] sandwich panel under different impact energy levels.

Table 6.5.

LVI experiment data of hybrid and non-hybrid sandwich composite panels with 10 mm thick PET foam cores.

Panels stacking sequence	Impact energy [J]	1st peak force [kN]	2nd peak force [kN]	Max. tup displacement [mm]	After-impact dent depth [mm]	After-impact dent's edge depth [mm]	After-impact rear side deformation [mm]	Dissipated energy [J]
[G/PET^{10}/G]	15	2.60	-	13.02	2.08	1.44	1.12	11.4
	17.5	2.81	-	13.97	2.16	1.52	0.81	13.4
	20	2.05	1.11	23.08	Top facesheet perforation	1.47	1.08	20.4
	30	2.84	1.88	25.52	Top facesheet perforation	1.09	1.98	29.8
	40	2.62	2.40	31.45	Top facesheet perforation	0.64	4.45	40.5
[G/M/PET^{10}/G]	30	4.77	-	13.99	3.33	2.16	0.89	23.8
	40	4.77	-	17.27	5.89	2.41	2.18	38.8
	50	4.24	-	22.25	8.92	3.28	2.54	51.6
	52.5	4.56	-	22.91	Top facesheet perforation	3.15	2.34	53.9
	55	4.04	2.25	26.55	Top facesheet perforation	3.00	2.34	57.4
	65	4.31	2.24	27.85	Top facesheet perforation	3.23	2.67	62.4

By reducing the core thickness, the impactor requires less distance to perforate before hitting the rear facesheet. Besides, upon reaching the top facesheet penetration threshold, the core quickly crushes under the compression load of the striker and transfers the load to the rear skin; therefore,

the plateau duration was considerably reduced for [G/PET[10]/G] samples, exhibiting a quicker rise after the initial load drop, as the rear composite skin rapidly intervenes the impact loading. Additionally, the measured after-impact rear deformation of the [G/PET[10]/G] was considerably higher since thin sandwich panels are more prone to bending loads.

Figure 6.14 depicts the section view damage pattern of the [G/PET[10]/G] samples, following the damage propagation and transitions similar to the 20 mm PET foam core thick panels. Yet, the level of impact energy at which each damage type has been determined was quite different for these thinner sandwich panels. At low impact energies, core shear cracks and PET foam core crush are the dominant energy-absorbing phenomena. Once the top facesheet penetration limits were exceeded, a combination of fiber breakage, core shear, core crush, and delamination occurred within the samples.
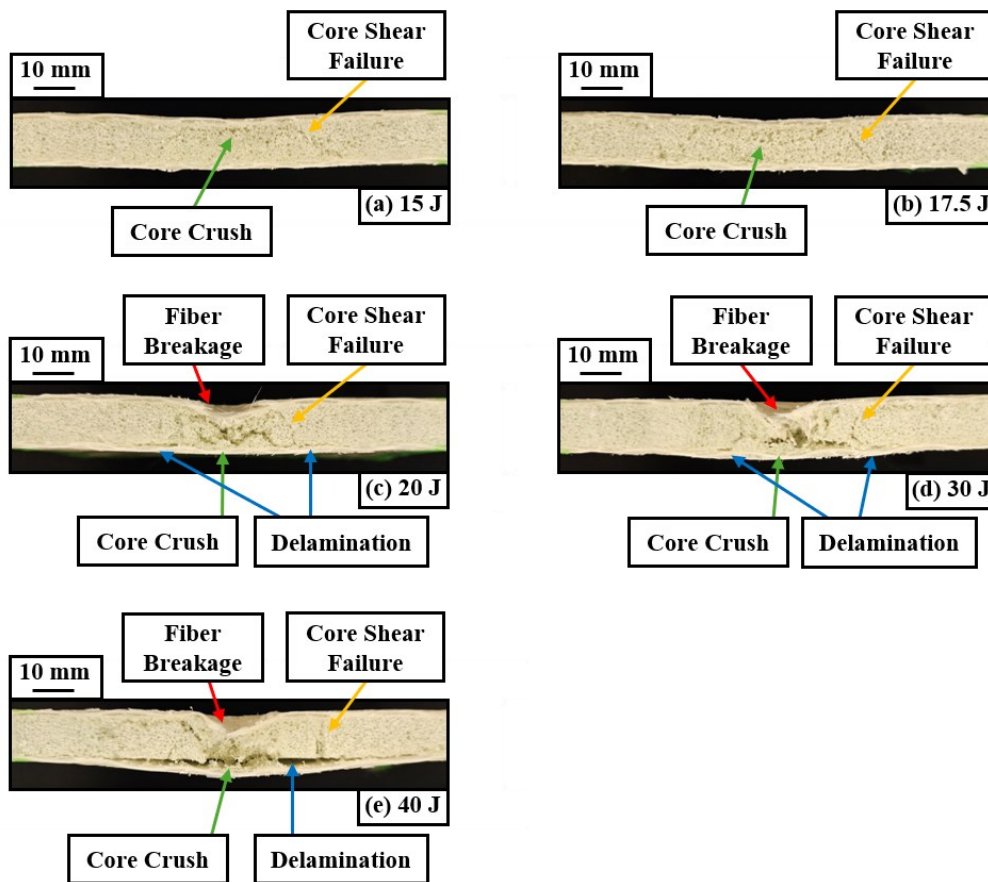
Figure 6.14. The after-impact section views of the non-hybrid [G/PET[10]/G] composite sandwich panel under different impact energies.

113

To assess the effect of hybridization and core thickness, reinforced composite sandwich panels with recycled PET foam cores were examined at different energy levels. Figure. 6.15 depicts the results of the LVI tests, revealing a significant improvement in the top facesheet penetration threshold of the sandwich panels reinforced with a resin-impregnated metal mesh layer. The sandwich panels with strengthened top facesheet withstood impact energies of up to 52.5 J, representing a substantial improvement of 162.5% over the non-hybrid [G/PET^{10}/G] panels. This increase in the perforation threshold energy is attributed to the specific elasto-plastic response of the hybrid facesheet, which can effectively absorb the impact energy.
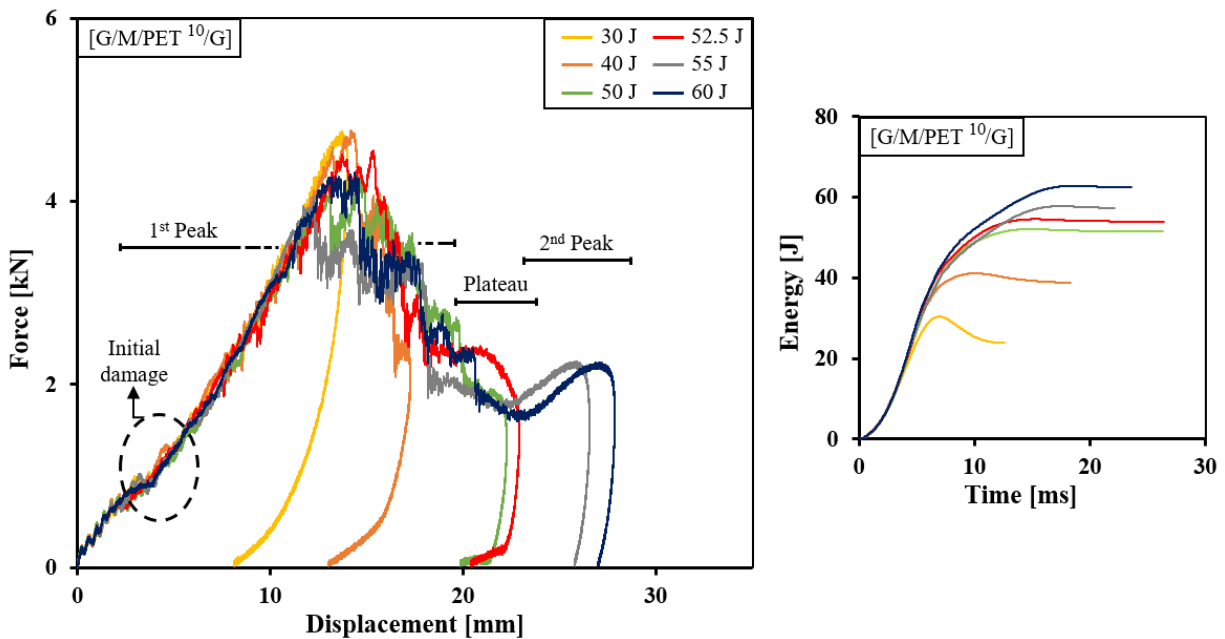
Figure. 6.15. Force-displacement, and energy-time response of the hybrid [G/M/PET^{10}/G] under different impact energy levels.

A comparison between the reinforced sandwich panels and non-hybrid ones proved the capability of hybridization in enhancing the energy absorption capacity of the hybrid foam core panels. In addition to their unique elasto-plastic response, the hybrid [G/M/PET^{10}/G] panels absorbed a considerable portion of energy through permanent plastic deformation of the strengthening metallic layer. Matrix cracks are commonly observed as one of the initial damages within the impregnated stainless-steel mesh layer. Moreover, examinations depicted plastic deformation of metal wires in the form of necking, particularly at the wire breakage points. These

characteristic responses indicate the energy-absorbing phenomenon of the hybrid panels under LVI loading.

Continuing the LVI tests beyond the top facesheet penetration threshold, post-penetration core shear cracks have been distinguished. This specific damage occurs due to the shear load distribution from the deformed hybrid composite layer to the sides of crushed PET foam beneath the strike point. Under 40 J impact energy, the non-hybrid [G/PET^{10}/G] sandwich panel was severely damaged and no longer functional, with delamination extending nearly to full skin-to-core debonding. Nonetheless, hybridization demonstrated a notable influence in improving the LVI performance. At the same energy level, the reinforced skin of the [G/M/PET^{10}/G] sandwich panel did not reach the perforation, absorbing the impact energy through a combination of complex damage phenomena, presented in Figure 6.16.
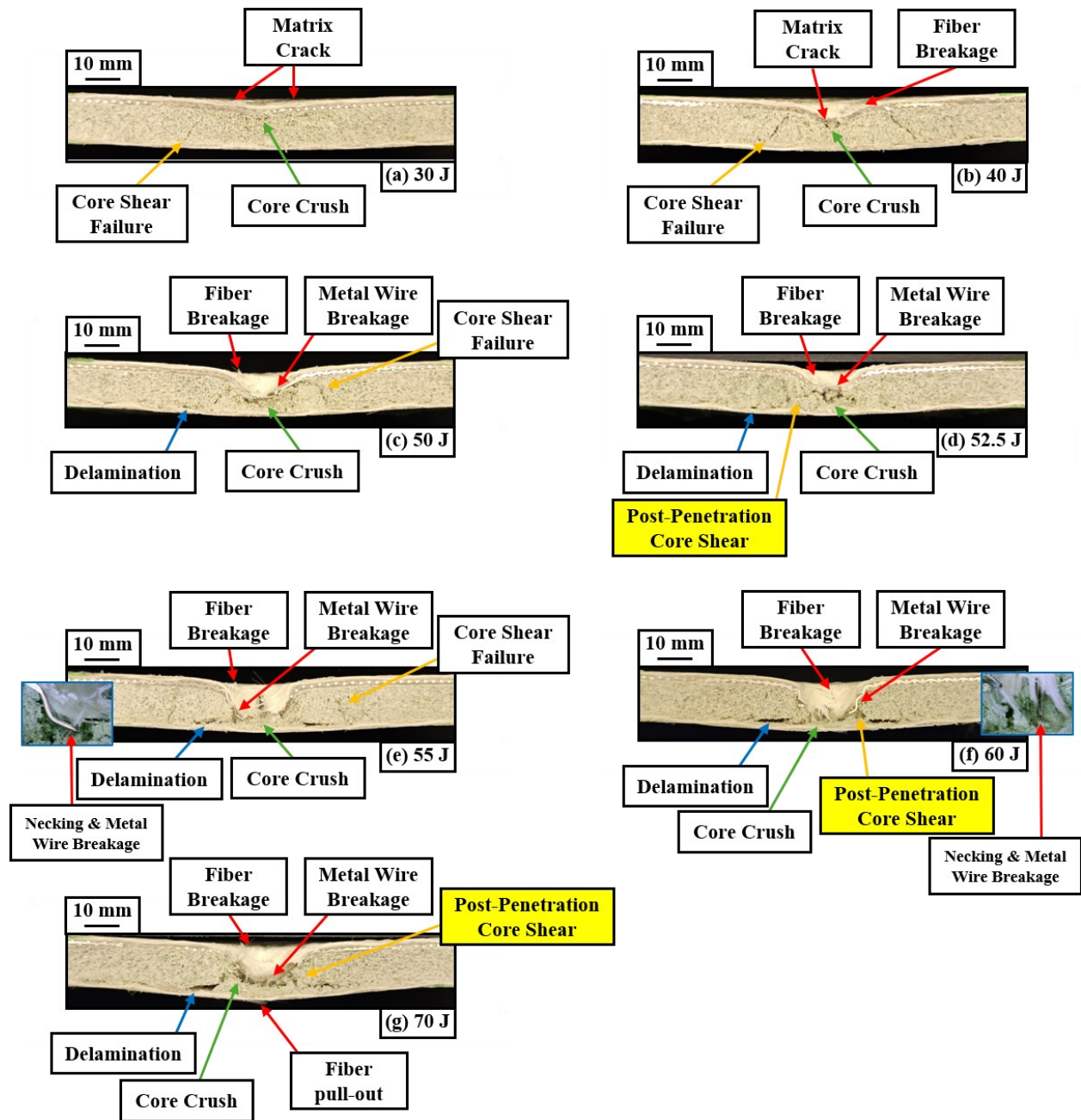
Figure 6.16. Damage progression of the hybrid [G/M/PET^{10}/G] composite sandwich panel under various impact energies.

While the composite skin loses its load-bearing capacity after failure, the deformed stainless-steel mesh layer withstands the impact load. The reinforcing metallic layer experiences a permanent deformation surrounding the collision site. Despite the breakage of certain mesh wires, this reinforcing layer transfers the load to the lower layers, leading to secondary core shear failure,

propagating from the corners of the perforated PET foam core. The detected damages in conjunction with the global deformation of the sandwich panel and particularly the plastic response of the hybrid composite skin, assist with enhancing energy absorption during the LVI tests. Even at the highest examined LVI energy, despite perforation, the level of delamination is considerably less in hybrid sandwich panels compared to non-hybrid ones.

In summary, hybridization was revealed to be a sustainable method to improve energy-absorbing elasto-plastic behavior introduced to the composite PET foam core sandwich panels. The deformation and damage pattern of the reinforced panels contributed to higher energy thresholds to penetrate the hybrid skin. This will finally delay the full perforation and reduce the extent of skin-to-core debonding observed in the after-impact section views. Even though hybridization is beneficial in impact scenarios, it comes with a trade-off in increased cost, manufacturing complexity and weight. Hence, the choice of product will depend on the specific application, and the users' decision to compromise these parameters for enhanced impact resistance.

All in all, these reinforced composite sandwich panels with recycled PET foam cores were designed in a collaborative effort with the industrial partner (ICP Inc.) to be suitable for heavy-duty applications, such as cargo trucks or stationary structures like modular housing and cold storage rooms. These panels could also be beneficial in protecting electrical facilities where enhanced resistance to external forces is required. Therefore, the choice depends on the balance between performance, cost, and production feasibility based on the intended use.

6.6 Conclusion

A two-phase compression molding fabrication method was used to laminate sandwich panels reinforced with PP resin-impregnated stainless-steel mesh. By optimizing the manufacturing parameter, proper adhesion was achieved between the composite skin and recycled PET foam material, which was confirmed by flatwise tensile tests and microscopic assessment. This study thoroughly investigated the LVI response of sandwich panels with two different recycled PET foam core thicknesses. Moreover, the influence of incorporating stainless steel metal mesh as an industrially viable solution to enhance the energy absorption capacity of composite sandwich panels was evaluated.

Reinforcing the impacted composite skin with a metallic mesh layer improved the energy-absorbing behavior of the sandwich panels. Considering the top skin penetration as the threshold, the hybrid sandwich panels outperformed the non-hybrid ones. The permanent plastic deformation of the hybrid composite facesheet, and the combination of complex damages within the skin and PET foam were the main energy-absorbing phenomena. Furthermore, full cross-section views of the after-impact samples depicted comprehensive damage propagation under various impact energies. Post-penetration core shear cracks, specifically attributed to the hybridization influence on load distribution to the PET foam core, were determined under impact energies exceeding the top facesheet perforation threshold.

Examining the sequence of facesheets being hit by the striker, revealed that placing the hybrid composite skin at the collision side improves the total energy required to fully perforate the panels. Since hybridization affects the elasto-plastic response of the sandwich panels and modifies the load distribution to the PET foam core, positioning the reinforced side in front of the impactor increased the LVI resistance. Finally, sandwich panels made of PET foam with lower core thicknesses were shown to be more susceptible to impact loading conditions.

Reducing the distance between the load-bearing composite skin and the neutral line directly affects the bending performance of sandwich panels, and in this case, decreases the maximum measured force values in the LVI diagrams. Besides, modifying the core thickness affects the plateau duration, detected during the PET foam core perforation stage. A comparison between the deformation of panels, beyond the impact zone, showed a global deformation of hybrid panels compared to the non-hybrid ones, while their top facesheets were locally damaged. In conclusion, the empirical study on the LVI behavior of sandwich panels with recycled PET foam core introduced the hybridization of composite skin as a viable solution capable of improving the overall energy absorption of panels.

Chapter 7:

Shape Memory Alloy Assisted Healing of Thermoplastic Composite Laminates under Repeated Impact Loading

7. Shape Memory Alloy Assisted Healing of Thermoplastic Composite Laminates under Repeated Impact Loading

7.1 Abstract

This study investigates the Low-Velocity Impact (LVI) performance and recovery capabilities of thermoplastic glass fiber composite laminates reinforced with Nitinol Shape Memory Alloy (SMA) wires. The potential of SMA-reinforced composite plates to absorb energy, restore the after-impact deformations and mitigate the properties degradation has been evaluated under repeated low-energy strikes and heat-treatment cycles. Repeated LVI tests were conducted at three distinct energy levels, with both hybrid and non-hybrid control sample groups subjected to impact and effective thermal recovery cycles. It was revealed that this newly presented hybridization method followed by thermal healing cycles enhanced the laminates' resistance, significantly increasing the perforation threshold number of impacts. Moreover, the SMA-assisted recovery process effectively reduced permanent dent deformation, achieving over 50 % healing in specific iterations.

7.2 Introduction

Composite structures are known to be vulnerable to impact damages, that might occur during installation, maintenance, or regular operation. Numerous studies revealed that the Low-Velocity Impact (LVI) response of composite laminates is highly dependent on various factors, such as the resin and fibers' properties, volume fraction, fiber orientation, stacking sequence, and fiber architecture. In addition to the testing boundary conditions, composites do show different behaviors changing the humidity and temperature of the environment [2,3,6,39,57,130,131,136,137,142,143,166–169]. Due to their specific mechanical properties, manufacturing feasibility, and enhanced environmental sustainability, thermoplastic composites are being widely used in industry. Notably, these materials tend to exhibit improved energy absorption characteristics, offering an advantage in impact resistance [52,56,138,139].

Composite laminates repeatedly being subjected to impacts at energies relatively lower than the perforation threshold experienced cumulative damages, which led to degradation in stiffness,

strength, and energy absorption capacity. Even though the initial impacts may cause barely visible matrix cracking or delamination, subsequent impacts increase the state of damages, resulting in more critical failures and fiber breakage [170–172]. The choice of a multiple-impact scenario is desired to determine the cumulative effects of repeated impact damages on the composite laminates' response. Such loading circumstances are mostly relevant to real-world applications where structures are exposed to dynamic loads within their service life. Other than waves themselves which frequently hit the marine structures, ship hulls and offshore platform structures can experience repeated impacts by hard objects or floating debris [78,173–175]. Arikan and Sayman revealed that the thermoplastic-based composite laminates outperformed the thermoset epoxy plates under repeated LVI loading [78]. While thermoset samples experienced local deformations with localized damaged regions, damages had propagated to the entire body of the thermoplastic counterpart, showing a considerable increase in the number of impacts required to penetrate the thermoplastic plates [46,78].

Hybridization with metal reinforcement layers has proven to be a viable approach to improve the impact performance of composites [9,10,75,149]. The integration of metallic layers, wires or mesh layers within composite laminates has been shown to enhance the elasto-plastic response, increasing the overall impact perforation threshold [11,71,72,117]. Studies have shown that metal wire diameter, stacking sequence, and orientation can significantly influence the LVI performance of these hybrid composite structures [68,69,123,176]. Furthermore, Shape Memory Alloy (SMA) wires have been explored for their ability to improve hybrid composite energy absorption. Research has demonstrated the significant advantages of embedding SMA wires in composite laminates, particularly for enhancing impact resilience and enabling self-healing capabilities [88–91]. There are different existing self-healing approaches, among which SMA-assisted heat treatment is considered an extrinsic technique capable of recovering specific damages within polymer-based composites [79–82,84–87]. C-scan imaging of reinforced composite laminates has revealed that SMA wire stitching can effectively result in crack closure and healing after-impact damages within the plate under various LVI energies [92]. Konlan et al. [18] employed a z-pinning approach using Flexinol SMA wires to reinforce glass composite laminates, demonstrating the potential to enhance impact resilience. This technique allowed for the closing or narrowing of post-impact delamination during thermal healing cycles, further improving the composite's performance [12–18].

The unique recovery capability of the SMA materials is valuable, especially when embedded in the composite laminate assisting with the healing of impact damages; therefore, the current study is an attempt to determine the capability of SMA-reinforced thermoplastic-based composite plates to improve the energy absorption and deformation recovery of damaged parts under repeated impacts and heat treatment cycles. Differential Scanning Calorimetry (DSC) examinations were performed to optimize the thermal recovery cycles, ensuring the best conditions for activating the SMA wires and healing the deformations within the PP-based composites. Upon determining the appropriate heat treatment temperature cycles, the panels were subjected to sets of repeated LVI tests followed by healing cycles. To evaluate the influence of hybridization on the perforation threshold impact count and after-impact dent recovery, repeated LVI tests were conducted at three distinct energy levels for hybrid and non-hybrid plates. In addition to evaluating the impact response of every test repetition, the after-impact deformation and percentage of SMA-assisted dent recovery have been evaluated. This method provided an advanced strategy for enhancing impact resistance and extending the operational life of composite materials.

7.3 Materials and fabrication process

In the current research, 1 mm thick 2/2 twill weave cloth with 60 present E-Glass fiber weight fraction and 40 present comingled Polypropylene (PP) thermoplastic resin was used to fabricate composite laminates. To reinforce these composite laminates, 0.635 mm thick SMA Nickel-Titanium alloy, commonly known as Nitinol, was utilized in wires with a plain appearance and black oxide final finish. The selection of Nitinol as the reinforcing SMA material is primarily attributed to its high toughness, and thermally activated properties. These characteristics of Nitinol are expected to enhance the energy-absorbing behavior of the composite plates, making it a preferred choice for the operational temperature range examined in the current study. As presented in Figure. 7.1,, a compression molding technique was optimized to properly laminate the composite plates. Plain composite laminates were made of 2 layers of dry glass/PP cloth simply stacked in the same fiber direction. In addition to that, when manufacturing the reinforced plates, the SMA wires were carefully distributed in an equidistant spacing with gaps equal to the wire thickness aligning the 0° fiber direction. It is worth mentioning that these metallic wires were merely placed at one side, covering the width of 20 mm on the laminate middle surface. The reason for such reinforcement lies within the striker's most effective local area which is directly governed by the

size of the impactor as depicted in Figure. 7.1,. The localized volume fraction of Nitinol SMA wires in hybrid composite laminates reached 10.4 ± 0.4 % within the strengthened region. It is worth noting that, in this manuscript, since the Nitinol wires were merely used to locally reinforce the composite plate at the mid-section, the SMA wire volume fraction was measured considering this specific portion of the samples.
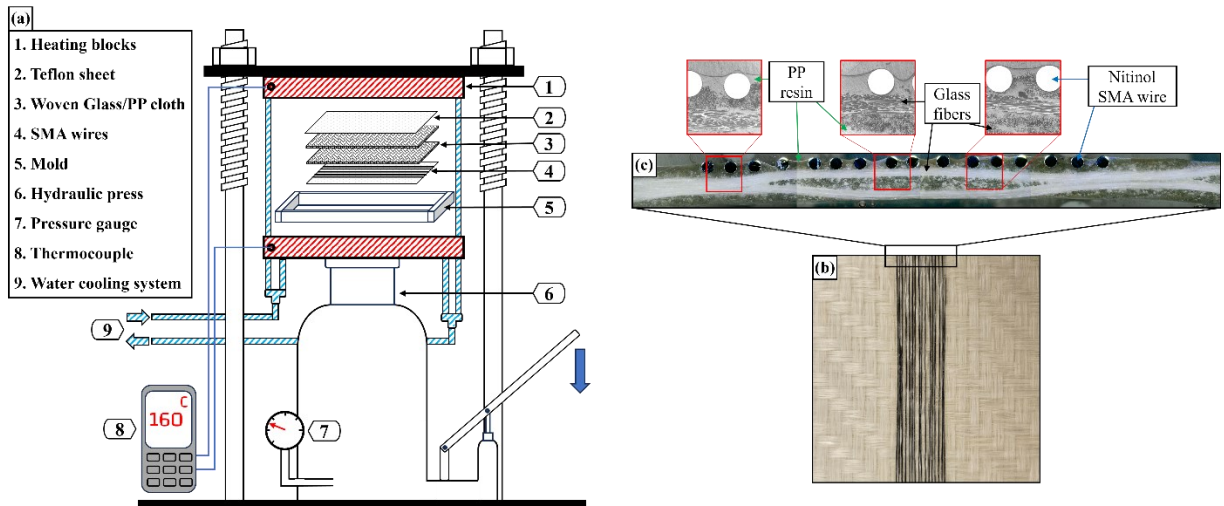
Figure. 7.1. (a). Schematic display of compression molding technique used for fabrication, (b). Localized reinforcement of composite laminates with SMA wires, and (c). Microscopic evaluation of the reinforced cross-section.

The stacked layers of raw material were heated to a temperature range of 160-165° C and were subjected to a constant pressure of 1.5 MPa for a duration of 3 minutes. In order to prevent fiber washout due to the unexpected resin flow at the PP melting temperature, a 2.46 mm thick steel mold supports the plate, which assists with the control over pressure and final thickness. Finally, with water running through the mold, the composite plates were cooled down at a controlled rate of 15° C/min to the ambient temperature. A set of experimental trials and errors was performed to optimize these selected process parameters [118,124,164]. This fabrication procedure showed a proper bonding formed between the SMA wires and the composite laminate. It should be noted that the existing PP resin in the composite laminate was sufficient to properly fill the gaps and connect the wires to the plate. Nevertheless, introducing any additional PP sheets to the process causes unfavorable glass fiber and SMA wire deformation because of fiber washout. Due to the hot press machine dimensional constraints, composite plates were manufactured in 120 mm × 120 mm

and were trimmed to 110 mm × 110 mm, to remove any pre-existing damages related to the fabrication procedure near the edges.

7.4 Experimental procedures

7.4.1 Differential Scanning Calorimetry (DSC)

DSC assessments were required to identify the temperatures at which the mechanical behavior of each material changes. This step was necessary to perfectly present a heating process suitable to heal the after-impact deformations. Hence, DSC tests were performed for both raw composite cloth and intact samples of Nitinol wires employing a TA Instrument Q200 DSC machine coupled with a Refrigerated Cooling System (RCS 90). The glass/PP cloth was examined at the temperature range of 0° C to 250° C, while the Nitinol wire sample was assessed from -50° C to 200° C, respectively for 2 and 3 heating and cooling cycles. These experiments were performed at a programmed heating rate of 10° C/min using Aluminium hermetic sample pans. Moreover, to ensure the reliability of the results and each material's behavior, the initial cycle of heating and cooling was removed from the final data as it is usually recommended for final DSC test evaluations [125,177,178].

7.4.2 Repeated Low-Velocity Impact tests

Previous evaluations performed on the perforation threshold of composite laminate made of two layers of plain glass/PP determined that the LVI perforation energy limit was 30 J [123]. Since this manuscript focuses on the behavior of the same composite laminate under repeated LVI loading, lower impact energies should be considered; therefore, three different LVI energy levels of 10 J, 15 J, and 20 J were chosen. To apply these energies to the system, the impactor mass has been kept constant at 3.265 kg, while the impactor was released at different distances of 312 mm, 468 mm, and 625 mm. As Figure. 7.2 shows, An Instron 9340 drop tower impact machine equipped with a 16 mm diameter hemispheric tup and a 22 kN load cell was used to perform the LVI tests, in accordance with the ASTM D7136 and D3763 standards [152,153]. Composite plates were secured in place with the grip force of a pneumatic circular clamp with an inner diameter of 76 mm. The force-time data were collected at a sampling rate of 2000 kHz, enough to capture the data during the entire impact test, offering considerable accuracy on the collected data. Furthermore, to

ensure precise timing for data collection, a photogate sensor detects impactor movement just before the strike to trigger the data acquisition system. Finally, these measured data have been used to calculate the impactor velocity, displacement and energy [6,154].
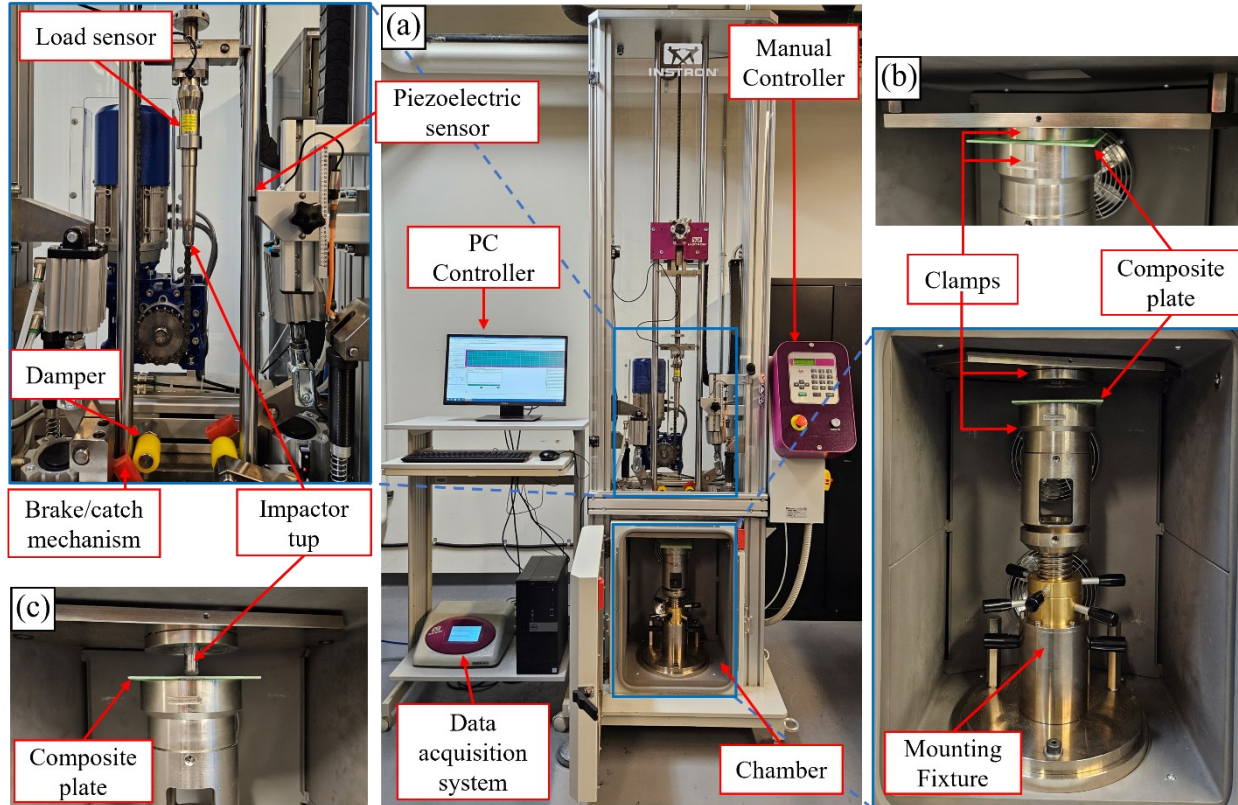
Figure. 7.2. (a). Instron 9340 drop weight impact test machine, (b). The engaged circular clamp with 76 mm inner diameter tightly secures the plate, and (c). Impactor tup positioned at the lowest height to properly set the exact location of collision.

In order to make sure that the impactor exactly hits the same spot during the repeated LVI tests, the sticker should be manually controlled and brought to the impact reference point (relative height of 0 mm), for the laminate to be perfectly positioned. This step, presented in Figure. 7.2. (c), should be carefully managed and repeated every time before running each impact test.

7.4.3 Heat treatment

To properly evaluate the effect of SMA wires on the energy absorption and recovery of the reinforced composite laminates, two separate control groups have been examined. "RH" represents

the reinforced composite plates subjected to iterations of LVI tests and recovery procedures done by heating in the oven. In addition to this reinforced group, plain composites with and without after-impact heat treatments were separated as two different virgin control groups, respectively referred to as "VH" and "V". Figure. 7.3 represents a schematic flowchart of the repeated impact tests, subsequent heating and recovery procedures while distinguishing each experimental group.
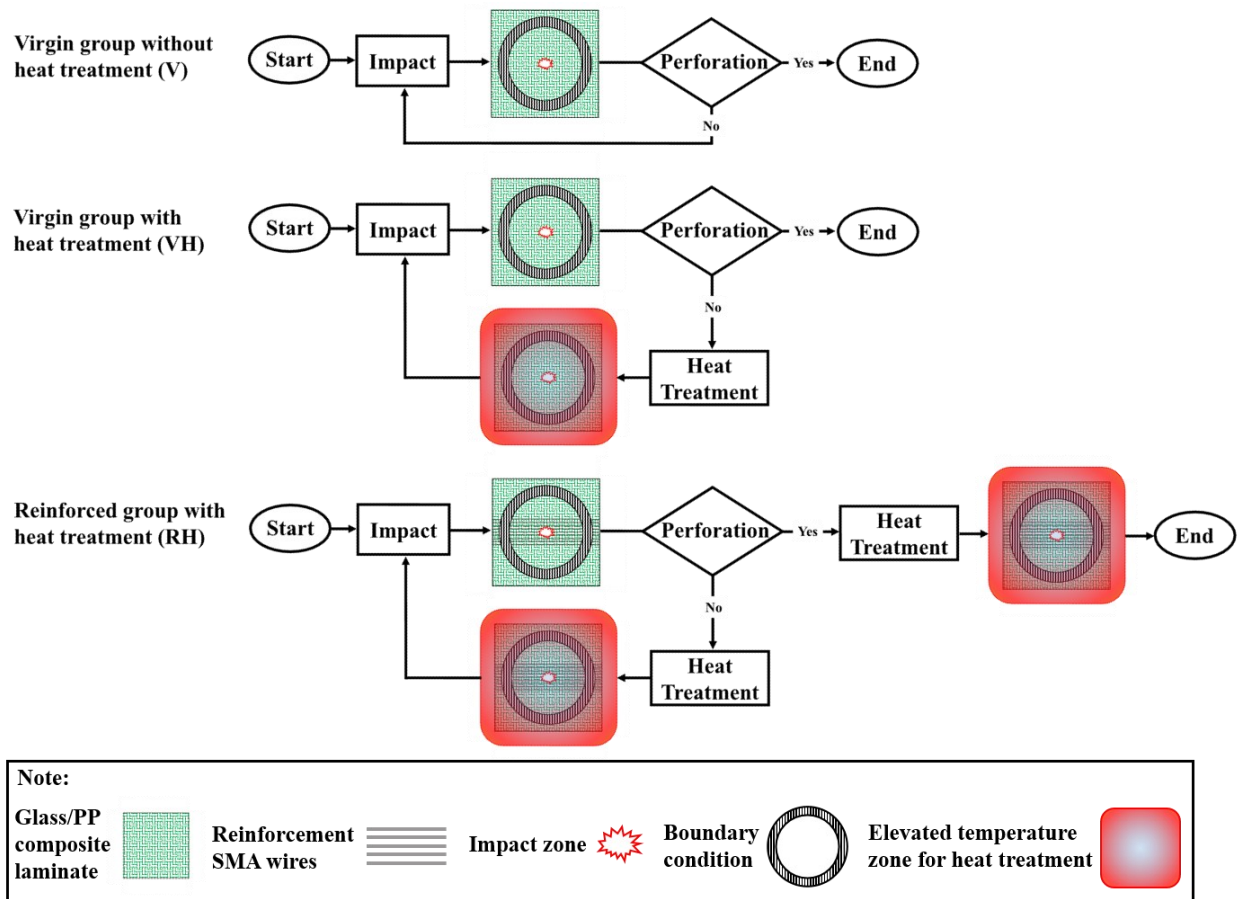
Figure. 7.3. Schematic flowchart of the repeated LVI loading and recovery heating cycles of V, VH, and RH specimens.

After each impact test, samples were clamped on an open circular fixture and placed in a preheated oven, as demonstrated in Figure. 7.4. Through this heating process, composite plates were exposed to a temperature of 160° C, gradually increasing to 175° C at a rate of 2.5° C/min. This temperature rate was compelled by the system because of the oven limitations. Passing a 2-minute mark hold time, at the temperature of 175° C, the samples were exposed to the ambient air

126

to cool down to room temperature. Previous attempts by the authors showed that the reinforced composite laminates need to be secured by the clamp force during the heating procedure. Otherwise, the SMA wires tend to separate from the composite plate at one side due to the wire shape recovery. This issue was considered to be resolved in large samples where the wires are long enough to withstand the separation force. Yet, because of the dimensional constraints, the reinforced samples need to be gripped where the SMA wires were positioned, during the heating and recovery stage.
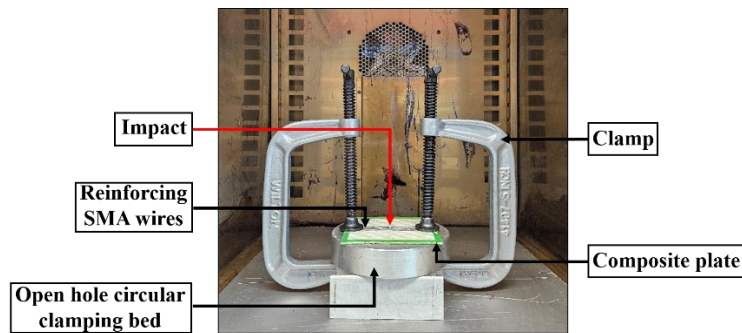
Figure. 7.4. The assembly of the reinforced composite plate secured by C-clamps during the heating process at the oven.

To measure the dent deformation of composite plates, both sides of the laminate were examined after each impact test using a dial gauge with a precision of 0.001 inches. This process was repeated for the RH composite group after each heating cycle to evaluate the recovery of the reinforced plates. Furthermore, side-view pictures of the composite plates were taken to indicate the permanent deformation of laminates and the extent of damages that occurred within the impacted region.

7.5 Results and discussion

DSC examination was crucial to determine the temperature at which the healing process should be performed. The after-impact heating cycles were supposed to be perfectly designed to melt the PP resin while activating the Nitinol wires recovery stage. Furthermore, both the SMA wire material and resin must be carefully selected being able to restore some of the initial mechanical properties after cooling down to the ambient temperature. Table 7.1 presents the important temperature measurements of the DSC tests for the intact sample of the Nitinol wire and

glass/PP cloth used to fabricate the reinforced composite laminates without accumulation of deformation and subsequent thermal cycles. Moreover, Figure. 7.5 (a) and (b) depict the DSC diagrams, respectively following the phase transformation temperatures of the Nitinol SMA material, and the melting and crystallization temperatures of PP resin.

Table 7.1. Thermal transition and phase transformation temperatures of thermoplastic PP resin and Nitinol SMA wire measured from DSC examinations.

	Melting start temperature (T_{ms})	Melting peak temperature (T_m)	Melting finish temperature (T_{mf})	Crystallization start temperature (T_{cs})	Crystallization peak temperature (T_c)	Crystallization finish temperature (T_{cf})
PP resin	137.7 °C	164.2 °C	173.1 °C	130.0 °C	118.5 °C	105.3 °C
	Austenite start temperature (A_s)	Austenite finish temperature (A_f)	Pre-martensite start temperature (R_s)	Pre-martensite finish temperature (R_f)	Martensite start temperature (M_s)	Martensite finish temperature (M_f)
Nitinol SMA wire	70.0 °C	97.8 °C	70.8 °C	53.8 °C	46.8 °C	24.6 °C
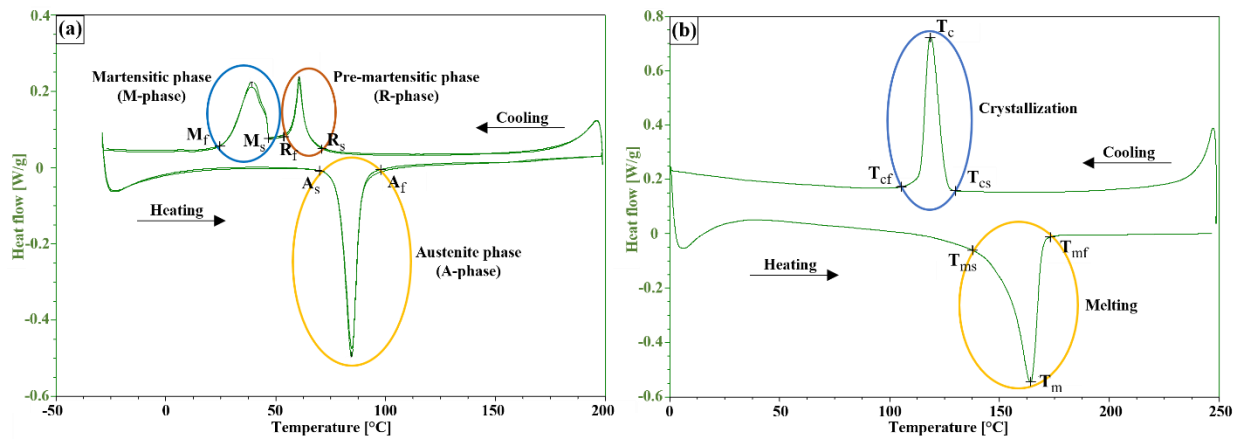
Figure. 7.5. DSC heat cycle curves, (a). Nitinol SMA wire phase transformation, and (b). Melting and crystallization of commingled PP resin within the glass/PP cloth.

The SMA material was capable of returning to its originally straight shape fully exceeding the Austenite phase (A-phase) transition temperature. Nevertheless, cooling down to the

environment temperature from a high temperature, the material resets itself experiencing the pre-martensitic phase (R-phase) and Martensitic phase (M-phase) [178]. Unlike the B19 Martensite, which has a monoclinic crystalline structure, the R-phase is an intermediate martensite phase transformation with an orthorhombic and less distorted crystal structure. This pre-martensite R-phase transformation, which occurs between the Austenite and B19 Martensite during the cooling process, is less stable than the Martensite phase transformation, yet, easier to reach because of its entropy state [179]. Thus, the chosen Nitinol material can be used at its full capacity at the examined temperature range. DSC assessment was also necessary to capture the melting range of the PP resin of the thermoplastic composite laminates. Finally, based on the DSC results, the maximum heating temperature of 175° C was assigned for the heating process which was high enough to completely melt the PP resin and soften the composite plate to be reshaped by the activated SMA wires.

Moreover, the consistency of DSC results in several test repetitions indicated that the wire materials used in the system retain their properties after multiple heating and cooling cycles. It is worth noting that the stability of SMA materials, subjected to repetitions of thermal cycles, is crucial to be assessed. It has been determined that, even though the NiTiCo SMA material experiences minimal performance degradations, it still maintains its shape memory effect and pseudoelastic properties over numerous thermal cycles [180]. While the stabilization shifts the phase transformation temperatures to higher values, the respective phase transformational energies have been decreased. In the case of this research, since the Nitinol SMA hybrid composite plates were subjected to the oven temperature of 175° C, and cooled to the ambient room temperature, possible phase transformation temperature deviation falls within the heat-treatment limits.

As discussed in the experimental procedure section, the perforation LVI energy threshold of 30 J was captured in former research on plain non-hybrid composite laminates [123]. Since the current paper tried to assess the after-impact recovery of hybrid composites under repeated LVI loadings, lower impact energy levels were required. By lowering the impacting energy below the perforation limits, the striker experiences a bounce back upon the initial drop. In such impact conditions, a portion of the energy is absorbed by a complex combination of phenomena namely friction, plastic deformation and damage propagations. The rest of the energy is restored by the tup which pushes the impactor upward causing a rebound situation. As discussed, the LVI tests were

continued until the laminates underwent full penetration, which can be noticed by the striker's movement passing through the laminate and not bouncing back after the collision. At this stage, the applied impact energy is entirely absorbed by the system.

Repeated LVI can lead to progressive damage accumulation compromising the structural integrity of the composite laminate, because of which the plates get perforated after several impacts with the same input energy. Nonetheless, the integration of SMA wire reinforcement within these composite plates can offer a viable solution. SMA wires have shown a unique ability to dissipate the impact energy, reducing the extent of damage in composite structures [18,90,91]. In addition to the wires' capability in energy absorption, SMA wires were specifically considered to recover damages or plastic deformations, which are responsible for permanent deformations. When subjected to thermal activation, the SMA wires' tendency to restore their original shape can source an out-of-plane force that can recover the plate's deformation [14,17,18].

Instead of the presented approach, replacement techniques such as patching could be potentially used to reinforce the impacted area. Yet, this method requires the damaged area to be accessible, while considerably timely operations need to be done manually. Furthermore, it may introduce stress concentration and material properties mismatch which could affect the load transfer and stiffness of the structure. In contrast, incorporating the Nitinol SMA wires enables an in-situ deformation recovery of impacted areas, possibly performed through external or electrical current heating, which simplifies the repair process reducing the risk of introducing new weak points [15]. Although replacement of the damaged area remains a viable option, these SMA-reinforced composite plates could present a promising alternative rapid repairing technique.

In the current study, in addition to the potential of SMA wires to improve the repeated impact preformation threshold, the level of recovery of the hybrid composite laminates after heat treatment cycles was deeply examined. The relevant data on the repetitions of 20 J impact tests for each sample group were collected in Figure. 7.6 to facilitate a comprehensive comparison of their response. The analysis of force-displacement results revealed a reduction in the slope of the diagrams after each impact which conveyed the loss of laminate stiffness. This observed degradation in the mechanical properties was attributed to the accumulation of damage, during each loading set. The collision of the striker to the composite plate at energy levels close to the perforation threshold can cause significant damage, such as matrix cracking, delamination, and

localized fiber breakage or fiber pull-out which substantially diminishes the stiffness and strength of these laminates [6,123]. These findings underscore the impact of repeated LVI on the structural integrity of composites, emphasizing the importance of strategies taking advantage of the hybridization technique.
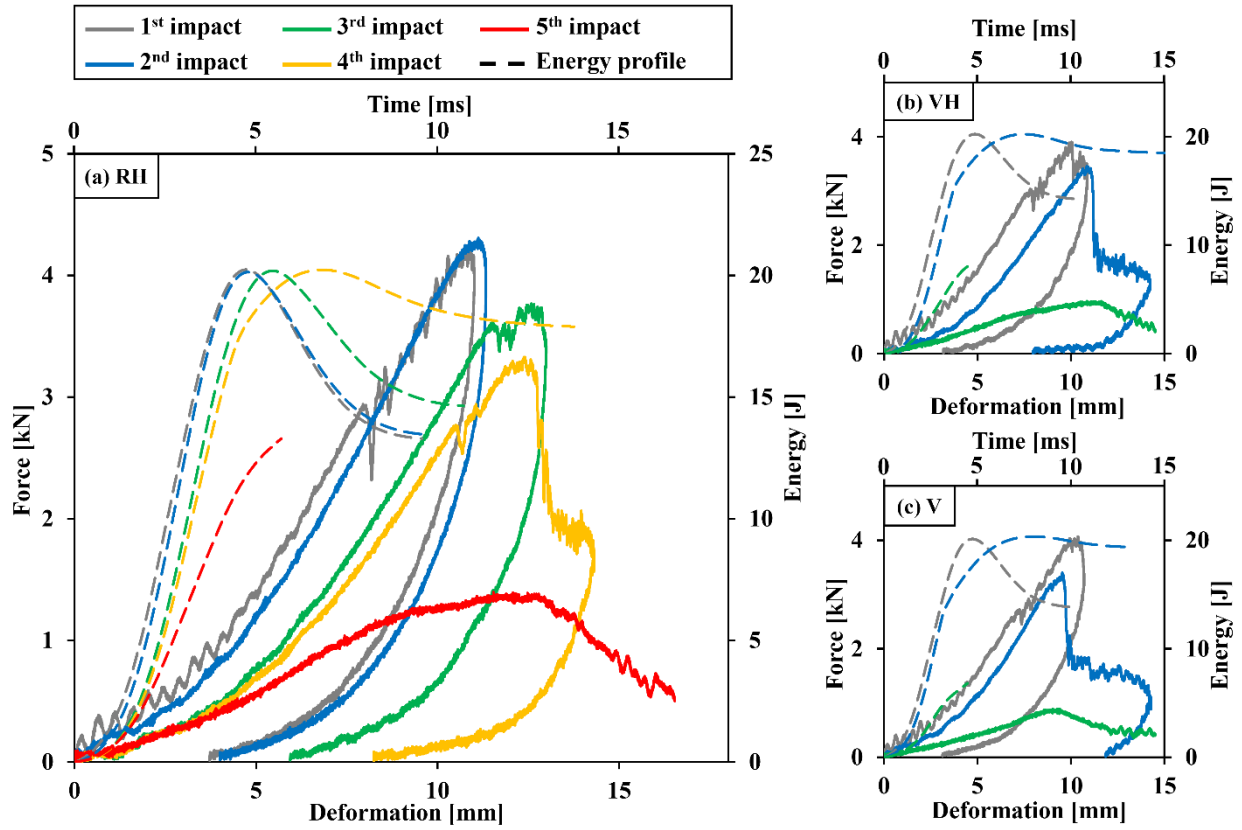
Figure. 7.6. Force-displacement and energy-time diagrams of the (a) SMA reinforced composite laminate subjected to heat treatment cycles (RH), (b) Virgin non-hybrid composite plates with heat treatment (VH), and (c) Virgin non-hybrid untreated composite groups (V) under repeated 20 J impacts.

Both non-hybrid V and VH sample groups exhibited a sudden load drop after reaching the maximum load at the second impact, which caused catastrophic damage to the laminates. The extent of damage was substantial at the second 20 J impact, with most of the applied energy being absorbed by the sample leaving only a small portion to rebound the tup. Despite the significance of damage at this stage, the panels were not fully penetrated as some of the deformation was

recovered. Thus, the third repetition of the 20 J strike was counted to be the maximum number of impacts required to fully perforate the plain composite laminates.

Here, the VH control group has been investigated in order to identify any significant defects or respective deterioration in the mechanical properties related to thermal cycles, that could potentially accelerate the LVI perforation. Due to the high viscosity of the thermoplastic PP resin used in this research, the thermal cycles did not have a substantial negative effect on the quality or appearance of the composite plates. Even though minor defects are expected to occur because of the heat treatment cycles, they do not necessarily govern the threshold number of repeated LVI tests required to perforate the composite laminates.

Reinforcing the laminates with SMA wires was shown to be beneficial in increasing the number of impacts required to fully penetrate the composite plate. The sudden load drop, which is an indication of catastrophic damage within the laminate, occurred at the fourth 20 J impact, while full penetration of the RH hybrid composite group was observed at the fifth one. In addition to the energy-absorbing capability of reinforcing metallic wires, the recovery cycles performed on the RH laminates effectively reset the SMA wires' properties and restored some of the plate's deformation. This healing process mitigated the severity of damages, thereby increasing the maximum number of 20 J impacts required to perforate the plate.

Although the SMA wires are positioned in the in-plane direction within the hybrid composite plates, under the impact condition they experience an out-of-pane deformation due to the bending force applied by the striker. Being subjected to heat-treatment cycles, the Nitinol SMA wires undergo a crystalline phase transformation, causing them to return to their original straight form. As the SMA wires straighten during this healing phase, they induce out-of-plane pressure on the deformed composite laminate, contributing to the after-impact deformation recovery in the z-direction. This out-of-plane force is a result of the intrinsic behavior of Nitinol SMA wires returning to their initial straight shape, applying a compressive force that recovers a good portion of the deformations and possibly healing some damages.

Moreover, following each treatment cycle, the molecular orientation of Nitinol wires enters a series of phase transitions from the A-phase to the M-phase and vice versa. These material phase changes reset the metallic reinforcement system that allows it to absorb a considerable share of

impact energy through plastic deformation. Despite the localized recovery of some out-of-plane deformations, the RH samples experienced a stiffness reduction after each impact. Furthermore, the maximum level of force that the panels can withstand decreases with impact repetitions due to the propagation of damages within the composite. Lastly, observations revealed that, in addition to introducing a chance to recover some of the damage and deformations through heating and cooling cycles, the threshold number of 20 J LVI tests needed to perforate the RH composite sample was improved by 66.7% compared to the control groups.

As mentioned, one of the main goals of this study was to evaluate the capability of SMA reinforcing wires on the scale of recovery on after-impact permanent deformation. While this new technique can improve the perforation threshold number of LVI tests, it introduces a novel and relatively simple method to mitigate after-impact dent deformation. Figure. 7.7 presents side-view pictures of the plates showing the permanent indentation of the impact zone, associated damage, and the recovery of the RH laminate group after every loading and healing cycle. Exceeding the melting temperature of the resin, which is higher than the Nitinol A-phase, the SMA wires tend to return to their original straight shape. This reversion applies an out-of-plane load to the softened composite laminate that assists in the recovery of a considerable portion of the dent's permanent deformation. For instance, 76 % of the front surface dent deformation, after the third 20 J impact test, has been restored during the heat treatment cycle. During the initial impacts, where the damage has not yet reached a catastrophic state, the healing cycles allows the front surface indentation to be reasonably flattened. Unlike the RH composite samples, which were assessed after each impact and heat treatment cycle, the VH group was evaluated focusing on capturing potential property changes. The VH sample group was examined to monitor the effect of heating cycles on the subsequent impact test responses and does not necessarily experience deformation changes when subjected to heating cycles.
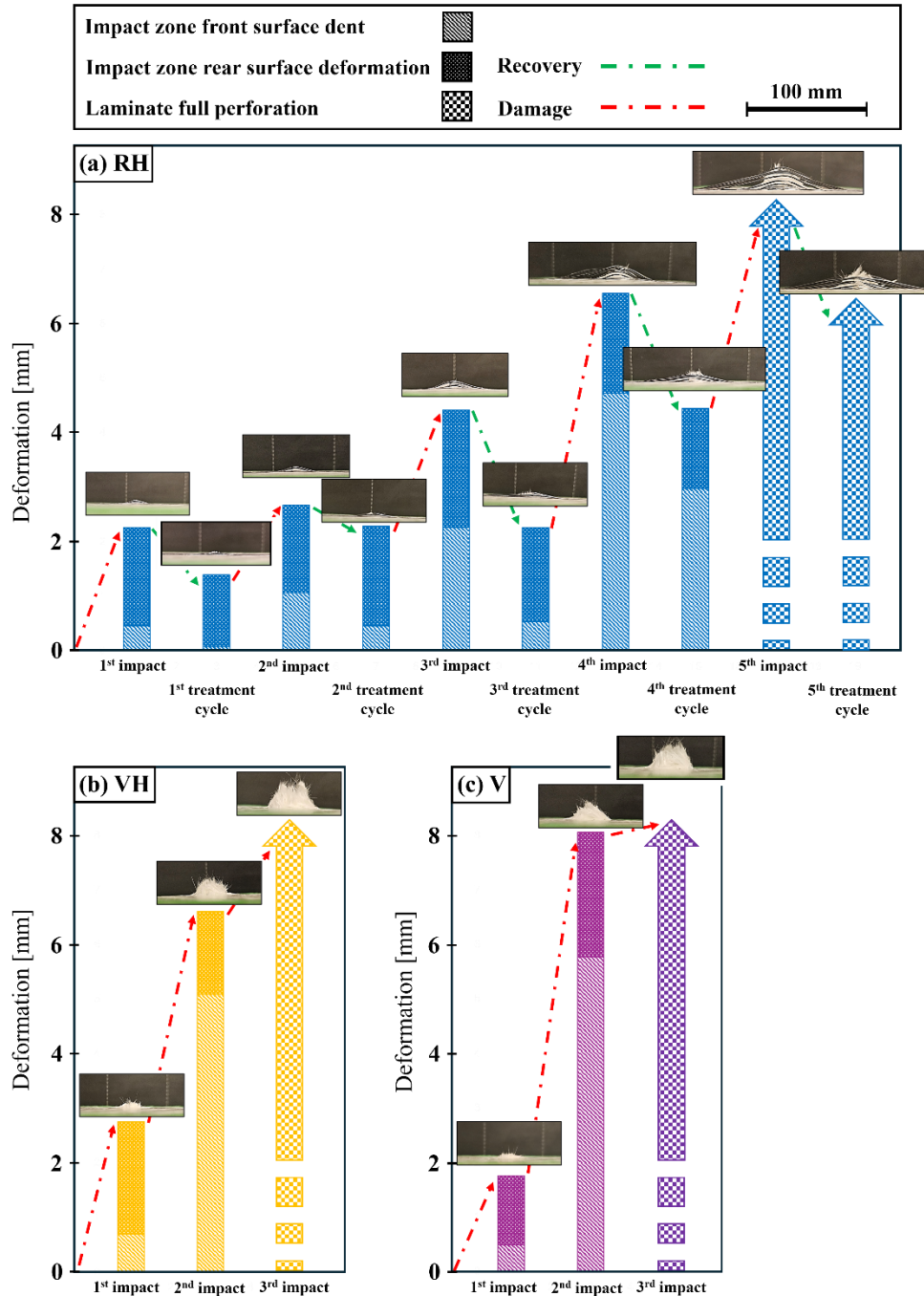
Figure. 7.7. The evaluation of after-impact deformation and recovery of (a). RH, (b). VH, and (c). V group composite plate subject to repeated 20 J LVI tests.

Nonetheless, evaluations of the post-treatment plates revealed that certain damages cannot be healed through this process, either due to the nature of the damage or the insufficient out-of-plane force exerted by the SMA wires. Catastrophic damages such as fiber breakage are unlikely

to be affected by this method. The damages that were not resolved by the heat treatment, are the main source of stiffness reduction during the repetition of LVI tests on the RH composite group. However, since thermoplastic composites experience elasto-plastic deformation, a portion of plastic deformations can be recovered during the heating process. Moreover, minor matrix cracks and localized delamination have a good chance of being healed by the out-of-plane force applied to the system due to SMA wires at high temperatures. Lastly, the SMA wires themselves fully reset after each healing process, improving the laminate's resistance to subsequent impacts.

It should be acknowledged that there are potential challenges associated with the in-situ healing process. Considering the current approach, relatively larger damaged structures cannot be simply dealt with, since these components may experience non-uniform heating, leading to undesirable thermal expansions, warping or uneven recovery. Besides, heating the hybrid composite plate locally can induce thermal stresses due to the thermal coefficient mismatch between the component and untreated areas. Prolonged exposures to such high temperatures, required to melt the thermoplastic PP resin, can result in resin flow or matrix softening, negatively affecting the stability of the composite structure, which requires further investigation.

By reducing the impact energy, the threshold number of impacts required to perforate the composite plates is expected to increase. While the laminates were perforated after five 20 J impacts, seven repetitions of 15 J LVI tests were necessary for the tup to fully penetrate the RH composite plates. A similar trend was observed in the Virgin control group, where the number of LVI tests required for perforation increased by one. Although the number of impacts needed to perforate the VH group plates remained unchanged at this lower energy level, the force and energy responses exhibited a clear deviation from the previous tests. This behavior was captured and presented in Figure. 7.8 for all the repetition of impact tests. It was revealed that the sudden load drop represents a significant level of damage after which even the already heat-treated RH group sample experienced perforation. Furthermore, because the extent of damage was lower after a set number of repeated 15 J impacts, the maximum load-bearing values were higher.
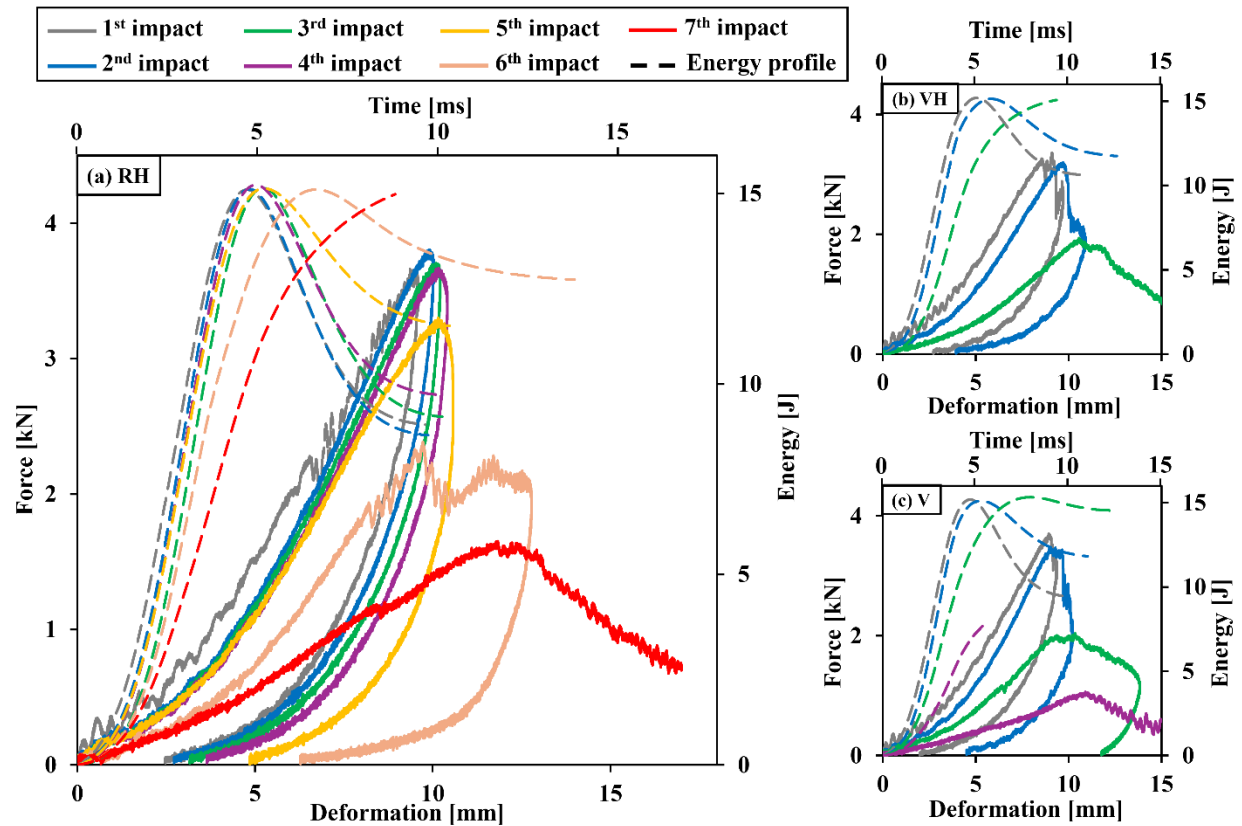
Figure. 7.8. Repeated LVI test diagrams of the (a) RH, (b) VH, and (c) V composite groups under 15 J impacts.

Reducing the applied impact energy in each strike directly diminished the extent of subsequent damages; therefore, the stiffness reduction, related to the propagation of damages within the composite laminates, was less pronounced under a series of 15 J impacts compared to the 20 J impact responses. Unlike the V and VH control groups, a considerable portion of plastic deformation of the RH composite laminate was recovered by the heating process. Not only SMA wires are good absorbents of energy because of their specific pseudoelastic behavior, but also can recover their mechanical properties through the healing process. As discussed, this shape restoration applied out-of-plane force on the composite laminate, healing some of the deformations and damages, which is evidenced by the comparatively lower stiffness drop in the RH sample group.

The Nitinol SMA wires are predominantly in the Martensitic phase characterized by a twinned structure, at room temperature. The applied stress during the impact tests leads to a

136

reorientation of these Martensitic variants to the detwinned ones. Even though the energy dissipation within this process is moderate compared to the phase transformation, it is significant enough to contribute to the LVI energy absorption. Upon heating, the SMA wires experience a phase transformation from Martensite to a relatively more ordered and structurally symmetrical Austenite phase [181–183]. During this process, the wires recover their original straight shape, rearranging their crystalline structure. In contrast to the mechanical deformation of the impacted samples, this step offers higher energy dissipation. Finally, being cooled down to the ambient temperature, the Nitinol SMA wires undergo a reverse Martensite phase transformation, releasing a portion of previously absorbed energy to reset the wires. Nevertheless, it is worth mentioning that due to the hysteresis input and recovery energy differences, there is net energy dissipation within a full thermal cycle.

Comparing the number of 15 J impact strikes required to reach full perforation, the RH composite group outperformed the VH and V control groups by 133.3% and 75%, respectively. Furthermore, the deformation of each sample group after repeated striker collisions was depicted in Figure. 7.9, which highlights the significant recovery in the RH composites due to the heating cycles, with approximately 70 % of the plastic deformation from the front impact dents being healed in all four initial strikes. Nonetheless, the SMA wires were unable to sufficiently recover the sample to its former state especially healing the puncture created by the impactor's penetration. Because of the extensive damage progression, which ultimately exceeded the recovery capacity, the material's integrity has been compromised and failed to recover during the heating cycles. This limitation was also evident in the composite plates' loss of stiffness. Even though at the early impacts, treatment effectively prevented a sudden drop in material properties, the final impacts led to a significant stiffness reduction due to the propagation of damages beyond the state of recovery.
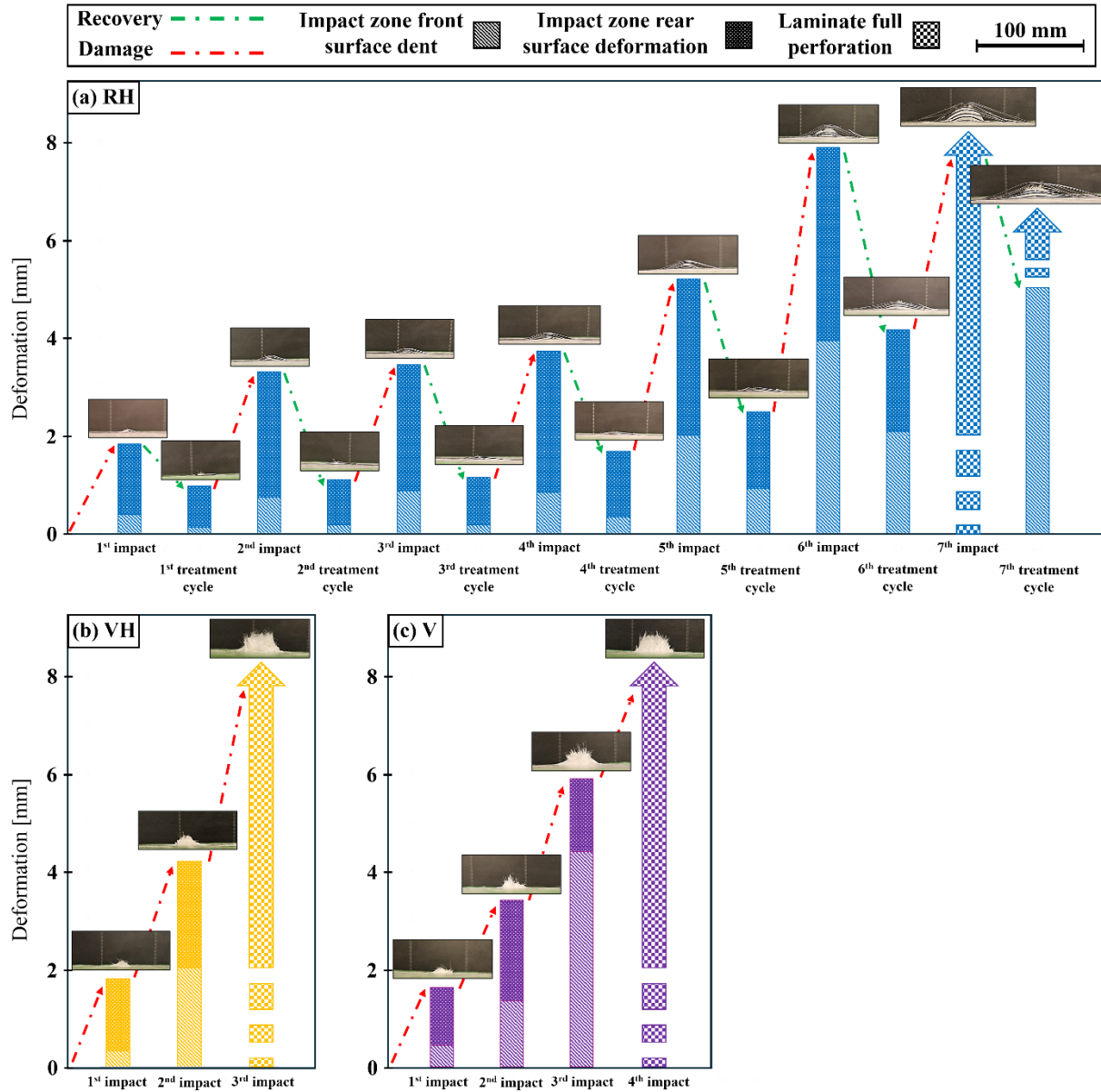
Figure. 7.9. A comparative assessment of after-impact deformation and recovery of (a). RH, (b). VH, and (c). V group plates after repetitions of 15 J impact tests.

The heat treatment procedure performed on RH composite sample groups was revealed to play a critical role in repeated impacts, particularly when minor damage and deformation were formed. Thus, to further support the observations, the repeated LVI tests were replicated at 10 J impacting energy, during which the threshold number of strikes for penetration was dramatically increased. Indeed, the V group plain composite sample withstood a maximum of 15 repetitions of

10 J impacts, with the perforation threshold increasing by four times compared to the 20 J LVI tests.

Due to its relatively low impact energy, each repetition of the LVI test does not necessarily result in a significant change in performance, particularly in the early and mid stages of the impact sequence. In other words, at such low energies, minimal deformation occurs which results in a gradual damage propagation and delays the onset of catastrophic failure. Subsequently, the reduction in stiffness after each impact is less pronounced. However, as the number of impacts increases and the system approaches the perforation threshold, a rapid accumulation of internal damages leads to noticeable reductions in stiffness and deviations in laminate behavior, illustrated in Figure. 7.10. While both non-hybrid composite sample groups have been penetrated, the SMA-reinforced sample continued to absorb impact energy and demonstrated the ability to recover. With the employed heat-treatment cycles, the hybrid composite samples recovered about 64 % of the front and 47 % of the rear dent deformation at the 25th strike.
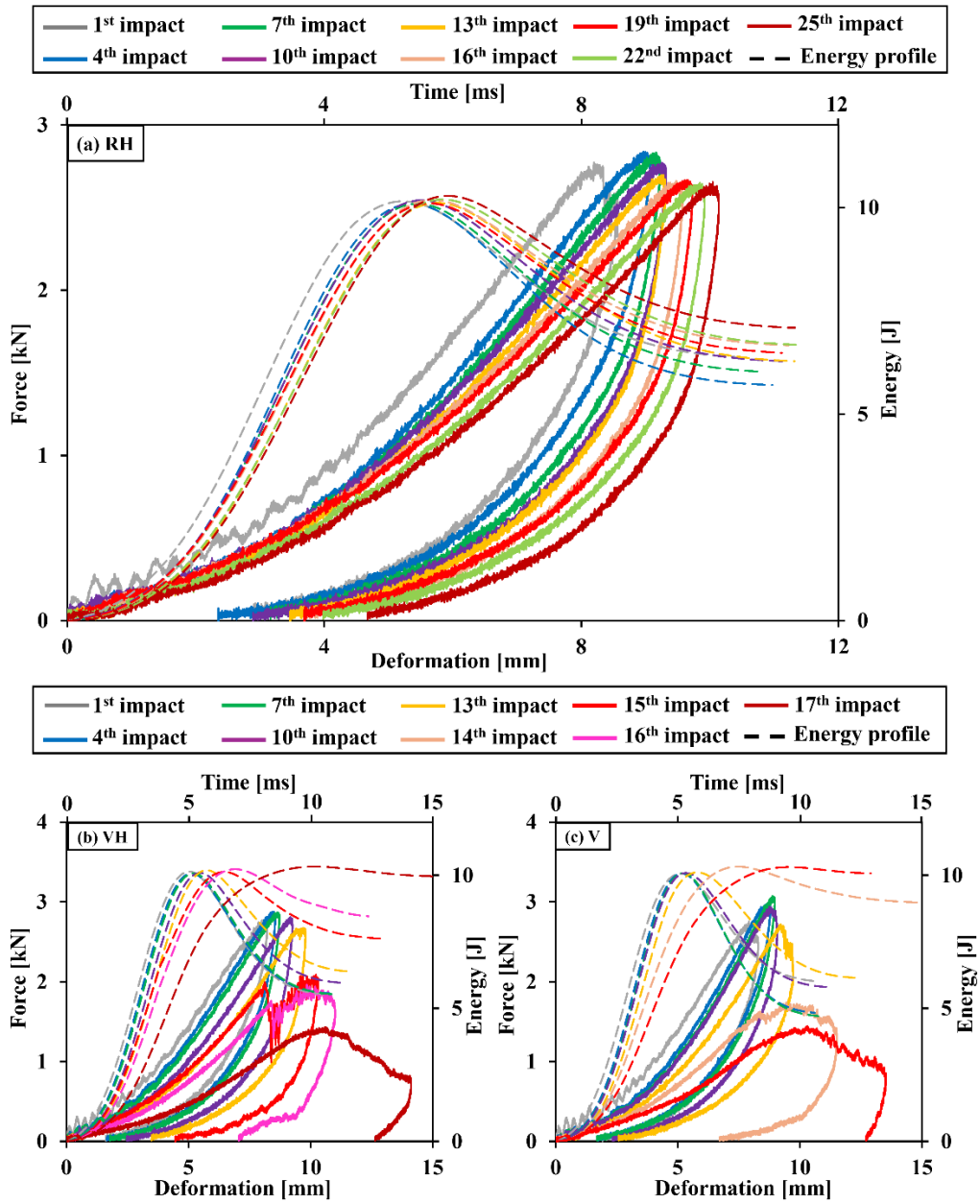
Figure. 7.10. Repeated 10 J impact test diagrams of the (a) RH, (b) VH, and (c) V composite groups.

Figure. 7.11 presented the post-impact dent deformations for all three sample groups subjected to repeated 10 J impact tests. As discussed, relatively slower damage accumulation and permanent deformation were observed during the initial impacts. Continuing the impact tests, damage propagation accelerated in non-hybrid composite laminates experiencing catastrophic failures. Nonetheless, the reinforced hybrid samples demonstrated the ability to withstand 25

collisions while maintaining structural integrity. Even though the RH composite group has been damaged, the energy-absorbing capabilities of the embedded SMA wires, combined with heat-treatment cycles, allowed these plates to outperform the non-hybrid ones. This behavior has been captured by the almost steady state of after-impact dent deformation and recovery measurements of the RH hybrid composite group, compared to the progressively increasing dent measurements of virgin composite laminates.
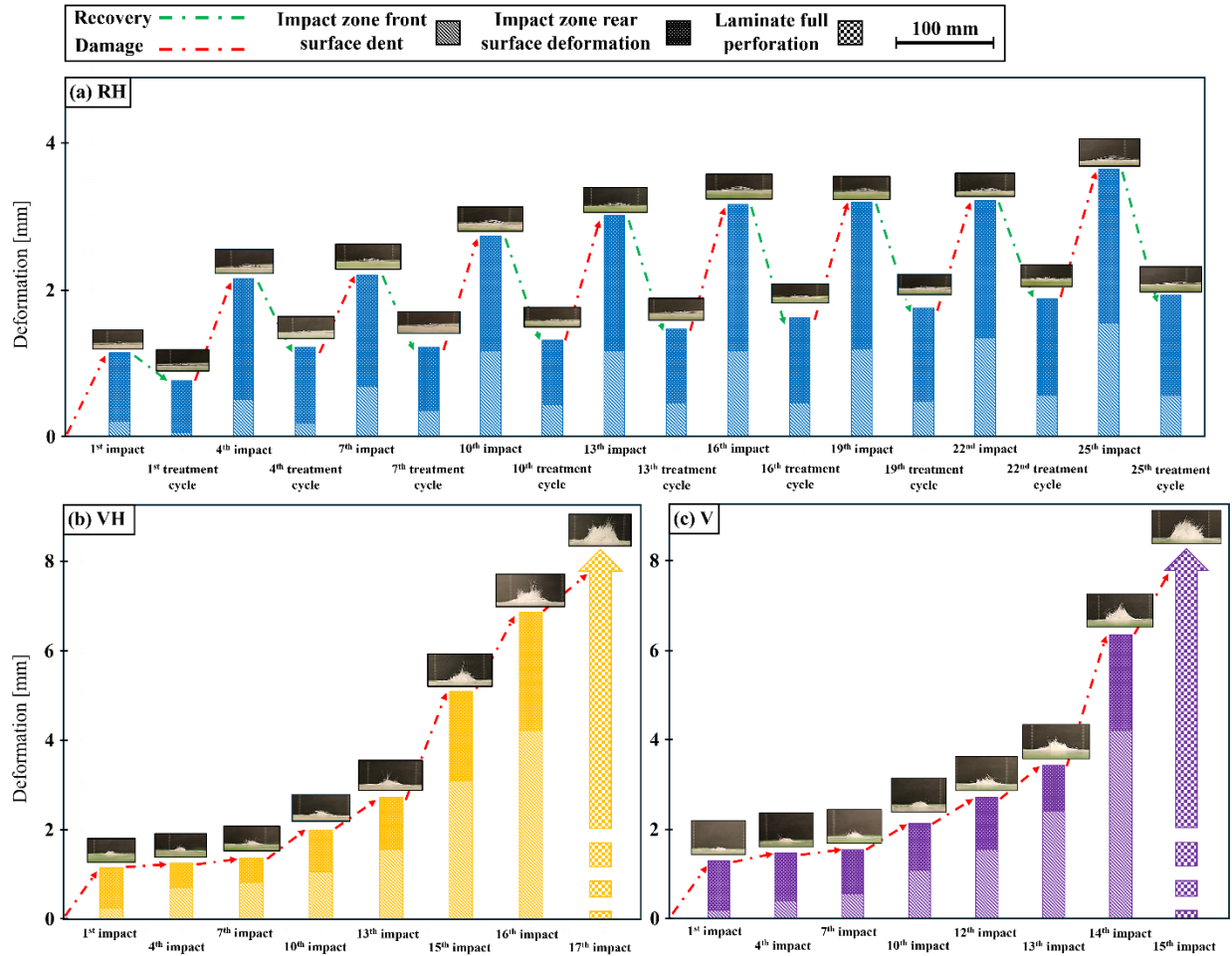
Figure. 7.11. After-impact deformation and SMA-assisted healing of (a). RH, (b). VH, and (c). V composite plates under repeated 10 J LVI tests.

In this investigation, the authors mainly focused on the extent and feasibility of recovery that hybridization with Nitinol SMA wires could offer to the composite structure after each set of impact and heat treatment cycles. At this stage, our goal was to investigate the potential benefits of

SMA hybridization in terms of restoring the structural form and mitigating damage in composite laminates. This recovery of deformation does not necessarily translate into damage recovery or strength property improvement during the healing cycle. Hence, the evaluation of the residual strength of the samples after each impact and recovery stage performing Compression After Impact (CAI) tests could be an interesting topic to follow up on. Evaluating the post-impact strength of these materials, though complementary CAI examinations, will provide valuable information about the structural integrity and post-impact residual strength of the SMA-assisted recovered composite laminates.

7.6 Conclusion

A comprehensive investigation of thermoplastic composite laminates strengthened with SMA wires was performed, focusing on their repeated impact performance and effectiveness of heat treatment healing. The repeated LVI leads to the accumulation of damages leading to deterioration of the mechanical properties. To address this issue, a novel method was developed utilizing SMA wires to reinforce the composite plates, presenting them with an ability to recover. Using a compression molding technique, SMA wires were embedded within the PP-based plates, reinforcing the structural rear side of the impacting location. DSC examinations were conducted on both composite cloth and SMA Nitinol materials to determine a proper heat-treatment cycle ensuring effective recovery of damages and deformations occurred during the LVI test repetitions.

In addition to the improvement in the threshold number of impacts required to perforate the plates, the hybridization approach used in this research has been evaluated for its applicability to recover after-impact deformations during a thermal healing process. Under repeated impact loading, conducted at three different energy levels, the composite plates reinforced with SMA wires demonstrated a significant enhancement in the perforation threshold impact counts. The experimental findings showed that the hybrid samples subjected to 10 J impact tests exhibited remarkable resilience, with no perforation occurring even after 25 impacts. At higher energy levels of 15 J and 20 J, the number of impacts required to penetrate the hybrid samples demonstrated respective improvements of 75 % and 66 %, compared to the virgin non-hybrid composite sample groups.

Moreover, the after-impact dent deformation of all LVI test iterations was carefully measured to better capture the healing effect of SMA wires. It was revealed that the SMA-assisted recovery process effectively restored a substantial portion of the permanent dent deformation, particularly at the early impacting stages where damages did not reach a catastrophic level. Despite some residual damages remaining, which can affect the residual strength of the hybrid composites, the SMA wires could recover a considerable amount of dent deformation even exceeding the 50 % healing by the heat-treatment procedure. Therefore, the heating process can be introduced as a reliable method for recovering some of the plastic deformation and minor damages in the SMA-reinforced composites, thereby enhancing their response to repeated impacts. By restoring the material's integrity, this thermal treatment process extended the composite plates' lifespan and offered a smart, adaptive solution for after-collision deformation recovery of structural applications.

Chapter 8:

Conclusions and Future Work

8. Conclusions and Future Work

8.1 Conclusions

In conclusion, this thesis provided a comprehensive investigation into the development and performance of thermoplastic-based composite laminates and sandwich panels, with a focus on optimizing fabrication methods, reinforcing these structures through hybridization techniques, and assessing their LVI response. Thus, a variety of approaches were explored to enhance the mechanical performance, energy absorption, and damage recovery of these composite systems.

Firstly, the optimization of the double-belt lamination and compression molding methods was thoroughly examined to produce fully recycled PET foam core sandwich panels. The studies revealed that both techniques can produce high-quality panels, with the double-belt process being particularly advantageous for continuous large-scale production. However, compression molding demonstrated superior control over lamination parameters, such as temperature and pressure, leading to fewer defects and enhanced flexural performance. Despite some limitations, both methods produced viable and structurally qualified sandwich panels with proper skin-to-core bonding, as confirmed by flexural, peel-off, and flatwise tensile test results.

Secondly, the introduction of stainless-steel mesh as a reinforcing layer significantly improved the energy absorption and mechanical behavior of both thermoplastic laminates and sandwich panels under LVI loading. The hybridization of glass/PP composite laminates with metallic mesh layers improved their ability to withstand higher impact energies, delaying perforation and improving impact resistance. The positioning of the mesh within the laminate, along with factors such as wire diameter, stacking sequence, and layup orientation, was found to critically influence the LVI response, with the $[G/M^{0.70}/G]$ hybrid laminate exhibiting the best performance. For sandwich panels, the incorporation of stainless-steel mesh in the impacting skin side significantly improved energy absorption, altered load distribution to the PET foam core, and modified damage propagation. This hybridization process, using stainless-steel metal mesh to reinforce the panels' composite facesheets, resulted in superior performance compared to non-hybrid composite sandwich panels.

Finally, the use of SMA wires in thermoplastic laminates introduced a novel adaptive solution for improving impact resistance and in-situ recovery. By embedding SMA wires into the composite structure and heat treatment cycles, enhanced recovery of permanent dent deformations after repeated LVI impacts was achieved. The hybrid laminates with SMA wires not only withstood a higher number of impacts before perforation but also exhibited significant recovery capabilities, with over 50% of dent deformation being restored in certain cases. This SMA-assisted recovery process underscores the potential for extending the operational lifespan of composite structures, particularly in applications involving repeated low-energy impacts.

8.2 Future Work

There are several future works that were planned to be covered or have the potential for upcoming studies:

- This study primarily focused on optimizing the process to achieve proper bonding between the composite skin and PET foam without melting the core material. It is well-known that viscosity plays a crucial role in the fabrication process, and it has been acknowledged that further research is needed to measure the viscosity of PP resin and PET molten thermoplastics, as well as to explore a lamination procedure that would facilitate molecular bonding.

- Further investigations could evaluate the degree of polymer chain entanglement at the interface and measure the level of interdiffusion between the thermoplastic PP resin and the PET foam core. While operating the double-belt process at temperatures near the melting point of the PET foam presents challenges, exploring the possibility of laminating panels by melting the PET core surface could be a potential research scope.

- In order to fully expand upon the potential of this research, Finite Element analysis has been considered in our group as part of future work. Specific steps have been taken to characterize the mechanical properties of each layer. These steps include tensile, compression, and shear tests for the glass/PP skin and impregnated mesh layer, as well as mechanical tests for the PET foam core material, ensuring the accuracy of the entry data for the FE simulations. It is planned to model the LVI behavior of the composite laminates and sandwich panels in ABAQUS, treating each layer independently.

Moreover, the potential of using UMAT or VUMAT subroutines could be considered to better capture the failures based on the specific damage criteria available for composites and foam materials.

- The influence of SMA wire thickness and orientation on the impact performance and recovery capabilities of the composite laminates could be further investigated. Optimizing these parameters may lead to enhanced energy absorption and higher recovery efficiency.

- More detailed study on the extent of repeated LVI damage and thermal recovery could be conducted using CT scan imaging technique. These methods would allow for precise monitoring of crack closure and delamination recovery after heat-treatment cycles, providing deeper insights into the effectiveness of SMA-assisted healing in composite laminates.

References

[1]   Caprino G, Lopresto V. The significance of indentation in the inspection of carbon fibre-reinforced plastic panels damaged by low-velocity impact. Compos Sci Technol 2000;60:1003–12. https://doi.org/10.1016/S0266-3538(99)00196-7.

[2]   Caprino G, Lopresto V. On the penetration energy for fibre-reinforced plastics under low-velocity impact conditions. Composite Science and Technology 2001;61:65–73. https://doi.org/10.1016/S0266-3538(00)00152-4.

[3]   Caprino G, Langella A, Lopresto V. Indentation and penetration of carbon fibre reinforced plastic laminates. Compos B Eng 2003;34:319–25. https://doi.org/10.1016/S1359-8368(03)00002-7.

[4]   Lopresto V, Caprino G. Dynamic failure of composite and sandwich structures. Dynamic Failure of Composite and Sandwich Structures, 2013, p. 209–90. https://doi.org/10.1007/978-94-007-5329-7.

[5]   Sunith BL, Pradeep Kumar K V, JayaChristiyan KG. Studies on factors influencing low velocity impact of composite materials - A review. IOP Conf Ser Mater Sci Eng 2021;1126:012079. https://doi.org/10.1088/1757-899x/1126/1/012079.

[6]   Shah SZH, Karuppanan S, Megat-Yusoff PSM, Sajid Z. Impact resistance and damage tolerance of fiber reinforced composites: A review. Compos Struct 2019;217:100–21. https://doi.org/10.1016/j.compstruct.2019.03.021.

[7]   Grünewald J, Parlevliet P, Altstädt V. Manufacturing of thermoplastic composite sandwich structures: A review of literature. Journal of Thermoplastic Composite Materials 2016;30:437–64. https://doi.org/10.1177/0892705715604681.

[8]   Mines RAW, Worralls CM, Gibson AG. Low velocity perforation behavior of polymer composite sandwich panels. Int J Impact Eng 1998;21:855–79. https://doi.org/10.1016/S0734-743X(98)00037-2.

[9]   Truong GT, Tran H van, Choi KK. Tensile behavior of on- and off-axis carbon fiber reinforced polymer composites incorporating steel wire mesh. Mechanics of Materials 2019;137. https://doi.org/10.1016/j.mechmat.2019.103131.

[10]   Truong GT, Choi KK. Tensile behavior of hybrid composites of carbon fibers—steel wire mesh reinforced polymer. Mechanics of Advanced Materials and Structures 2021;28:154–66. https://doi.org/10.1080/15376494.2018.1553256.

[11]   Mosleh Y, Clemens D, Gorbatikh L, Verpoest I, Van Vuure AW. Penetration impact resistance of novel tough steel fibre-reinforced polymer composites. Journal of Reinforced Plastics and Composites 2015;34:624–35. https://doi.org/10.1177/0731684415574538.

[12]   Suslu H, Fan J, Ibekwe S, Jerro D, Mensah P, Li G. Shape memory alloy reinforced vitrimer composite for healing wide-opened cracks. Smart Mater Struct 2020;29:065008. https://doi.org/10.1088/1361-665X/AB85A7.

[13]   Saeedi A, Shokrieh MM. A novel self-healing composite made of thermally reversible polymer and shape memory alloy reinforcement. Journal of Intelligent Material Systems and Structures. 2019;30(10):1585–93. https://doi.org/10.1177/1045389X19844015.

[14]   Cohades A, Hostettler N, Pauchard M, Plummer CJG, Michaud V. Stitched shape memory alloy wires enhance damage recovery in self-healing fibre-reinforced polymer composites. Compos Sci Technol 2018;161:22–31. https://doi.org/10.1016/j.compscitech.2018.03.040.

[15]   Wang CC, Ding Z, Purnawali H, Huang WM, Fan H, Sun L. Repeated instant self-healing shape memory composites. J Mater Eng Perform 2012;21:2663–9. https://doi.org/10.1007/S11665-012-0374-1/metrics.

[16]   Kirkby EL, Michaud VJ, Månson JAE, Sottos NR, White SR. Performance of self-healing epoxy with microencapsulated healing agent and shape memory alloy wires. Polymer. 2009;50:5533–8. https://doi.org/10.1016/j.polymer.2009.05.014.

[17] Konlan J, Mensah P, Ibekwe S, Li G. A laminated vitrimer composite with strain sensing, delamination self-healing, deicing, and room-temperature shape restoration properties. J Compos Mater 2022;56:2267–78. https://doi.org/10.1177/00219983221098225.

[18] Konlan J, Mensah P, Ibekwe S, Crosby K, Li G. Vitrimer based composite laminates with shape memory alloy Z-pins for repeated healing of impact induced delamination. Compos B Eng 2020;200: 108324. https://doi.org/10.1016/j.compositesb.2020.108324.

[19] Åkermo M, Åström BT. Modeling compression molding of all-thermoplastic honeycomb core sandwich components. Part A: Model development. Polym Compos 2000;21:245–56. https://doi.org/10.1002/pc.10182.

[20] Åkermo M, Åström BT. Modeling compression molding of all-thermoplastic honeycomb core sandwich components. Part B: Model verification. Polym Compos 2000;21:257–67. https://doi.org/10.1002/pc.10183.

[21] Skawinski O, Binetruy C, Krawczak P, Grando J, Bonneau E. All-thermoplastic composite sandwich panels - Part I: Manufacturing and improvement of surface quality. Journal of Sandwich Structures and Materials 2004;6:399–421. https://doi.org/10.1177/1099636204040094.

[22] Skawinski O, Binetruy C, Krawczak P, Grando J, Bonneau E, Scanzi JM, et al. All-thermoplastic composite sandwich panels - Part II: Modelling of bending behaviour. Journal of Sandwich Structures and Materials 2004;6:423–46. https://doi.org/10.1177/1099636204040093.

[23] Akermo M, Tomas Astrom B. Experimental Investigation of Compression Molding of Glass/PP-PP Foam Core Sandwich Components. Journal of Thermoplastic Commposite Materials 1999;12:297–316. https://doi.org/10.1177%2F089270579901200404.

[24] Mazzuca P. Flexural behaviour of GFRP sandwich panels with eco-friendly PET foam core for the rehabilitation of building floors. Structures, Elsevier 2024;60:105815. https://doi.org/10.1016/j.istruc.2023.105815.

[25] Oliveira PR, dos Santos JC, Ribeiro Filho SLM, Torres Ferreira B, Panzera TH, Scarpa F. Eco-friendly sandwich panel based on recycled bottle caps core and natural fibre composite facings. Fibers and Polymers 2020;21:1798–807. https://doi.org/10.1007/s12221-020-9818-7.

[26] Laria JG, Gaggino R, Kreiker J, Peisino LE, Positieri M, Cappelletti A. Mechanical and processing properties of recycled PET and LDPE-HDPE composite materials for building components. Journal of Thermoplastic Composite Materials 2023;36:418–31. https://doi.org/10.1177/0892705720939141.

[27] Kassab R, Sadeghian P. Effects of material non-linearity on the structural performance of sandwich beams made of recycled PET foam core and PET fiber composite facings: Experimental and analytical studies. Structures 2023;54:1259–77. https://doi.org/10.1016/j.istruc.2023.05.119.

[28] Bocz K, Ronkay F, Vadas D, Molnár B, Gere D, Czigány T, et al. Flame retardancy of PET foams manufactured from bottle waste. J Therm Anal Calorim 2023;148:217–28. https://doi.org/10.1007/s10973-022-11423-3.

[29] Bocz K, Ronkay F, Molnár B, Vadas D, Gyürkés M, Gere D, et al. Recycled PET foaming: Supercritical carbon dioxide assisted extrusion with real-time quality monitoring. Advanced Industrial and Engineering Polymer Research 2021;4:178–86. https://doi.org/10.1016/j.aiepr.2021.03.002.

[30] Liu H, Antwi-Afari MF, Mi H, Liu C. Research on the feasibility of polyethylene terephthalate foam used in wind turbine blades. Environ Prog Sustain Energy 2023;42:e13956. https://doi.org/10.1002/ep.13956.

[31] Kang G, Joung C, Kim H, Im S, Kang S, Ji W, et al. Manufacturing, thermoforming, and recycling of glass fiber/PET/PET foam sandwich composites: DOE analysis of recycled materials. Polym Compos 2022;43:8807–17. https://doi.org/10.1002/pc.27063.

[32] Åkermo M, Tomas åström B. Modeling compression molding of all-thermoplastic honeycomb core sandwich components. Part A: Model development. Polym Compos 2000;21:245–56. https://doi.org/10.1002/pc.10182.

[33] Åkermo M, Tomas åström B. Modeling compression molding of all-thermoplastic honeycomb core sandwich components. Part B: Model verification. Polym Compos 2000;21:257–67. https://doi.org/10.1002/pc.10183.

[34] Trende A, Ström BTA˚, Wöginger A, Mayer C, Neitzel M. Modelling of heat transfer in thermoplastic composites manufacturing: double-belt press lamination. Compos Part A Appl Sci Manuf 1999;30:935–43. https://doi.org/10.1016/S1359-835X(99)00016-0.

[35] Wang X, Mayer C, Neitzel M. Some issues on impregnation in manufacturing of thermoplastic composites by using a double belt press. Polym Compos 1997;18:701–10. https://doi.org/10.1002/pc.10323.

[36] Mayer C, Wang X, Neitzel M. Macro-and micro-impregnation phenomena in continuous manufacturing of fabric reinforced thermoplastic composites. Compos Part A Appl Sci Manuf 1998;29:783–93. https://doi.org/10.1016/S1359-835X(98)00056-6.

[37] Ishida O, Kitada J, Uzawa K. Experimental study of manufacturing thermoplastic composites using double belt press with different press modules. Materials System 2023;40:29–35. https://doi.org/10.34401/materialssystem.40.0_29.

[38] Liu D, Zhu Y, Ding J, Lin X, Fan X. Experimental investigation of carbon fiber reinforced poly(phenylene sulfide) composites prepared using a double-belt press. Compos B Eng 2015;77:363–70. https://doi.org/10.1016/j.compositesb.2015.03.062.

[39] Robinson P, Davies GAO. Impactor mass and specimen geometry effect in low velocity impact of laminated composites. Int J Impact Eng 1992;12:189–207. https://doi.org/10.1016/0734-743X(92)90408-L.

[40] Artero-Guerrero JA, Pernas-Sánchez J, López-Puente J, Varas D. Experimental study of the impactor mass effect on the low velocity impact of carbon/epoxy woven laminates. Compos Struct 2015;133:774–81. https://doi.org/10.1016/j.compstruct.2015.08.027.

[41] Zabala H, Aretxabaleta L, Castillo G, Urien J, Aurrekoetxea J. Impact velocity effect on the delamination of woven carbon-epoxy plates subjected to low-velocity equienergetic impact loads. Compos Sci Technol 2014;94:48–53. https://doi.org/10.1016/j.compscitech.2014.01.016.

[42] Liu H, Liu J, Ding Y, Hall Z, Luo L, Zhou J, et al. Investigations on the impact behaviour of fibre-reinforced composites: Effect of impact energy and impactor shape. Procedia Structural Integrity 2020;28:106–15. https://doi.org/10.1016/j.prostr.2020.10.014.

[43] Shyr TW, Pan YH. Impact resistance and damage characteristics of composite laminates. Compos Struct 2003;62:193–203. https://doi.org/10.1016/S0263-8223(03)00114-4.

[44] Baucom JN, Zikry MA, Rajendran AM. Low-velocity impact damage accumulation in woven S2-glass composite systems. Compos Sci Technol 2006;66:1229–38. https://doi.org/10.1016/j.compscitech.2005.11.005.

[45] Bandaru AK, Chavan V V., Ahmad S, Alagirusamy R, Bhatnagar N. Low velocity impact response of 2D and 3D Kevlar/polypropylene composites. Int J Impact Eng 2016;93:136–43. https://doi.org/10.1016/j.ijimpeng.2016.02.016.

[46] Richardson MOW, Wisheart MJ. Review of low-velocity impact properties of composite materials. Compos Part A Appl Sci Manuf 1996;27:1123–31. https://doi.org/10.1016/1359-835X(96)00074-7.

[47] Bibo GA, Hogg PJ. The role of reinforcement architecture on impact damage mechanisms and post-impact compression behaviour. J Mater Sci 1996;31:1115–37. https://doi.org/10.1007/BF00353091.

[48] Cantwell WJ, Morton A. The impact resistance of composite materials-a review. Composites 1991;22:347–62. https://doi.org/10.1007/BF00353091.

[49] Reyes G, Sharma U. Modeling and damage repair of woven thermoplastic composites subjected to low velocity impact. Compos Struct 2010;92:523–31. https://doi.org/10.1016/j.compstruct.2009.08.038.

[50]   Ghaseminejhad MN, Parvizi-Majidi A. Impact behaviour and damage tolerance of woven carbon fibre-reinforced thermoplastic composites. Constr Build Mater 1990;4:194–207. https://doi.org/10.1016/0950-0618(90)90040-8.

[51]   Vieille B, Casado VM, Bouvet C. About the impact behavior of woven-ply carbon fiber-reinforced thermoplastic- and thermosetting-composites: A comparative study. Compos Struct 2013;101:9–21. https://doi.org/10.1016/j.compstruct.2013.01.025.

[52]   Shah SZH, Megat-Yusoff PSM, Karuppanan S, Choudhry RS, Ahmad F, Sajid Z, et al. Performance comparison of resin-infused thermoplastic and thermoset 3D fabric composites under impact loading. Int J Mech Sci 2021;189:105984. https://doi.org/10.1016/j.ijmecsci.2020.105984.

[53]   Zhou J, Hassan MZ, Guan Z, Cantwell WJ. The low velocity impact response of foam-based sandwich panels. Compos Sci Technol 2012;72:1781–90. https://doi.org/10.1016/j.compscitech.2012.07.006.

[54]   ISO 6603-2 Plastics - Determination of puncture impact behaviour of rigid plastics - Part 2: Instrumented impact testing. ISO 2000.

[55]   ASTM D6264 / D6264M - 17 Standard test method for measuring the damage resistance of a fiber-reinforced polymer-matrix composite to a concentrated quasi-static indentation force. 2017.

[56]   Dogan A, Arikan V. Low-velocity impact response of E-glass reinforced thermoset and thermoplastic based sandwich composites. Compos B Eng 2017;127:63–9. https://doi.org/10.1016/j.compositesb.2017.06.027.

[57]   Ouadday R, Marouene A, Morada G, Kaabi A, Boukhili R, Vadean A. Experimental and numerical investigation on the impact behavior of dual-core composite sandwich panels designed for hydraulic turbine applications. Compos Struct 2018;185:254–63. https://doi.org/10.1016/j.compstruct.2017.11.007.

[58]   Sinmazçelik T, Avcu E, Bora MÖ, Çoban O. A review: Fibre metal laminates, background, bonding types and applied test methods. Mater Des 2011;32:3671–85. https://doi.org/10.1016/j.matdes.2011.03.011.

[59]   Vogelesang LB, Vlot A. Development of fibre metal laminates for advanced aerospace structures. J Mater Process Technol 2000;103:1–5. https://doi.org/10.1016/S0924-0136(00)00411-8.

[60]   Vlot A. Impact properties of fibre metal laminates. Composites Engineering 1993;3:911–27. https://doi.org/10.1016/0961-9526(93)90001-Z.

[61]   Lawcock GD, Ye L, Mai YW, Sun & CT. Effect of fibre/matrix adhesion on carbon-fibre-reinforced metal laminates-II. Impact behaviour. Compos Sci Technol 1998;57:1621–8. https://doi.org/10.1016/S0266-3538(97)00094-8.

[62]   Reyes G, Cantwell WJ. The mechanical properties of fibre-metal laminates based on glass fibre reinforced polypropylene. Compos Sci Technol 2000;60:1085–94. https://doi.org/10.1016/S0266-3538(00)00002-6.

[63]   Shi H, Fernandez-Villegas I, Bersee HEN. An investigation on the strain distribution of resistance welded thermoplastic composite joints. Collection of Technical Papers - AIAA/ASME/ASCE/AHS/ASC Structures, Structural Dynamics and Materials Conference, American Institute of Aeronautics and Astronautics Inc. Honolulu, Hawaii, 23-26 April 2012. https://doi.org/10.2514/6.2012-1448.

[64]   Villegas IF, Bersee HEN. Characterisation of a metal mesh heating element for closed-loop resistance welding of thermoplastic composites. Journal of Thermoplastic Composite Materials 2015;28:46–65. https://doi.org/10.1177/0892705712475012.

[65]   Callens MG, Gorbatikh L, Verpoest I. Ductile steel fibre composites with brittle and ductile matrices. Compos Part A Appl Sci Manuf 2014;61:235–44. https://doi.org/10.1016/j.compositesa.2014.02.006.

[66] Callens MG, Gorbatikh L, Bertels E, Goderis B, Smet M, Verpoest I. Tensile behaviour of stainless steel fibre/epoxy composites with modified adhesion. Compos Part A Appl Sci Manuf 2015;69:208–18. https://doi.org/10.1016/j.compositesa.2014.11.022.

[67] Callens MG, de Cuyper P, Gorbatikh L, Verpoest I. Effect of fibre architecture on the tensile and impact behaviour of ductile stainless steel fibre polypropylene composites. Compos Struct 2015;119:528–33. https://doi.org/10.1016/j.compstruct.2014.09.028.

[68] O'Brien C, Zaghi AE. Mechanical characteristics of hybrid composites with ±45° glass and 0°/90° stainless steel fibers. Materials 2018;11(8):1355. https://doi.org/10.3390/ma11081355.

[69] O'Brien C, McBride A, Zaghi AE, Burke KA, Hill A. Mechanical behavior of stainless steel fiber-reinforced composites exposed to accelerated corrosion. Materials 2017;10(7):772. https://doi.org/10.3390/ma10070772.

[70] McBride AK, Turek SL, Zaghi AE, Burke KA. Mechanical behavior of hybrid glass/steel fiber reinforced epoxy composites. Polymers 2017;9(4):151. https://doi.org/10.3390/polym9040151.

[71] Ahmed TJabeen. Hybrid composite structures : Multifunctionality through metal fibres an exploratory investigation. Ph.D. Thesis. Technical University of Delft, Netherlands, 2009.

[72] Ahmed TJ, Bersee HEN, Beukers A. Low velocity impact on woven glass composites reinforced with metal mesh layers. 16th International Conference on Composite Materials (ICCM16), Kyoto, Japan, 8–13 July 2007.

[73] He W, Wang L, Liu H, Wang C, Yao L, Li Q, et al. On impact behavior of fiber metal laminate (FML) structures: A state-of-the-art review. Thin-Walled Structures 2021;167:108026. https://doi.org/10.1016/j.tws.2021.108026.

[74] Karunagaran N, Rajadurai A. Effect of surface treatment on mechanical properties of glass fiber/stainless steel wire mesh reinforced epoxy hybrid composites. Journal of Mechanical Science and Technology 2016;30:2475–82. https://doi.org/10.1007/s12206-016-0507-9.

[75]   Hasselbruch H, Von Hehl A, Zoch HW. Properties and failure behavior of hybrid wire mesh/carbon fiber reinforced thermoplastic composites under quasi-static tensile load. Mater Des 2015;66:429–36. https://doi.org/10.1016/j.matdes.2014.07.032.

[76]   Tugirumubano A, Vijay SJ, Go SH, Shin HJ, Ku KL, Kim HG. The evaluation of electromagnetic shielding properties of CFRP/metal mesh hybrid woven laminated composites.   J   Compos   Mater   2018;52:3819–29. https://doi.org/10.1177/0021998318770511.

[77]   Jang BP, Huang CT, Hsieh CY, Kowel \v, Jak BZ. Repeated impact failure of continuous fiber   reinforced   thermoplastic   and   thermoset   composites.   J   Compos   Mater 1991;25(9):1171–1203. https://doi.org/10.1177/002199839102500906.

[78]   Arikan V, Sayman O. Comparative study on repeated impact response of E-glass fiber reinforced polypropylene & epoxy matrix composites. Compos B Eng 2015;83:1–6. https://doi.org/10.1016/j.compositesb.2015.08.051.

[79]   Reyes G, Sharma U. Modeling and damage repair of woven thermoplastic composites subjected   to   low   velocity   impact.   Compos   Struct   2010;92:523–31. https://doi.org/10.1016/j.compstruct.2009.08.038.

[80]   Pan Z, Zhao Q, Wei Q, Wu Z, Li N. Heat treatment on the multiple-impact mechanical responses and damage behaviors of 3D and 2D woven GF/PP/epoxy composites. Thin-Walled Structures 2023;183:110415. https://doi.org/10.1016/j.tws.2022.110415.

[81]   Patel AJ, Sottos NR, Wetzel ED, White SR. Autonomic healing of low-velocity impact damage in fiber-reinforced composites. Compos Part A Appl Sci Manuf 2010;41:360–8. https://doi.org/10.1016/j.compositesa.2009.11.002.

[82]   Selver E, Potluri P, Soutis C, Hogg P. Healing potential of hybrid materials for structural composites.   Compos   Struct   2015;122:57–66. https://doi.org/10.1016/j.compstruct.2014.11.027.

[83] Kirkby EL, Rule JD, Michaud VJ, Sottos NR, White SR, Månson JAE. Embedded shape-memory alloy wires for improved performance of self-healing polymers. Adv Funct Mater 2008;18:2253–60. https://doi.org/10.1002/adfm.200701208.

[84] Neuser S, Michaud V, White SR. Improving solvent-based self-healing materials through shape memory alloys. Polymer (Guildf) 2012;53:370–8. https://doi.org/10.1016/j.polymer.2011.12.020.

[85] Kirkby EL, Rule JD, Michaud VJ, Sottos NR, White SR, Månson JAE. Embedded shape-memory alloy wires for improved performance of self-healing polymers. Adv Funct Mater 2008;18:2253–60. https://doi.org/10.1002/adfm.200701208.

[86] John M, Li G. Self-healing of sandwich structures with a grid stiffened shape memory polymer syntactic foam core. Smart Mater Struct 2010;19. https://doi.org/10.1088/0964-1726/19/7/075013.

[87] Li G, John M. A self-healing smart syntactic foam under multiple impacts. Compos Sci Technol 2008;68:3337–43. https://doi.org/10.1016/j.compscitech.2008.09.009.

[88] Bor TC, Warnet L, Akkerman R, De Boer A. Modeling of stress development during thermal damage healing in fiber-reinforced composite materials containing embedded shape memory alloy wires. J Compos Mater 2010;44(22):2547–72. https://doi.org/10.1177/0021998310371532.

[89] Pappadà S, Rametta R, Largo A, Maffezzoli A. Low-velocity impact response in composite plates embedding shape memory alloy wires. Polym Compos 2012;33:655–64. https://doi.org/10.1002/pc.22170.

[90] Meo M, Marulo F, Guida M, Russo S. Shape memory alloy hybrid composites for improved impact properties for aeronautical applications. Compos Struct 2013;95:756–66. https://doi.org/10.1016/j.compstruct.2012.08.011.

[91] Li H, Liu J, Wang Z, Yu Z, Liu Y, Sun M. The low velocity impact response of shape memory alloy hybrid polymer composites. Polymers 2018;10(9):1026. https://doi.org/10.3390/polym10091026.

[92] Cohades A, Hostettler N, Pauchard M, Plummer CJG, Michaud V. Stitched shape memory alloy wires enhance damage recovery in self-healing fibre-reinforced polymer composites. Compos Sci Technol 2018;161:22–31. https://doi.org/10.1016/j.compscitech.2018.03.040.

[93] Xie H, Shen C, Fang H, Han J, Cai W. Flexural property evaluation of web reinforced GFRP-PET foam sandwich panel: Experimental study and numerical simulation. Compos B Eng 2022;234:109725. https://doi.org/10.1016/j.compositesb.2022.109725.

[94] ASTM C297/ C297M - 04 Standard test method for flatwise tensile strength of sandwich constructions. 2017.

[95] ASTM D3167 - 10 Standard test method for floating roller peel resistance of adhesives. 2017.

[96] ASTM C393 Standard Test method for flexural properties of sandwich constructions. 2017.

[97] Ozturk F, Cobanoglu M, Ece RE. Recent advancements in thermoplastic composite materials in aerospace industry. Journal of Thermoplastic Composite Materials 2024;37(9):3084-3116. https://doi.org/10.1177/08927057231222820.

[98] Ma Q, Rejab MRM, Siregar JP, Guan Z. A review of the recent trends on core structures and impact response of sandwich panels. J Compos Mater 2021;55:2513–55. https://doi.org/10.1177/0021998321990734.

[99] Yassin K, Hojjati M. Processing of thermoplastic matrix composites through automated fiber placement and tape laying methods: A review. Journal of Thermoplastic Composite Materials 2018;31:1676–725. https://doi.org/10.1177/0892705717738305.

[100] Dogan A. Low-velocity impact, bending, and compression response of carbon fiber/epoxy-based sandwich composites with different types of core materials. Journal of Sandwich Structures & Materials 2021;23:1956–71. https://doi.org/10.1177/1099636220908862.

[101] Rome JI, Goyal VK, Patel DN. Strength reduction of foam-core sandwich structures with core mismatches. Journal of Sandwich Structures & Materials 2023;25:44–60. https://doi.org/10.1177/10996362221115418

[102] Xie H, Li W, Fang H, Zhang S, Yang Z, Fang Y, et al. Flexural behavior evaluation of a foam core curved sandwich beam. Compos Struct 2024;328:117729. https://doi.org/10.1016/j.compstruct.2023.117729.

[103] Bragagnolo G, Crocombe AD, Ogin SL, Sordon A, Mohagheghian I. Flexural Behaviour of Foam Cored Sandwich Structures with Through-Thickness Reinforcements. Journal of Composites Science 2023;7:125. https://doi.org/10.3390/jcs7030125.

[104] Manalo A, Aravinthan T, Fam A, Benmokrane B. State-of-the-art review on FRP sandwich systems for lightweight civil infrastructure. Journal of Composites for Construction 2017;21:04016068. https://doi.org/10.1061/(asce)cc.1943-5614.0000729.

[105] Iyer SV, Chatterjee R, Ramya M, Suresh E, Padmanabhan K. A comparative study of the three point and four point bending behaviour of rigid foam core glass/epoxy face sheet sandwich composites. Mater Today Proc 2018;5:12083–90. https://doi.org/10.1016/j.matpr.2018.02.184.

[106] Fischer Kerche E, Silveira Caldas BG, Carvalho RF, Amico SC. Mechanical response of sisal/glass fabrics reinforced polyester–polyethylene terephthalate foam core sandwich panels. Journal of Sandwich Structures & Materials 2022;24:1993–2009. https://doi.org/10.1177/10996362221115057.

[107] Mei J, Liu J, Huang W. Three-point bending behaviors of the foam-filled CFRP X-core sandwich panel: experimental investigation and analytical modelling. Compos Struct 2022;284:115206. https://doi.org/10.1016/j.compstruct.2022.115206.

[108] Grünewald J, Orth T, Parlevliet P, Altstädt V. Modified foam cores for full thermoplastic composite sandwich structures. Journal of Sandwich Structures & Materials 2019;21:1150–66. https://doi.org/10.1177/1099636217708741.

[109] Sun C, Albustani H, Phadnis VA, Saleh MN, Cantwell WJ, Guan Z. Improving the structural integrity of foam-core sandwich composites using continuous carbon fiber stitching. Compos Struct 2023;324:117509. https://doi.org/10.1016/j.compstruct.2023.117509.

[110] Lee J-C, Yu S, Jung H-S, Kim K-Y, Lim DY. Measurement of interfacial bonding force between foam and CFRP in foam-cored CFRP sandwich composites. Fibers and Polymers 2021;22:1934–9. https://doi.org/10.1007/s12221-021-0236-2.

[111] Samareh-Mousavi SS, Chen X, McGugan M, Semenov S, Berring P, Branner K, et al. Monitoring fatigue delamination growth in a wind turbine blade using passive thermography and acoustic emission. Struct Health Monit 2024;23(5):2906-2921. https://doi.org/10.1177/14759217231217179.

[112] Rezaei M, Karatzas V, Berggreen C, Carlsson LA. The effect of elevated temperature on the mechanical properties and failure modes of GFRP face sheets and PET foam cored sandwich beams. Journal of Sandwich Structures & Materials 2020;22:1235–55. https://doi.org/10.1177/1099636218781995.

[113] Pyrzowski Ł, Sobczyk B. Local and global response of sandwich beams made of GFRP facings and PET foam core in three point bending test. Compos Struct 2020;241:112122. https://doi.org/10.1016/j.compstruct.2020.112122.

[114] Butler CA, Mccullough RL, Pitchumani R, Gillespie Jr JW. An analysis of mechanisms governing fusion bonding of thermoplastic composites. Journal of Thermoplastic Composite Materials 1998;11:338–63. https://doi.org/10.1177/089270579801100404.

[115] Yousefpour A, Hojjati M, Immarigeon J-P. Fusion bonding/welding of thermoplastic composites. Journal of Thermoplastic Composite Materials 2004;17:303–41. https://doi.org/10.1177/0892705704045187.

[116] Ageorges C, Ye L, Hou M. Advances in fusion bonding techniques for joining thermoplastic matrix composites: A review. Compos Part A Appl Sci Manuf 2001;32:839–57. https://doi.org/10.1016/S1359-835X(00)00166-4.

[117] Mandegarian S, Hojjati M. Low velocity impact behavior of thermoplastic glass fiber composites strengthen with stainless steel mesh layers. 23rd International Conference on Composite Materials (ICCM23), Belfast, Northern Ireland, UK, 31 July-4 August 2023.

[118] Mandegarian S, Hojjati M. Manufacturing and performance of sandwich composite panels with recycled PET foam core made by continuous roll forming. Manufacturing Letters. 2024;21:89-92. https://doi.org/10.1016/j.mfglet.2024.03.019.

[119] Ishida O, Kitada J, Uzawa K. Experimental study of manufacturing thermoplastic composites using double belt press with different press modules. Materials System, 2023;40:29–35. https://doi.org/10.34401/materialssystem.40.0_29.

[120] Armacell 2017. https://www.armacell.us/products/armaform/?CA (accessed April 24, 2024).

[121] Azad M. Manufacturing of sandwich panels using recycled thermoplastic composites in a continuous extrusion line. Concordia University, Montreal, QC, Canada, 2016.

[122] Innovative Composite Products Inc. (ICP Inc.) 2024. https://i-c-p.ca/ (accessed April 25, 2024).

[123] Mandegarian S., Hojjati M. Experimental investigation on the effects of stainless-steel mesh reinforcing layers on low-velocity impact response of hybrid thermoplastic glass fiber composites. J Compos Mater, 2024;58(16):1887-1904. https://doi.org/10.1177/00219983241253028.

[124] Mandegarian S, Hojjati M, Moghaddar H. Fabrication of thermoplastic composite sandwich panels with recycled PET foam core using hot press. 13th Canadian International Conference on Composites (CANCOM 2024), Waterloo, ON, Canada, 6-9 Aug 2024.

[125] ASTM D3418 - 21 Test method for transition temperatures and enthalpies of fusion and crystallization of polymers by differential scanning calorimetry. 2021.

[126] ASTM C365/ C365M - 22 Standard Test method for flatwise compressive properties of sandwich cores. 2022.

[127] ASTM D3039 / D3039M - 17 Standard test method for tensile properties of polymer matrix composite materials. 2017.

[128] ASTM D3410/ D3410M Standard test method for compressive properties of polymer matrix composite materials with unsupported gage section by shear loading. 2021.

[129] Djele A, Karakuzu R. An experimental study on quasi-static indentation, low-velocity impact and damage behaviors of laminated composites at high temperatures. Polymers and Polymer Composites 2021;29:S969–77. https://doi.org/10.1177/09673911211016932.

[130] Yalkın HE, Karakuzu R, Alpyıldız T. Experimental and numerical behaviors of GFRP laminates under low velocity impact. J Compos Mater 2020;54:2999–3007. https://doi.org/10.1177/0021998320906871.

[131] Dubary N, Taconet G, Bouvet C, Vieille B. Influence of temperature on the impact behavior and damage tolerance of hybrid woven-ply thermoplastic laminates for aeronautical applications. Compos Struct 2017;168:663–74. https://doi.org/10.1007/BF00353091.

[132] G.A.O.Davies, X.Zhang, G.Zhou, S.Watson. Numerical damage modelling of impact. Composites 1994;25:342–50. https://doi.org/10.1016/S0010-4361(94)80004-9.

[133] Kim JK, Sham ML. Impact and delamination failure of woven-fabric composites. Compos Sci Technol 2000;60:745–61. https://doi.org/10.1016/S0266-3538(99)00166-9.

[134] De Baere I, Jacques S, Van Paepegem W, Degrieck J. Study of the mode I and mode II interlaminar behaviour of a carbon fabric reinforced thermoplastic. Polym Test 2012;31:322–32. https://doi.org/10.1016/j.polymertesting.2011.12.009.

[135] Vallons K, Behaeghe A, Lomov S V., Verpoest I. Impact and post-impact properties of a carbon fibre non-crimp fabric and a twill weave composite. Compos Part A Appl Sci Manuf 2010;41:1019–26. https://doi.org/10.1016/j.compositesa.2010.04.008.

[136] Jung KH, Kim DH, Kim HJ, Park SH, Jhang KY, Kim HS. Finite element analysis of a low-velocity impact test for glass fiber-reinforced polypropylene composites considering mixed-mode interlaminar fracture toughness. Compos Struct 2017;160:446–56. https://doi.org/10.1016/j.compstruct.2016.10.093.

[137] Simeoli G, Acierno D, Meola C, Sorrentino L, Iannace S, Russo P. The role of interface strength on the low velocity impact behaviour of PP/glass fibre laminates. Compos B Eng 2014;62:88–96. https://doi.org/10.1016/j.compositesb.2014.02.018.

[138] Boria S, Scattina A, Belingardi G. Impact behavior of a fully thermoplastic composite. Compos Struct 2017;167:63–75. https://doi.org/10.1016/j.compstruct.2017.01.083.

[139] Boria S, Scattina A, Belingardi G. Experimental investigation on a fully thermoplastic composite subjected to repeated impacts. Proc Inst Mech Eng C J Mech Eng Sci 2019;233:6985–7002. https://doi.org/10.1177/0954406219866883.

[140] Vieille B, Casado VM, Bouvet C. Influence of matrix toughness and ductility on the compression-after-impact behavior of woven-ply thermoplastic- and thermosetting-composites: A comparative study. Compos Struct 2014;110:207–18. https://doi.org/10.1016/j.compstruct.2013.12.008.

[141] De Cicco D, Asaee Z, Taheri F. Low-velocity impact damage response of fiberglass/magnesium fiber-metal laminates under different size and shape impactors. Mechanics of Advanced Materials and Structures 2017;24:545–55. https://doi.org/10.1080/15376494.2016.1162343.

[142] Asaee Z, Taheri F. Experimental and numerical investigation into the influence of stacking sequence on the low-velocity impact response of new 3D FMLs. Compos Struct 2016;140:136–46. https://doi.org/10.1016/j.compstruct.2015.12.015.

[143] Asaee Z, Shadlou S, Taheri F. Low-velocity impact response of fiberglass/magnesium FMLs with a new 3D fiberglass fabric. Compos Struct 2015;122:155–65. https://doi.org/10.1016/j.compstruct.2014.11.038.

[144] Fan J, Cantwell WJ, Guan ZW. The low-velocity impact response of fiber-metal laminates. J Compos Mater 2010;30:26–35. https://doi.org/10.1177/0731684410386133.

[145] Tsartsaris N, Meo M, Dolce F, Polimeno U, Guida M, Marulo F. Low-velocity impact behavior of fiber metal laminates. J Compos Mater 2011;45:803–14. https://doi.org/10.1177/0021998310376108.

[146] Al-Mezrakchi R, Al-Ramthan A, Alam S. Designing and modeling new generation of advanced hybrid composite sandwich structure armors for ballistic threats in defense applications. AIMS Mater Sci 2020;7:608–31. https://doi.org/10.3934/matersci.2020.5.608.

[147] Bikakis GSE, Dimou CD, Sideridis EP. Ballistic impact response of fiber–metal laminates and monolithic metal plates consisting of different aluminum alloys. Aerosp Sci Technol 2017;69:201–8. https://doi.org/10.1016/j.ast.2017.06.028.

[148] Mahesh V. Comparative study on low velocity impact response of carbon-fiber-reinforced polymer/ thermoplastic elastomer based fiber metal laminates with and without interleaving of elastomeric layer. Journal of Thermoplastic Composite Materials 2024;37:604–24. https://doi.org/10.1177/08927057231180487.

[149] Uzay Ç, Geren N. Effect of stainless-steel wire mesh embedded into fibre-reinforced polymer facings on flexural characteristics of sandwich structures. Journal of Reinforced Plastics and Composites 2020;39:613–33. https://doi.org/10.1177/0731684420921952.

[150] Wang C, Ramakrishnan KR, Shankar K, Morozov E, Wang H, Fien A. Homogenized shell element-based modeling of LVI response of stainless-steel wire mesh. Mechanics of Advanced Materials and Structures 2020;28:1932–47. https://doi.org/10.1080/15376494.2020.1716415.

[151] Wang C, Wang H, Shankar K, Morozov E V., Hazell PJ. On the mechanical behaviour of steel wire mesh subjected to low-velocity impact. Thin-Walled Structures 2021;159:107281. https://doi.org/10.1016/j.tws.2020.107281.

[152] ASTM D7136 / D7136M - 15 Standard test method for measuring the damage resistance of a fiber-reinforced polymer matrix composite to a drop-weight impact event. 2015.

[153] ASTM D3763 - 18 Standard test method for high speed puncture properties of plastics using load and displacement sensors. 2018.

[154] Ghayour M, Hojjati M, Ganesan R. Effect of tow gaps on impact strength of thin composite laminates made by Automated Fiber Placement: Experimental and semi-analytical

approaches. Compos Struct 2020;248:112536. https://doi.org/10.1016/j.compstruct.2020.112536.

[155] Kakati S, Chakraborty D. Low velocity impact on fibre metal laminates: A review. J Compos Mater 2023;57:4731–50. https://doi.org/ 10.1177/00219983231212544.

[156] Erkendirci ÖF, Haque BZ. Quasi-static penetration resistance behavior of glass fiber reinforced thermoplastic composites. Compos B Eng 2012;43:3391–405. https://doi.org/10.1016/j.compositesb.2012.01.053.

[157] Taşyürek M, Kara M. Low-velocity impact response of pre-stressed glass fiber/nanotube filled epoxy composite tubes. J Compos Mater 2021;55:915–26. https://doi.org/10.1177/0021998320961552.

[158] Taşyürek M, Ödemiş O. Investigation of the effect of CNT reinforcement on low-velocity impact behavior of wooden plate honeycomb aircraft structures. International Journal of Aeronautics and Astronautics 2023;4:1–8. https://doi.org/10.55212/ijaa.1289145.

[159] Dogan A. Low-velocity impact, bending, and compression response of carbon fiber/epoxy-based sandwich composites with different types of core materials. Journal of Sandwich Structures and Materials 2021;23:1956–71. https://doi.org/10.1177/1099636220908862.

[160] Yalkın HE, Karakuzu R, Alpyıldız T. Low velocity impact behavior of sandwich composites with different structural configurations of foam core: An experimental study. Journal of Sandwich Structures & Materials 2022;24:1941–60. https://doi.org/10.1177/10996362221115050.

[161] Baran I, Weijermars W. Residual bending behaviour of sandwich composites after impact. Journal of Sandwich Structures & Materials 2018;22:402–22. https://doi.org/10.1177/1099636218757164.

[162] Guo H, Yuan H, Zhang J, Ruan D. Review of sandwich structures under impact loadings: Experimental, numerical and theoretical analysis. Thin-Walled Structures 2024;196:111541. https://doi.org/10.1016/j.tws.2023.111541.

[163] Zhang J, Ye Y, Qin Q, Wang T. Low-velocity impact of sandwich beams with fibre-metal laminate face-sheets. Compos Sci Technol 2018;168:152–9. https://doi.org/10.1016/j.compscitech.2018.09.018.

[164] Mandegarian S, Hojjati M, Moghaddar H. Thermoplastic composite sandwich panels with recycled pet foam core: A manufacturing process assessment. Journal of Thermoplastic Composite Materials 2024. https://doi.org/10.1177/08927057241291021.

[165] Lopresto V, Caprino G. Damage mechanisms and energy absorption in composite laminates under low velocity impact loads. In: abrate s, castanié b, rajapakse yds, editors. Dynamic Failure of Composite and Sandwich Structures, Dordrecht: Springer, 2013, vol 192, p. 209–89. https://doi.org/10.1007/978-94-007-5329-7_6.

[166] Lakshminarayana H V., Boukhili R, Gauvin R. Impact response of laminated composite plates: Prediction and verification. Compos Struct 1994;28:61–72. https://doi.org/10.1016/0263-8223(94)90006-X.

[167] Ma B, Cao X, Feng Y, Song Y, Yang F, Li Y, et al. A comparative study on the low velocity impact behavior of UD, woven, and hybrid UD/woven FRP composite laminates. Compos B Eng 2024;271:111133. https://doi.org/10.1016/j.compositesb.2023.111133.

[168] Alabbad M, Vel SS, Lopez-Anido RA. Computational model for predicting the low-velocity impact resistance and tolerance of composite laminates. Compos B Eng 2022;244:110187. https://doi.org/10.1016/j.compositesb.2022.110187.

[169] Lyu Q, Wang B, Guo Z. Predicting post-impact compression strength of composite laminates under multiple low-velocity impacts. Compos Part A Appl Sci Manuf 2023;164:107322. https://doi.org/10.1016/j.compositesa.2022.107322.

[170] Atas C, Sayman O. An overall view on impact response of woven fabric composite plates. Compos Struct 2008;82:336–45. https://doi.org/10.1016/j.compstruct.2007.01.014.

[171] Atas C, Icten BM, Küçük M. Thickness effect on repeated impact response of woven fabric composite plates. Compos B Eng 2013;49:80–5. https://doi.org/10.1016/j.compositesb.2013.01.019.

[172] de Morais WA, Monteiro SN, d'Almeida JRM. Effect of the laminate thickness on the composite strength to repeated low energy impacts. Compos Struct 2005;70:223–8. https://doi.org/10.1016/j.compstruct.2004.08.024.

[173] Atas C, Icten BM, Küçük M. Thickness effect on repeated impact response of woven fabric composite plates. Compos B Eng 2013;49:80–5. https://doi.org/10.1016/j.compositesb.2013.01.019.

[174] Zhu L, Faulkner D. Damage estimate for plating of ships and platforms under repeated impacts. Marine Structures 1996;9:697–720. https://doi.org/10.1016/0951-8339(95)00018-6.

[175] de Morais WA, Monteiro SN, d'Almeida JRM. Effect of the laminate thickness on the composite strength to repeated low energy impacts. Compos Struct 2005;70:223–8. https://doi.org/10.1016/j.compstruct.2004.08.024.

[176] Mandegarian S, Hojjati M, Moghaddar H. Recycled PET foam core sandwich panels with reinforced hybrid composite facesheets: A sustainable approach for enhanced impact resistance. Journal of Sandwich Structures and Materials, 2025;27(2):396-428. https://doi.org/10.1177/10996362241298164.

[177] ASTM F2004-24 Standard test method for transformation temperature of nickel-titanium alloys by thermal analysis. 2024.

[178] Shaw JA, Churchill CB, Iadicola MA. Tips and tricks for characterizing shape memory alloy wire: Part 1-differential scanning calorimetry and basic phenomena. Exp Tech 2008;32:55–62. https://doi.org/10.1111/J.1747-1567.2008.00410.x/metrics.

[179] Duerig TW, Pelton AR, Bhattacharya K. The Measurement and Interpretation of Transformation Temperatures in Nitinol. Shape Memory and Superelasticity 2017;3:485–98. https://doi.org/10.1007/S40830-017-0133-0/metrics.

[180] Cisse C, Zaki W, Ben T, Iyer S, Hubert P. Thermomechanical characterization of functionally stabilized nickel-titanium-copper shape memory alloy. Engineering Research Express 2022;4:015031. https://doi.org/10.1088/2631-8695/AC2BF1.

[181] Sahli ML, Necib B. Characterisation and modelling of behaviour of a shape memory alloys. International Journal of Advanced Manufacturing Technology 2014;70:1847–57. https://doi.org/10.1007/S00170-013-5416-9/metrics.

[182] Bhardwaj A, Gupta AK, Padisala SK, Poluri K. Characterization of mechanical and microstructural properties of constrained groove pressed nitinol shape memory alloy for biomedical applications. Materials Science and Engineering: C 2019;102:730–42. https://doi.org/10.1016/J.MSEC.2019.04.070.

[183] Guo Y, Klink A, Fu C, Snyder J. Machinability and surface integrity of Nitinol shape memory alloy. CIRP Annals 2013;62:83–6. https://doi.org/10.1016/J.CIRP.2013.03.004.

Appendix:

Supplementary information for: "Experimental Investigation on the Effects of Stainless-Steel Mesh Reinforcing Layers on Low-Velocity Impact Response of Hybrid Thermoplastic Glass Fiber Composites"
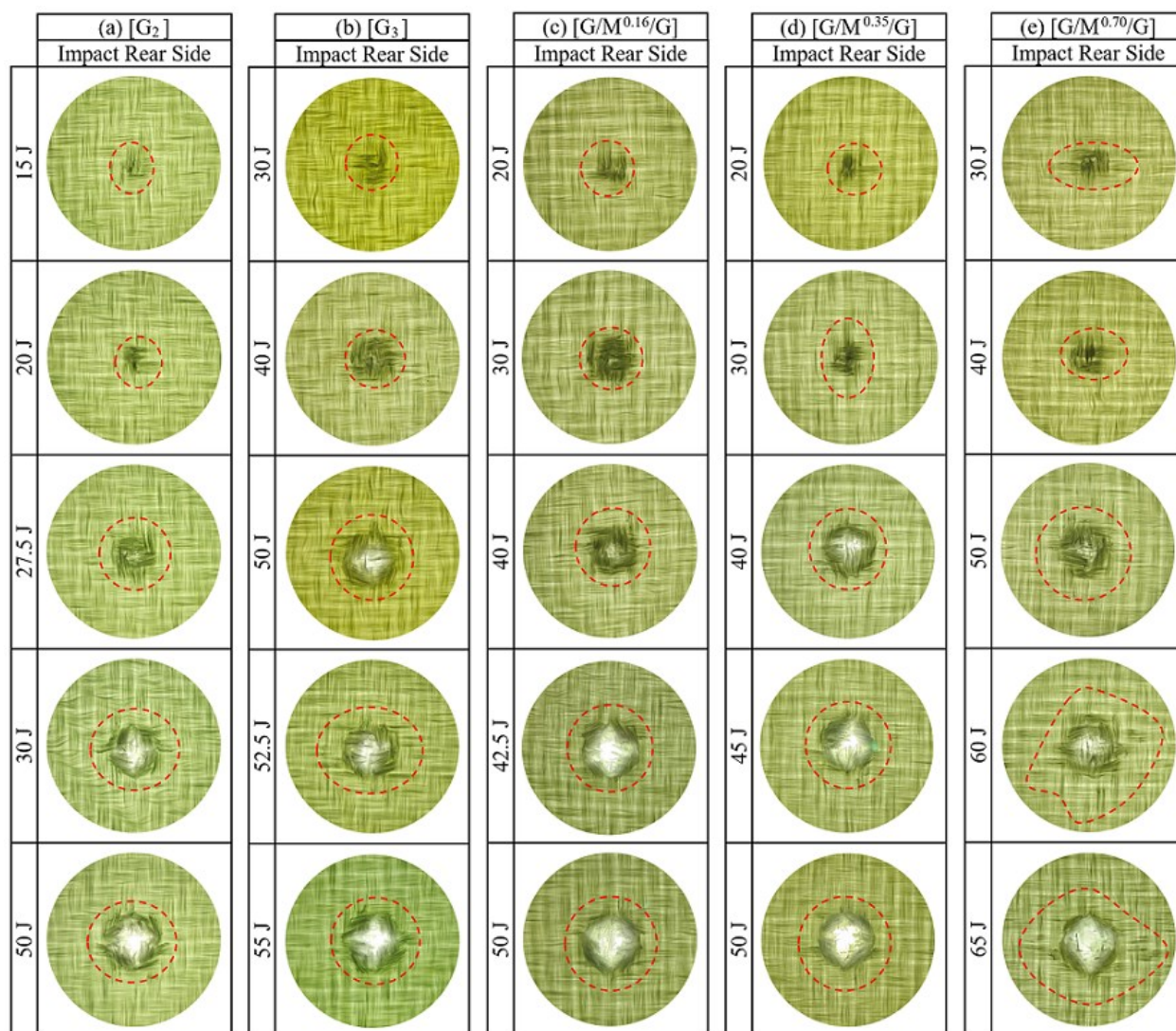
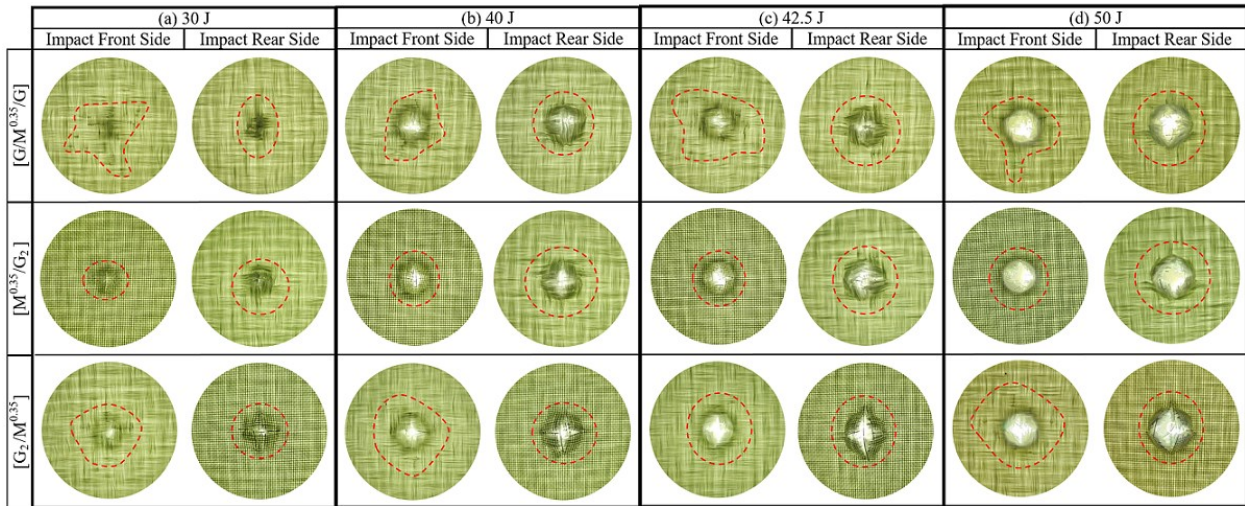Figure A.1. The extent of damage under various LVI energies (rear impact side).

Figure A.2. Comparison of the damage extent of [G/M$^{0.35}$/G], [M$^{0.35}$/G$_2$], and [G$_2$/M$^{0.35}$] hybrid composite laminates under various LVI energies.
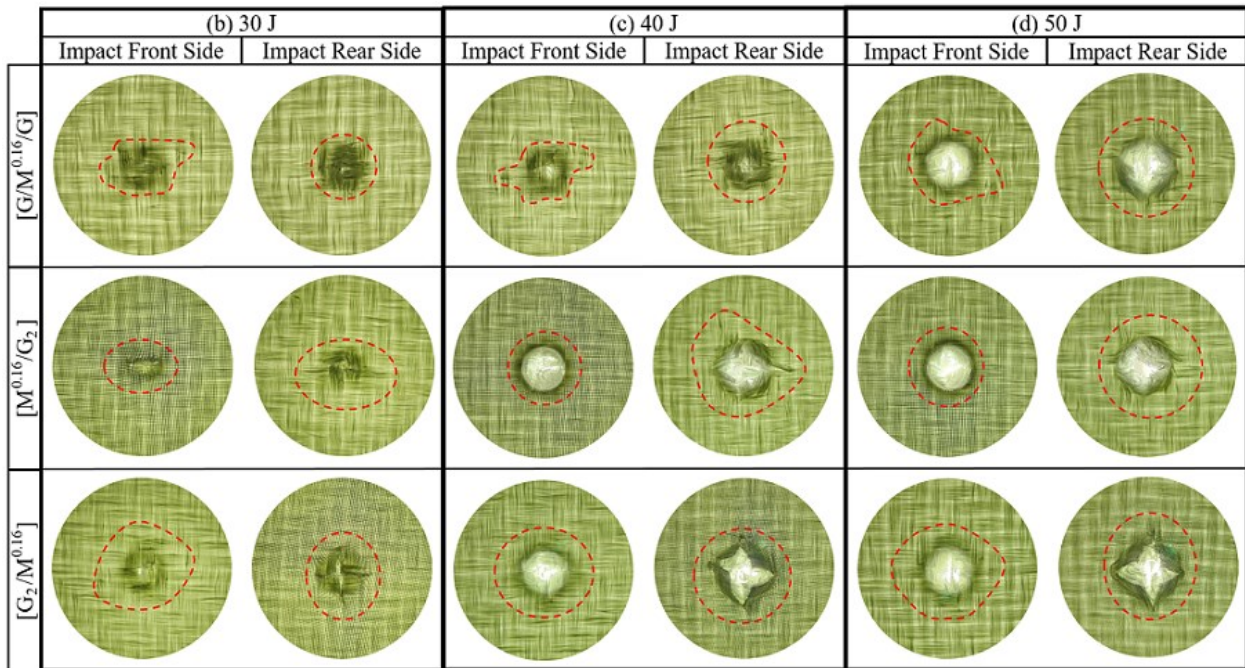

Figure A.3. Evaluation of the [G/M$^{0.16}$/G], [M$^{0.16}$/G$_2$], and [G$_2$/M$^{0.16}$] hybrid composite laminates damage extent under various LVI energies.

Table A.1.

Summary of the LVI test results of $[M^{0.35}/G_2]$, $[G_2/M^{0.35}]$, $[M^{0.16}/G_2]$ and $[G_2/M^{0.16}]$ hybrid composite laminates.

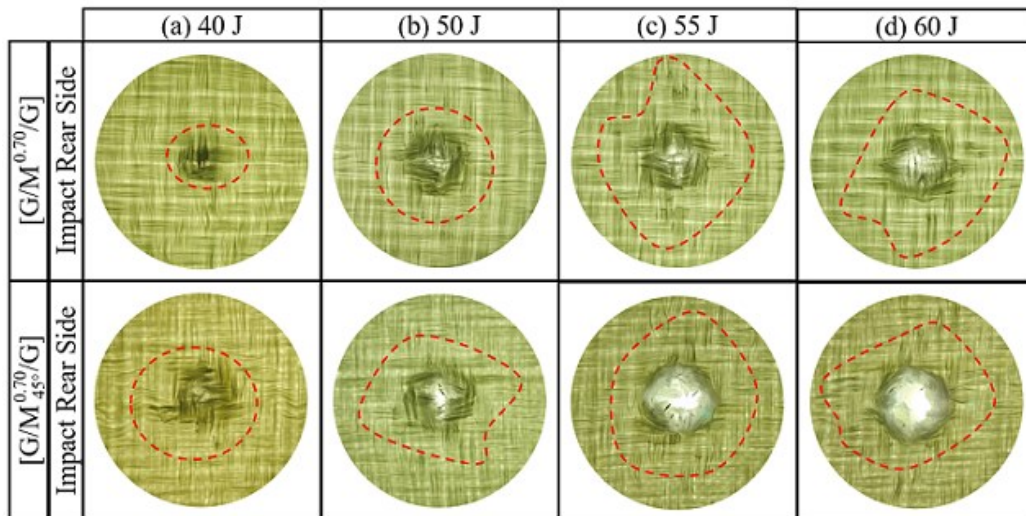| Laminate stacking sequence	Impact energy [J]	Peak force [kN]	Disp. at peak force [mm]	Max. displacement [mm]	After-impact dent depth [mm]	After-impact dent's edge depth [mm]	Dissipated energy [J]
$[M^{0.35}/G_2]$	20	4.40	9.41	9.77	1.65	1.22	12.81
	30	5.07	11.00	12.86	4.60	1.78	25.52
	40	5.11	11.13	17.28	8.15	2.03	38.62
	42.5	5.28	11.46	18.98	9.80	2.64	42.14
	45	4.22	10.34	-	P	0.56	43.77
	50	4.56	10.22	-	P	0.76	43.51
$[G_2/M^{0.35}]$	20	4.36	10.12	10.62	1.47	0.97	14.23
	30	6.16	10.42	14.25	5.28	1.73	27.42
	40	4.79	10.77	18.95	7.11	1.91	39.76
	42.5	4.59	10.86	-	P	2.54	42.55
	45	5.35	11.94	-	P	1.63	45.02
	50	4.36	10.64	-	P	0.99	39.20
$[M^{0.16}/G_2]$	30	4.53	11.89	12.54	4.32	1.37	24.35
	35	3.81	9.37	18.38	9.07	1.40	34.93
	37.5	4.14	9.90	-	P	0.99	37.79
	40	4.67	10.90	-	P	0.69	39.31
	50	4.05	10.01	-	P	0.69	35.65
$[G_2/M^{0.16}]$	20	3.96	9.77	10.31	1.45	0.58	14.61
	30	4.99	10.48	13.02	3.86	1.55	26.44
	35	4.72	10.97	17.05	7.75	1.65	34.50
	37.5	4.42	11.05	-	P	0.81	37.28
	40	4.44	10.87	-	P	0.43	37.52
	50	4.38	9.66	-	P	0.90	36.08

Figure A.4. Damage extent of [G/M$^{0.70}$/G], and [G/M$^{0.70}_{45°}$/G] hybrid laminates under (a) 40 J, (b) 50 J, (c) 55 J and (d) 60 J impact energies (rear impact side).
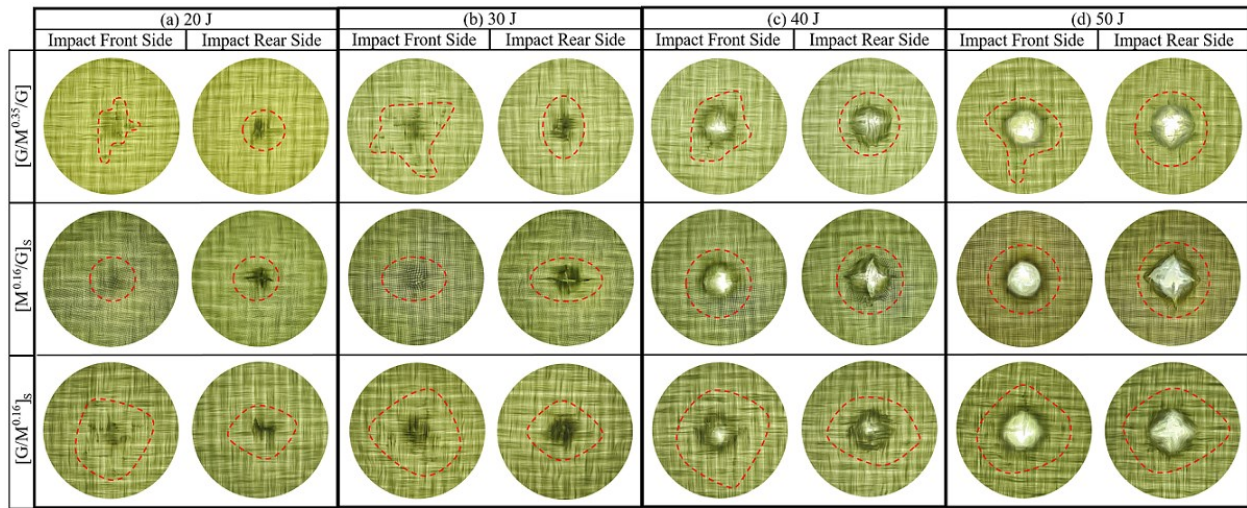

Figure 05. Assessments of the damage response of the [G/M$^{0.35}$/G], [G/M$^{0.16}$]$_s$ and [M$^{0.16}$/G]$_s$ hybrid composites subjected to (a) 20 J, (b) 30 J, (c) 40 J and (d) 50 J impact energies.

Table A.2.

Summary of LVI test results of [G/M$^{0.16}$]$_s$ and [M$^{0.16}$/G]$_s$ plates at different impact energies.

Laminate stacking sequence	Impact energy [J]	Peak force [kN]	Disp. at peak force [mm]	Max. displacement [mm]	After-impact dent depth [mm]	After-impact dent's edge depth [mm]	Dissipated energy [J]
[M$^{0.16}$/G]$_s$	20	4.18	9.81	10.06	2.21	1.09	14.44
	30	5.34	11.47	12.09	4.42	2.29	25.03
	40	4.82	9.62	17.20	8.51	2.41	38.71
	42.5	4.57	10.30	-	P	1.68	42.51
	45	4.87	9.28	-	P	1.02	43.70
	50	4.66	10.86	-	P	0.51	43.70
[G/M$^{0.16}$]$_s$	20	4.17	9.34	9.47	0.97	0.38	13.23
	30	4.87	11.22	11.75	2.39	0.58	24.66
	40	5.21	10.88	15.75	4.80	1.09	36.68
	42.5	5.58	11.56	16.52	4.34	1.32	40.14
	45	5.11	10.75	-	P	0.91	44.95
	50	4.45	10.35	-	P	0.58	45.82